EFFICIENT TECHNIQUE FOR ARRHYTHMIA DETECTION AND CLASSIFICATION USING ECG SIGNAL

A Thesis Submitted
In Partial Fulfillment of the Requirements for the
Degree of

DOCTOR OF PHILOSOPHY
in
Electronics & Communication Engineering
by

Shikha Singhal
(Roll No. 2k20/PHDEC/511)

Under the Supervision of

Dr. Manjeet Kumar
Assistant Professor, Department of Electronics & Communication Engineering
Delhi Technological University

Department of Electronics & Communication Engineering

DELHI TECHNOLOGICAL UNIVERSITY
(Formerly Delhi College of Engineering)
Shahbad Daulatpur, Main Bawana Road, Delhi-110042, India

December, 2025

DELHI TECHNOLOGICAL UNIVERSITY
(Formerly Delhi College of Engineering)
Shahbad Daulatpur, Main Bawana Road, Delhi-42

<u>CANDIDATE'S DECLARATION</u>

I **Shikha Singhal** hereby certify that the work which is being presented in the thesis entitled **"Efficient Technique for Arrhythmia Detection and Classification Using ECG Signals"** in partial fulfilment of the requirements for the award of the Degree of Doctor of Philosophy, submitted in the Department of Electronics & Communication Engineering, Delhi Technological University is an authentic record of my own work carried out during the period from January 2021 to September 2025 under the supervision of **Dr. Manjeet Kumar**, Assistant Professor in Department of Electronics & Communication Engineering, Delhi Technological University, Delhi, India. The matter presented in the thesis has not been submitted by me for the award of any degree of this or any other Institute.

Candidate's Signature

This is to certify that the student has incorporated all the corrections suggested by the examiners in the thesis and the statement made by the candidate is correct to the best of our knowledge.

Signature of Supervisor(s)   **Signature of External Examiner**

DELHI TECHNOLOGICAL UNIVERSITY
(Formerly Delhi College of Engineering)
Shahbad Daulatpur, Main Bawana Road, Delhi-42

CERTIFICATE BY THE SUPERVISOR

Certified that **Shikha Singhal** (2k20/PHDEC/511) has carried out her research work presented in this thesis entitled **"Efficient Technique for Arrhythmia Detection and Classification Using ECG Signals"** for the award of **Doctor of Philosophy** from Department of Electronics & Communication Engineering, Delhi Technological University, Delhi, under my supervision. The thesis embodies results of original work, and studies are carried out by the student herself and the contents of the thesis do not form the basis for the award of any degree to the candidate or to anybody else from this or any other University/Institution.

Dr. Manjeet Kumar
Department of ECE
Delhi Technological University
Delhi-110042, India

Date:

<u>ACKNOWLEDGEMENT</u>

I am deeply indebted and sincerely grateful to the many individuals whose support and guidance have been instrumental in helping me complete this research program. This challenging yet rewarding journey has contributed significantly to my personal growth and academic development. It is a great pleasure to now take this opportunity to express my heartfelt gratitude to all those who have supported me along the way.

First and foremost, I would like to express my heartfelt gratitude and sincere appreciation to my supervisor, **Dr. Manjeet Kumar**, for his invaluable guidance, insightful suggestions, unwavering support, and constant encouragement throughout the course of my research work. His keen interest and constructive feedback have been instrumental in shaping this study. I have learned immensely from him, not only in the academic domain but also in various other aspects of life. I am deeply grateful for his unwavering support and cooperation, which I received from the very beginning of this work until its completion in the form of this thesis. His meticulous and comprehensive approach, coupled with his genuine passion for research, has transformed this journey into a truly enriching and rewarding experience.

I would like to extend my heartfelt thanks to Prof. Dinesh Kumar for motivating and supporting me throughout my research journey. I am truly grateful for their insightful advice, patience, and encouragement, which have played a pivotal role in shaping both my academic and personal growth. I am thankful and extend my feelings towards my colleagues and friends Dr. Vishal Jain, Dr. Rajeev Saini, Dr. Pankaj Batra, Dhruv, Roli, Bhawna, Kavita, Monika for their consistent support in this journey.

I am grateful to my brother and sister who stands by me at every part of my journey. I extend my heartfelt gratitude to my beloved parents for their unconditional love, unwavering encouragement, and constant blessings. They have been a guiding force throughout my life, and I have always strived to live up to their expectations. They constantly provided unwavering support, which allowed me to fully focus on my

research work. Lastly, I would like to thanks all who supported me, guiding me in this journey.

Shikha Singhal

2K20/PHDEC/511

Department of Electronics and Communication Engineering

Delhi   Technological   University

Delhi-110042, India

ABSTRACT

Cardiovascular health-related problem is a rapidly increasing integrated field concerning the processing and fetching the information from cardiovascular systems for early detection and treatment of cardiovascular diseases. Artificial Intelligence (AI) techniques, especially machine and deep learning techniques are more impactful and powerful tools for upgrading the capabilities of an application, and they have been applied to medical data for analysis and disease detection purposes. The work represents a comprehensive view of AI-based computational modelling with the abilities of powerful AI techniques that can play a crucial role in developing smart and enhanced systems in a real-world application. It consists of different techniques that are imposed over distinct ECG signals to evaluate the cardiovascular disease. It outlines the broad overview of AI-based modelling that can be utilized in various application domains. An electrocardiogram (ECG) plays a major role in biomedical applications to record the heartbeat activity. Regular monitoring of ECG through wearable devices like the band, watches, etc. can be done for early detection of cardiovascular diseases. The competency of each method discussed is related to ECG classification approaches that have been compared in terms of some parameters like accuracy, sensitivity, specificity, positive predictivity, and F1-score.

The noise affects the ECG signal which may deteriorate the features of the respective signal that leads to improper treatment. De-noising has been done by pre-processing of the signal, which enables the prediction of the heart condition. Key morphological and statistical features are then extracted and used to train machine learning models for accurate classification of various arrhythmia types, such as atrial fibrillation, ventricular tachycardia, and premature contractions. The efficiency of ECG classification with different computational methods was evaluated with the executed algorithms by using different available databases. The challenges of existing techniques to analyse the ECG signal for the classification and detection of arrhythmia are summarized. The work demonstrates high accuracy, sensitivity, and specificity, highlighting its potential in automated cardiac monitoring systems. The findings

underscore the effectiveness of integrating ECG signal analysis with intelligent classification models, offering a reliable tool for early detection and management of arrhythmias in clinical and remote healthcare settings.

Here, arrhythmia detection and classification have been addressed through the integration of signal processing and time–frequency analysis techniques across different datasets. For segmentation and pre-processing of time-domain signal, a Group Sparse Mode Decomposition (GSMD) technique is employed to extract intrinsic mode functions, enabling detailed representation of ECG signals in terms of frequency and bandwidth. The noise and artefact present in ECG signal affect the signal in every aspect whether it is frequency, peak location, existence of ECG peaks etc. To eliminate the noise and artifacts present, a high resolution, Superlet Transform is applied, offering superior localization of transient features is necessary for identifying arrhythmic patterns. Additionally, Dynamic Mode Decomposition (DMD) is utilized to decompose ECG signals into distinct modes, capturing dynamic behaviors that support accurate arrhythmia classification. It is further applied to real-time ECG dataset to validate the model efficiency over arrhythmia detection. When integrated with machine learning classifiers, the features derived from DMD contribute to robust and accurate real-time arrhythmia classification, demonstrating its potential for practical deployment in clinical and wearable health monitoring systems. Together, these methods provide a comprehensive framework that significantly improves the detection and characterization of arrhythmias, contributing to more reliable and effective diagnostic tools.

To ensure accurate localization of cardiac events, R-peak detection is carried out using Parallel Cluster Wavelet Analysis (PCWA). This method leverages the multi-resolution capability of wavelets along with unsupervised clustering to identify sharp variations in ECG signals that correspond to R-peaks. By operating across multiple frequency bands simultaneously, PCWA enhances the detection of peaks even in the presence of baseline wander, muscle artifacts, and noise.

TABLE OF CONTENTS

LIST OF TABLES

xii

xiii

LIST OF FIGURES

List of Algorithms

LIST OF SYMBOLS AND ABBREVIATIONS

ANN	Artificial neural network
Adaboost	Adaptive Boosting
AFL	Atrial Flutter
APB	Atrial Premature Beat
BaROA	Bat-Rider optimization algorithm
BBNN	Block-Based Neural Network
BLSTM	Bidirectional Long Short Term Memory
CCDD	Chinese Cardiovascular Disease Database
CEEMD	Complete Ensemble Empirical Mode Decomposition
cECG	Capacitive ECG
CHF	Congestive Heart Failure
CVDs	Cardiovascular disease
CPSC	China Physiological Challenge
CBCTA	Chopper-Based Continuous-Time Amplifier
CNN	Convolutional neural network
CRNN	Convolutional and Recurrent Neural Network
CUVT DB	Creighton University Ventricular Tachyarrhythmia Database
CQNSGT	Constant-Q Non-Stationary Gabor Transform
DBM	Deep Boltzmann Machine
DFOD	Digital Fractional Order Differentiator
DNN	Deep Neural Network
DWT	Discrete Wavelet Transform
ECG	Electrocardiogram
EMCA	Expectation-Maximization Clustering Algorithm
EMG noise	Electromyographic noise
EMD	Empirical Mode Decomposition
FCResNet	Fast Compression Residual CNN
FrFT	Fractional Fourier Transform
FVNB	Fusion of Ventricular and Normal Beat

GAF	Gramian Angular Field
GAN	Generative Adversarial Network
GCNN	Generic CNN
Grad-CAM	Gradient-Weighted Class Activation Mapping
GRU	Gated Recurrent Unit
GTR1DA	Generalized Tensor Rank One Discriminant Analysis
HA-ResNet	Hidden Attention Residual Network
HIT	Homeomorphically Irreducible Tree
HOS	Higher Order Statistics
HPF	High Pass Filter
HR-WPD	High-Resolution Wavelet Packet
HPSDM	High Pass Sigma-Delta Modulator
ICA	Independent Component Analysis
IVR	Idioventricular Rhythm
LBBB	Left Bundle Branch Block
LC-CNN	Lightweight Custom Convolutional Neural Network
LPF	Low pass Filter
MCC value	Matthews Correlation Coefficient Value
MECG	Maternal ECG
MFF	Multimodal Feature Fusion
MIT-BIH Arrhythmia DB	Massachusetts Institute of Technology-Beth Israel Hospital Arrhythmia database
MIT-BIH NST	MIT-BIH Noise Stress Test
MIAT	Mixup Asymmetric Tri-training
MIF	Multimodal Image Fusion
MLP	Multilayer Perceptron
MOWPT	Maximal Overlap Wavelet Packet Transform
MRFO	Manta ray foraging optimization
NEO-CCNN	Non-linear Energy Operator- Compact 1D Conventional Neural Network

NSTDB	Noise Stress Test Database
PAC	Premature Atrial Contraction
PB	Pacemaker Rhythm
PCA	Principal Component Analysis
PCICC2011	Physionet. PhysioNet/Computing in Cardiology Challenge 2011
PLI	Powerline Interference
PSO	Particle Swarm Optimization
PTBDB	Physikalisch-Technische Bundesanstalt diagnostic 12-lead ECG database
PVC	Premature Ventricular Contraction
QDA	Quadratic Discriminant Analysis
RBBB	Right Bundle Branch Block
RMSE	Root Mean Square Error
RRHOS	RR intervals and Higher-Order Statistics
SDGs	Sustainable Development Goals
SA node	Sinoatrial node
SBCX	Symbolic Baseline-Corrected Approximation
SC-FRD	Self-calibrating fetal R-peak detection
SDAE	Stacked Denoising Autoencoders
SDHB	Second Degree Heart Block
Self-ONNs	Self-Organised Operational Neural Networks
STA-CRNN	Spatio-temporal Attention Based Convolutional Recurrent Neural Network
ST-Res U-net	Spatio-temporal Residual U-net;
SUVT DB	Supraventricular Database
SVEB	Supraventricular Ectopic Beat
SVM	Support vector machine
SVTA	Supraventricular Tachyarrhythmia
SWT	Stationary Wavelet Transform

u-MDFA	Unidirectionally processed multifractal detrended fluctuation analysis
VB	Ventricular Bigeminy
VEB	Ventricular Ectopic Beat
VMD	Variational Mode Decomposition
Vtri	Ventricular Trigeminy
WPW	Pre-excitation

CHAPTER 1

INTRODUCTION

In the last few decades, cardiovascular diseases (CVDs) are the major cause of death and fatality in the world [1] [2], depicted in Fig 1.1. For processing the encrypted signals, more attention has been given to the development of various tools in the last few years [3]. Approximately, 17.9 million people died from CVDs every year globally which represents 35% of total global deaths [4]. Early detection and diagnosis of CVDs are one of the leading research areas in today's world.
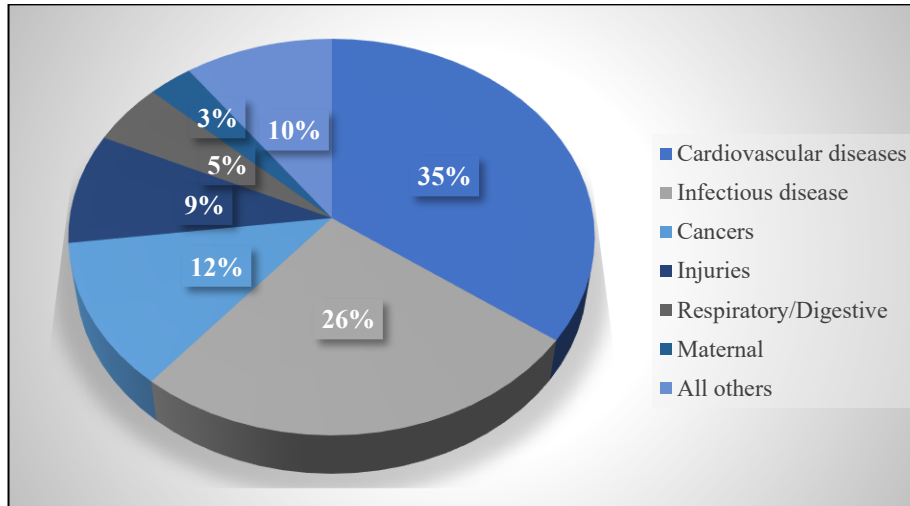
Fig 1.1 The leading global cause of fatality [1]

As an important endless disease, CVD can be caused by the accumulative effects of tobacco usage, deleterious diet, and inadequate physical activities that degrade the overall health status. The regular monitoring of heart rate is the key factor to analyse the cardiovascular health status of an individual. However, some wearable devices, such as bands and watches, can be implemented to avoid any calamity at an early stage. An electrocardiogram (ECG) has been a significant and unique tool in investigating and recognizing cardiovascular diseases [5]. Any deviation in the heart rate is an indication of some fundamental pathology changes which can be identified by the ECG signal. ECG signal represents the time evolution of the electrical activity of the heart which consists of electrical depolarisation-repolarisation patterns of the heart [6]. By

monitoring the heart rate or rhythm, abnormalities in the functioning of the heart can be identified. Body sensor networks are helpful to diagnose the irregularity in the activity of the heart [7]. In recent years, the analysis of ECG signals has drawn much attention to the automatic detection and diagnosis of heart diseases [8]. There are several advantages of ECG technology for heart rate monitoring, but the major drawback is the noise introduced during ECG signal acquisitions like baseline wander, power line interference, EMG noise, and motion artifacts [9] which degrades the performance of the signal. ECG contributes to the Sustainable Development Goals (SDGs) by advancing healthcare diagnostics, promoting early detection of cardiovascular diseases (CVDs), and supporting health equity. ECG research plays a significant role in strengthening health systems, expanding access to care, and reducing unavoidable deaths, all of which are central for achieving the SDGs, especially SDG 3-Good Health and Well Being.

1.1 Basic principle of ECG

ECG signal measures the electrical activity of the heart and the deviation from the normal one through which the disease can be detected. ECG comprises the depolarisation-repolarisation of cells after the resting membrane potential (RMP) reaches the threshold. When sodium ions (Na+) strike the sinus-atrial (SA) node, the rest membrane potential reaches the threshold and loses the electronegativity after which depolarization occurs. After the completion of depolarization, potassium ions (K+) leave the cell area, and calcium (Ca+) ions reach the cell area. The process continues and after a few cycles, it loses all of its electropositivity through potassium (K+) ions and the cell attains electronegativity again. This process represents repolarization [10]. During the depolarization process, all the cells get depolarised in the atrium and a total vector of the electromagnetic force is directed towards the left and downward near the ventricle. As the atria myocardium is thin and does not comprise any specialized conduction system, hence, the generation of the vector is small and directed with moderate velocity towards the ventricle. Now, depolarization occurs in the ventricular area through the atrial ventricular (AV) node which is a slow conductor. Once it enters the ventricular area through the AV node, conduction takes

2

place very fast due to Purkinje fibers and depolarization occurs. After depolarization of the ventricular area, repolarisation occurs in the next step. This makes the complete process of depolarisation and repolarisation. The overall process of depolarisation and repolarisation is termed as action potential. The ECG waveform along with different segments and intervals is shown in Fig 1.2.
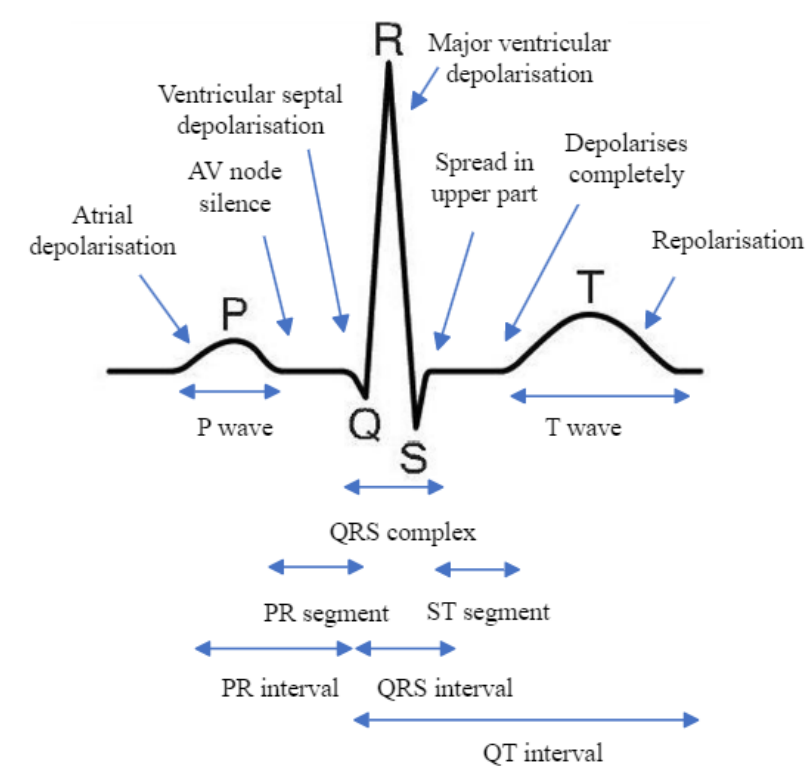
Fig 1.2 Representation of different segments and intervals of ECG signal

Table 1.1 summarizes the range of amplitude, frequency, and duration of different ECG waves. The duration of different intervals of ECG waveform is reported in Table 1.2. ECG leads are split into bipolar limb leads and unipolar leads. The twelve leads of the ECG recorder represent twelve electrical views of the heart from twelve different angles. The leads of the ECG recorder are depicted in Fig 1.3. The conventional 12-lead procedure involves connecting ten electrodes to the body: one to each limb and six across the chest. There are six limb leads and six chest leads [10].

Table 1.1 Amplitude, frequency, and duration range of ECG waveform

Features	Amplitude (mV)	Frequency (Hz)	Duration (sec)
P-wave	0.20 - 0.25	0.7-8	0.08 – 0.10
R-wave	1.40 - 1.60	-	-
Q-wave	0.20 - 0.40	10-50	0.07 – 0.11
T-wave	0.10 - 0.50	1-8	0.12 – 0.18
QRS-complex	-	10- 40	0.08 – 0.10

Table 1.2 Different intervals of ECG signal

Features	Duration (sec)
PR-interval	0.12 – 0.22
QT-interval	0.35 – 0.44
ST-interval	0.05 – 0.15
QRS-interval	0.09 – 0.10
RR-interval	0.6 – 1.2
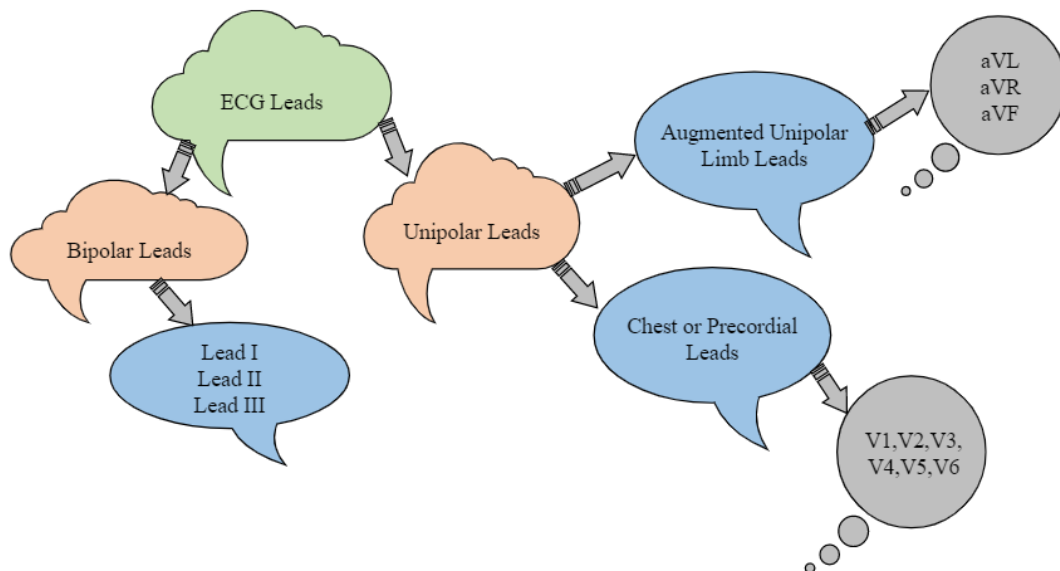
Fig 1.3 Representation of ECG leads of 12-lead ECG recorder

The six limb leads look at the heart in a vertical plane and are obtained from three electrodes attached to the right arm, left arm, and left leg. The electrode on the right

leg is an earth electrode. The measurement of the voltage requires two poles: negative & positive. The negative pole is used as zero references. Limb leads I, II, and III are bipolar as they measure the electric potential between two of the three limb electrodes. Leads aVR, aVL, and aVF are unipolar leads. They use one limb electrode as the positive pole & take the average of inputs from the other two as the zero references. Hence, aVR looks at the upper right side of the heart; aVL looks at the upper left side of the heart, and aVF looks at the inferior wall of the heart. From twelve leads, the magnitude of the heart's electrical potential can be measured and recorded over some time. The details about lead placement are reported in Table 1.3. The positioning of different bipolar, unipolar, and chest leads is shown in Fig 1.4.

Table 1.3 Summary of the placement of ECG leads [10]

Types of leads	Leads	Placement of leads
Bipolar leads	Lead I	LA – RA (left arm-right arm) (between the left arm and right arm)
	Lead II	LL – RA (left leg-right arm) (between left leg and right arm)
	Lead III	LL – LA (left leg-left arm) (between left leg and left arm)
Unipolar leads	Lead aVR (right arm)	RA (+) to [LA & LF] (-) (Rightward)
	Lead aVL (left arm)	LA (+) to [RA & LF] (-) (Leftward)
	Lead aVF (left leg)	LF (+) to [RA & LA] (-) (Inferior)
Unipolar chest leads or precordial leads	V1, V2, V3, V4, V5, V6	Along the horizontal axis
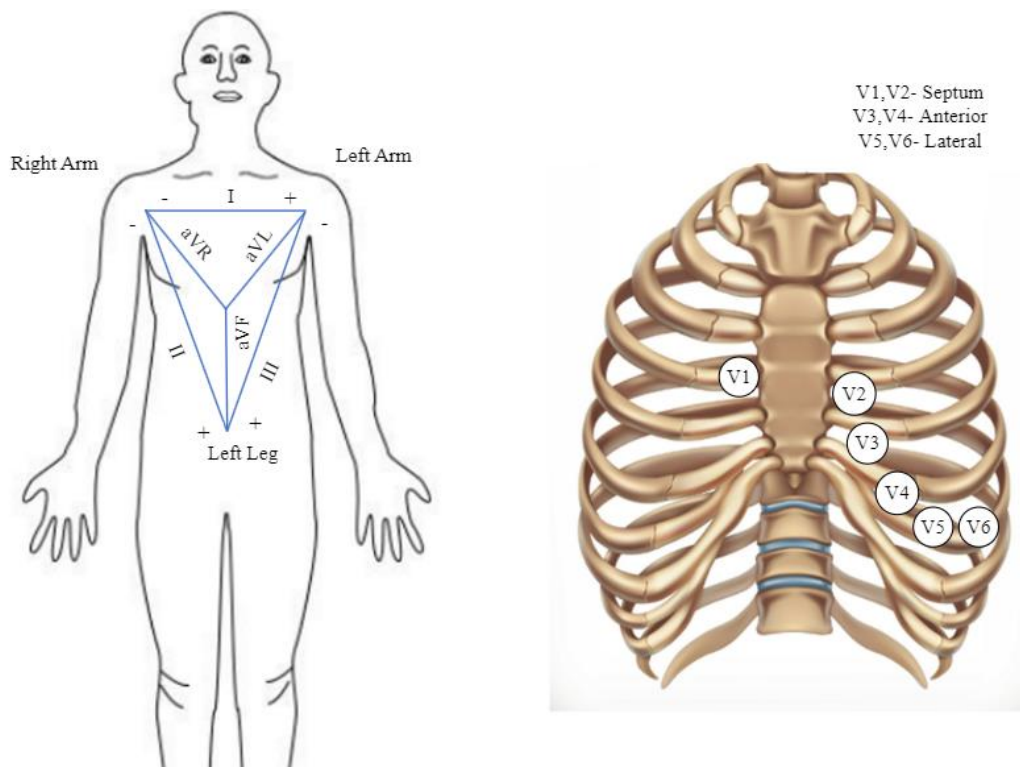
Fig 1.4 Positions for the placement of unipolar limb leads, bipolar limb leads, and precordial leads.

Chest leads are unipolar leads and are used to determine the potential difference between the positive electrode and virtual electrode. V1 and V2 are oriented over the right side of the heart but they are sensitive to septal electrical activity of the heart. Functionally, V1 and V2 are septal leads. V3 and V4 are oriented over the septum and are sensitive to anterior myocardial infarction. V5 and V6 are positioned at the left that are sensitive to major ventricular depolarisation. If infarction occurs in (V1, V2, V3, V4) and (V3, V4, V5, V6) are referred to as anteroseptal leads and anterolateral leads, respectively [10].

1.1.1 Heart Rate Estimation Using ECG

The average number of times a heart beats per minute (bpm) represents the heart rate. The deviation in heart rate from the normal range shows cardiac arrhythmia [11]. Arrhythmia is a condition where heartbeats show an irregular pattern. The normal heart rate is about 60-80 bpm. The heart rate lower than 60 bpm indicates a disorder known

as bradycardia. During athletic activity, the instantaneous heart rate can reach up to 200 bpm which exhibits a disorder named tachycardia [12]. The classification of different types of arrhythmias based on heart rate is listed in Table 1.4.

Table 1.4 Heart rate relationship with different types of arrhythmias [12]

Range of Heart rate (bpm)	Types of Arrhythmias
>350	Atrial Fibrillation
250-350	Atrial Flutter
150-250	Paroxysmal tachyarrhythmia
100-150	Simple tachyarrhythmia
40-60	Mild bradyarrhythmia
20-40	Moderate bradyarrhythmia
0-20	Severe bradyarrhythmia

Arrhythmia which originates in the sinus and atria is classified into a different category. Sinus Arrhythmia is divided into physiological sinus arrhythmia, sinus tachycardia, and sinus bradycardia. Physiological sinus arrhythmia shows the inspiration and expiration phase results in different RR-interval [13]. During inspiration, RR-interval decreases as heart rate increases due to vagal inhibitory action, and RR-interval increases during expiration by vagal stimulatory action. In Sinus tachycardia overstimulation is done on the Sinoatrial (SA) node that increases the heart rate, occurs due to fever, more exercise, etc. Sinus bradycardia occurs in athletes, patients with hyperthermia, jaundice, etc. which slow down the activity of an SA node. SA node initially works well but later it slows down which is termed tachybradysyndrome or sick sinus syndrome [13]. Whereas, atrial tachyarrhythmia is split into atrial tachycardia, atrial flutter, and atrial fibrillation. In Atrial tachycardia, multiple P-waves followed by one QRS-complex show ventricular activity. A very rapid and fast rhythm appears in atrial flutter. In atrial fibrillation, directed vectors are not synchronized in the atrium due to which there is no electrical vector in the atrial area. Different stages of ECG classification are shown in Fig 1.5.

1.2 Different types of noise present in ECG signal

(a) **Power line Interference (PLI):** It is the ordinary noise in ECG signal caused by inductive coupling between the power lines and the electronics of ECG recording equipment. PLI can reach up to 50% of the ECG's peak-to-peak amplitude. Its frequency is typically $60\ Hz$ and its harmonics (or $50 \pm 0.2\ Hz$ in certain datasets). The amplitude and frequency of signal varies with PLI. The bandwidth level of this noise lies below $1\ Hz$.

(b) **Electrode Contact Noise:** It is a sporadic type of noise with an amplitude that can reach the maximum output of the recorder [9]. It occurs when the contact between the skin and the electrodes is disrupted, resulting in transient interference lasting about one second. This disruption can be permanent or intermittent, often caused by a loose electrode making or losing contact with the skin due to vibration or movement. The primary effect of this noise is a baseline shift that gradually returns to the original value in an exponential manner.

(c) **Baseline Wander or Baseline shift:** It is a low-frequency noise within the range of $0.15 - 0.3\ Hz$, with an amplitude reaching up to 15% of the ECG's peak-to-peak amplitude. This noise is primarily caused by the subject's respiration, which forces shifts in the ECG signal's baseline. The extent of baseline wandering increases with higher breathing rates. Factors such as skin impedance, the subject's movement, electrode characteristics, and electrolyte properties also affect the amplitude and duration of this baseline shift.

(d) **Motion Artifacts:** It occurs due to electrode movement on the skin caused by the subject's physical activity. This movement alters the skin-electrode impedance, leading to variations in the ECG signal's baseline. The amplitude of motion artifacts can be as high as 500% of the ECG's peak-to-peak amplitude, lasting for $100 - 500\ ms$. These artifacts cause transient changes in the baseline and, along with baseline wander, can distort the low-frequency components and the ST-segment of the ECG signal. Inaccurate ST-segment generates erroneous prediction of several diseases like myocarditis, infarction, ischemia etc.
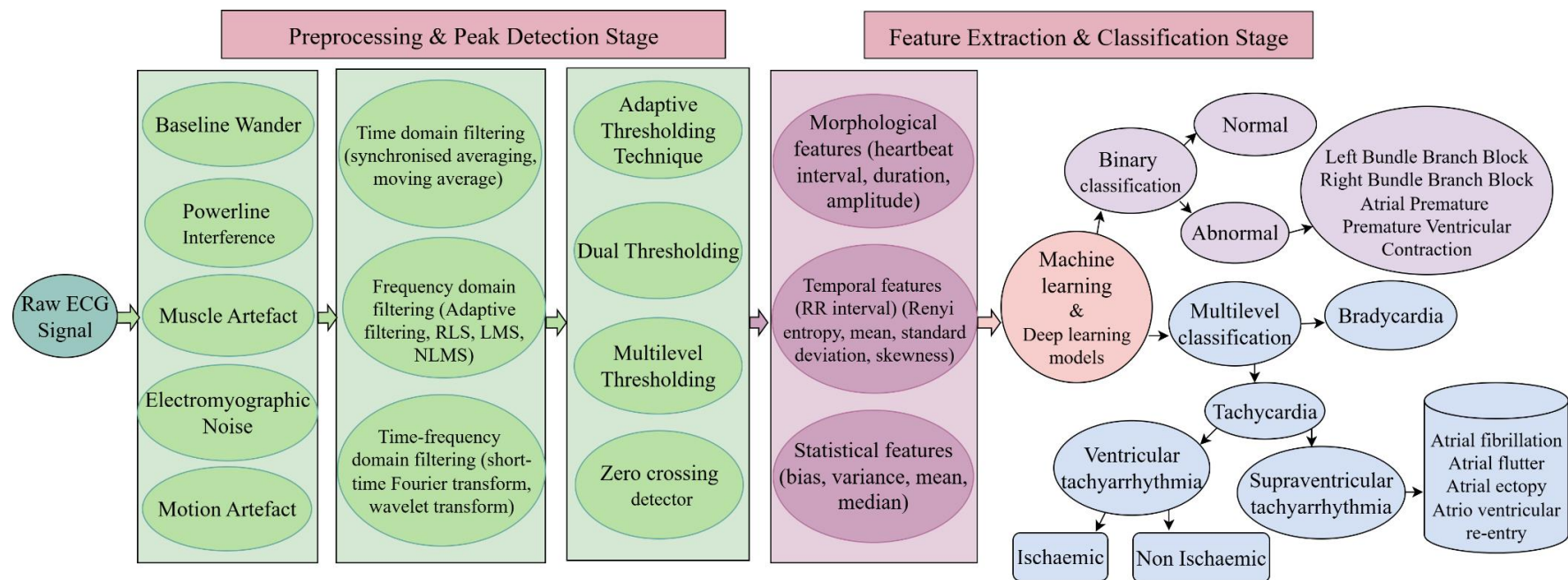
Fig 1.5 Block diagram representation of different stages in the classification of ECG signal

(e) **Electromyographic (EMG) noise:** It arises from muscle contractions, producing potentials in the millivolt range. This noise lasts approximately $50\ ms$ and includes frequency components spanning 0-10 KHz. Its average amplitude is about 10% of peak-to-peak ECG signal amplitude. EMG noise overlaps the ECG signal within frequency range of $0.01 - 0.1\ KHz$, making it challenging to differentiate between the two signals [9]. Discarding EMG noise without creating interference in the features of ECG signal is complicated.

(f) **Instrumentation Noise:** It is generated by irregular usage of electronic components utilised to capture ECG signals. An illustration of instrumentation noise is the amplitude saturation of an ECG signal caused by irregular biasing of an input amplifier, aids to unsuitable recording of ECG signal.

Table 1.5 Representation of ECG noise, its causes and features.

Noise	Cause	Features
Power line Interference (PLI)	Due to inductive coupling between powerlines	Freq: 60 Hz Bandwidth: <1 Hz
Electrode Contact Noise	Interference between skin and electrodes	Freq: Below 100 Hz
Baseline Wander	Breathing/ Respiration of the subject	Freq: low, below 0.5 Hz
Motion Artifacts	Variation of impedance due to movement of skin-electrode	Freq: Variable, low (<5 Hz) Duration: 100- 500 ms
Electromyographic (EMG) noise	Due to muscle contraction	Freq: Broad, $0.01 - 0.1\ KHz$ Duration: 50 ms
Instrumentation noise	Improper use of electronic components	-
Electrosurgical Noise	Due to medical apparatus and requirements	Freq: 0.1 to $1\ MHz$ Duration: 1-10 sec

(g) **Electrosurgical Noise:** It is generated by the presence of medical apparatus in the patient monitoring surroundings. This noise is characterized as a high-amplitude sinusoidal signal with frequencies ranging from 0.1 to 1 MHz and a duration of $1 - 10$ seconds. Its amplitude is approximately 200% of the ECG signal's peak-to-peak amplitude. The distinct noise associated with ECG signal along with features are represented in Table 1.5.

1.3 Challenges and Limitations

Cardiovascular disease (CVD) is one of the main causes of death all over the world. Various factors like diabetes, blood pressure, hypertension, and others degrade the functioning of the heart causing severe conditions resulting in death. Due to insufficient monitoring tools, the death rate due to cardiovascular disease increases very rapidly. Early detection and monitoring of the abnormality in the heart activity are helpful to prevent CVD. With regular checkups & treatment of heart-related problems, several diseases can be prevented by ECG diagnosis. There are various interferences in the acquisition process of ECG signals that may lead to the bad quality of the collected ECG signals. The major challenges while detecting the disease using ECG signals are as follows:

1) **Artifacts removal in ECG signals**: One of the key challenges is to eliminate the artifacts present in ECG signal. The accuracy of the system suffers due to several artifacts which increase the computational complexity and correspondingly reduce the performance. Analog filters are not efficient to filter out the unwanted artifacts from ECG signals. Due to some limitations, digital filters are more flexible than analog filters for denoising purposes [14]. It has been observed that various researchers implemented different filters like low pass filter (LPF), high pass filter (HPF), band pass filter (BPF), and notch filter for artifact removal. LPF [15] performs better as it removes all high-frequency noise like Powerline Interference (PLI), and Electromyographic noise (EMG) but also affects the QRS complex and attenuates the ECG characteristics. To overcome this, researchers prefer HPF and BPF to eliminate artifacts like EMG, PLI, and Baseline wander. Various algorithms are implemented to

design the adaptive filter like least mean square (LMS), recursive least square (RLS), and normalized least mean square (NLMS). The overall combined time–frequency domain approach showed better results for denoising the signal.

2) **QRS Complex detection**: Another challenge is the detection of the QRS complex as it shows cardiac dysfunction due to multiple premature QRS complexes which reflects the complexity of the detection process. Several thresholding techniques can be used to detect QRS complex but in all techniques, the adaptive threshold technique performs better which increases the probability of detecting QRS complex. Artificial neural networks are also useful and helpful in detecting QRS complex. One more important factor is the selection of sampling frequency. An appropriate selection of sampling frequency improves the accuracy of the detection algorithm of the QRS complex [16]. If the sampling frequency is low, produces an error due to the superimposition of high-frequency components on the low-frequency components.

3) **Real-time, non-intrusive approach for monitoring heart conditions**: Another key challenge is to develop an unobtrusive method to monitor heart conditions with physical activities. Heart rate can be calculated through wearable devices like bands or watches but the accuracy of wearable devices can be suffered through motion artifacts [17]. To address this problem, numerous solutions have been executed with advanced signal processing algorithms like adaptive noise cancellation methods, but it is still an obstruction to overcome with this artifact. Unobtrusive monitoring devices can be implemented in different ways, by inserting the wearable devices or sensors in different accessories, or by fixing the sensors in household objects like chairs, tables or furniture, etc.

1.4 Problem Statement

The challenges involved in arrhythmia detection and classification motivate to develop efficient algorithms to fulfil the purpose of developing robust detection techniques. In order to achieve this, the time-efficient and early detection techniques are designed which aids to classifying the disease accurately. The study worked over different features of ECG signal and also transforms the ECG signal into time-frequency pattern for better resolution which helps in recognising the disease using neural networks. The

ECG peak detection is also performed using wavelet analysis and thresholding techniques.

1.4.1 Basic Process of ECG Signal Analysis and Classification

ECG monitoring describes a set of common processes as data acquisition, pre-processing, feature extraction, and classification as shown in Fig 1.6. Data acquisition with wired or wireless sensor measures and record the activity of the heart. A high pass sigma-delta modulator is used for acquisition and digitization [7]. ECG signal is required to be pre-processed after data acquisition.
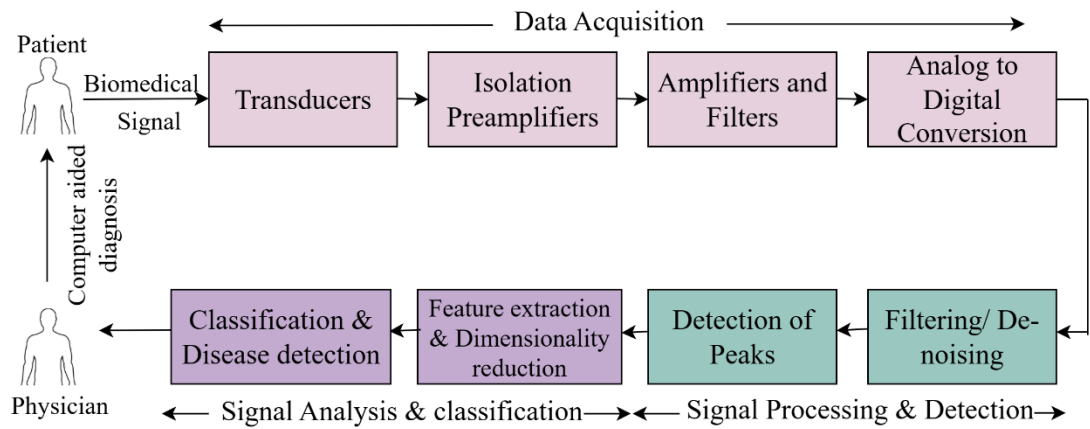
Fig 1.6 Computer aided-diagnosis based on Biomedical signal processing and classification

1.4.1.1 Data Acquisition

It is the process of raw data collection from various sources which is used to validate, train and test a model. The quality of the data directly impact the effectiveness and accuracy of all models. Data acquisition is an important part of overall processing of ant signal. Various sources can be used for data collection like sensors in IoT devices, public datasets etc.

1.4.1.2 Preprocessing

It is essential to remove noise from the ECG signals. In the acquisition stage, different frequency components are used that may produce interference in the signal recording process and may add noise to the ECG signal. This unwanted noise in the signal may corrupt the original information and leads to erroneous data. Filtering methods are implemented to remove the noise from the corrupted ECG signal. Based on the type

of noise present in the signal, an appropriate filter is to be selected. Baseline wander, Power line interference (PLI), Motion artifact, and Electromyographic (EMG) noise are the main noises that have to be suppressed for further processing. Baseline wander is a low-frequency noise in the range of $0.15 - 0.3\ Hz$ caused by respiration that creates a hurdle in the ECG signal. With the increase in breathing rate, baseline wandering increases. Low pass filter, wavelet transformation is implemented to remove the baseline wandering [2], [18], [19] for the signal to be processed. Motion artifact occurs due to the movement of the electrode over the skin resulting from the movement of the patient. EMG noise occurs due to the shrinking of muscles which reflects the potential in the range of millivolts. PLI is due to the interference between a power line and the ECG recording equipment.

For the removal of PLI, data is passed through median filters which is used to remove the QRS complexes and T wave. Finally, a notch filter centered at $60\ Hz$ (or $50\ Hz$) is used to remove the interference [4]. A low pass Butterworth filter can be used as a powerline interference canceller [18]. A wavelet filter is used to remove the Gaussian white noise, wavelet transform is applied to ECG signals for reducing the noise factor [6]. De-noising of ECG signal is performed by non-linear Bayesian filtering [20]. The main motive of pre-processing step is to reduce the noise level from the corrupted ECG signal to enhance the efficiency of the system. The detail of different pre-processing techniques available in the literature is presented in [9]. A comparison is made between several techniques to denoise the corrupted signal. Time-domain, frequency-domain, time–frequency domain (wavelet transform), and others presented in the last few decades are used as denoising techniques [21].

1.4.1.3 Feature Extraction

Feature sets: For any given task, an optimal set of features exists among a large number of features from the feature set [2]. Features are categorized into morphological features, temporal features, time-domain features, frequency-domain features, and non-linear features.

(1) *Morphological features*: Based on the position and amplitude of the P wave, Q wave, R wave, S wave, and T wave that calculate the depths and specifies the area, and power, of any signal. In ECG signal, P, Q, R, S, T peak points, QRS-complex duration, PR-interval, QT-interval, and ST-interval are the features extracted as morphological features.

(2) *Temporal features:* These are the most appropriate heart rate features based on the length of intervals, heart rate variability metrics (variations in RR-interval), QRS duration including the ECG wave acquired from time-domain signals [2], [11].

(3) *Time-domain features:* Statistical features completed the set of features including the maximum and minimum value of RR interval, histogram, variance, mean, standard deviation, and skewness.

(4) *Frequency-domain features:* Includes the wavelet transform coefficient, normalized low and high-frequency power, based on the ECG signal with a window. Spectral characteristics of the window are calculated as center frequency, and spectral frequency [11].

(5) *Non-linear features:* These are the characteristics of heart electrical activity which cannot be accurately described by linear models. It has been calculated by non-linear method like fuzzy entropy, sample entropy, that quantify signal predictability and complexity. The detailed feature of the ECG signal is summarised in Table 1.6.

This step is used to extract useful information from ECG signals for disease classification. All the characteristic waves are identified with their intervals in the feature extraction stage. It has been observed from the previous studies that the wavelet approach is the most favourable feature extraction approach. For the multiresolution analysis of ECG, discrete wavelet transform is employed [19] to attain more accurate results. Some distinctive noise-specific features like short term zero crossing for detection and classification are used [22].

In ECG diagnosis, R-peaks are detected by frequency domain analysis, and time-domain analysis is used to detect other characteristic waves [23]. The most appropriate technique for detection purposes is the thresholding technique in which pre-processed signal is compared with the adaptive threshold to detect the QRS-complex. Some

dimensionality reduction techniques like principal component analysis (PCA) and independent component analysis (ICA) are implemented to extract features from the ECG signal [24]. With these methods, the important part of information can be preserved by projecting to a low-dimensional space. Four temporal features are computed for the classification of each beat of Pre RR-interval, Post RR-interval, Local average RR interval, and Global average RR-interval.

Table 1.6 Summary of the detailed features of ECG signal

Type of Feature	Features
Morphological feature (based on amplitude, power, area)	QRS morphology P and T wave morphology PR-interval QT-interval ST-interval
Temporal feature (based on length of the interval)	Pre RR-interval Post RR-interval Average RR-interval P-wave duration QRS interval T-wave duration
Time-domain feature (based on histogram, mean, variance, standard deviation)	Mean of RR-interval Root mean square (RMS) value of the difference between RR interval
Frequency-domain feature (based on ECG signal with window)	Low frequency components: P wave and T wave High frequency components: QRS complex Spectral parameters: power spectral density
Non-linear features	Fuzzy entropy, sample entropy

1.4.1.4 Classification

For the detection of cardiac arrhythmia, the classification of ECG signals is necessary and it is one of the major challenges that reflect more efforts in this field [25]. Neural networks are used for the classification of ECG signals. It takes the extracted features as an input and the output is the desired result. It works as a computational algorithm based on the biological neural network. ECG Classification process consists of several classifiers which are widely used to improve the accuracy of the detection process. It has been observed from previous studies that various classifiers are used to classify the ECG signal in a modified way. The decision tree [26], linear support vector machine [27], Adaboost, SVM, ANN [28], 2-D CNN [29], SVM-RBF [30], Patient independent classifier [31], Multi-perspective CNN (MPCNN) [32], 1-D CNN, Deep RNN [33] are used to classify the ECG signal with improved accuracy and other specifications.

1.5 Database used for the analysis of ECG signal

The ECG databases play a supreme role in the development and enhancement of algorithms that are helpful in the classification and detection process. For the analysis of ECG signals, several databases are publicly available to scrutinize the initiated algorithms. The database increases the opportunity to produce the outcome in many different forms which will be helpful in real-world domain. The different database has been used by various researchers in the past few years. Details of some important databases are available below.

(a) **Physiobank database** [34] is an important database that consists of a well-characterized biomedical signal that represents 200 ECG signal recordings out of which 160 are to be treated as training data and the other 40 are treated as test data. It is used to characterize the data of patients with health implications such as myocardial infarction, sudden cardiac death, etc.

(b) **Massachusetts Institute of Technology-Beth Israel Hospital Arrhythmia database (MIT-BIH Arrhythmia DB)** [35] is the popular database used for arrhythmia detection which consists of (48-half hours each) ambulatory ECG recording. MIT-BIH dataset consists of 23 records where (inpatients-60%, outpatients-40%), and the rest

25 records show an uncommon but clinically significant arrhythmia. This includes 25 men aged from 32 to 89 years, and 22 women aged from 23 to 89 years. The sampling rate is 360 samples per second per channel is used with a resolution of 11 bits. The publication of the MIT-BIH Arrhythmia database can be regarded as a major achievement in the development of arrhythmia detectors that enhances the performance of the system.

(c) **MIT-BIH Atrial Fibrillation (AF) Database** [36] is an important database that includes 25 long-term ECG recordings with atrial fibrillation. The duration is of 10 hours each for an individual recording. Each signal is sampled at 250 samples per second with 12-bit resolution over a range of $\pm 10mV$.

(d) **Physikalisch-Technische Bundesanstalt diagnostic 12-lead ECG database (PTBDB)** [34] also plays a major role in the detection process of arrhythmia that consists of 549 records from 290 subjects from which 52 are considered healthy records. Each signal is sampled at 1000 samples per second with a resolution of 16 bits over a range of $\pm 16.384\,mV$. A detailed summary of 268 subjects is available, rest detailed summary of 22 subjects is not available.

(e) **The Fantasia database** [37] shows the effective development of detectors which consists of 40 ECG recordings, 20 records from the young generation aged 21 to 34 years, and 20 from elderly people aged 68 to 85 years. The duration of all the recordings is 120 min and the sampling rate is 250 Hz.

(f) **ECG ID** [34] database includes 310 recordings taken from 90 subjects. 44 men and 46 women from various fields are taken for the recordings. The sampling frequency of the ECG signal is 500 Hz with a 12-bit resolution over a range of $\pm 10mV$.

(g) **MIT- BIH SupraVentricular (SUVT)** [38] consists of 78 records of 30 min each sampled at 128 Hz.

(h) **Creighton University Ventricular Tachyarrhythmia Database (CUVT)** [39] includes 35 eight-minute ECG recordings of human subjects who experienced episodes of sustained ventricular tachycardia, ventricular flutter, and ventricular fibrillation. All signals were passed through an active second-order Bessel low-pass filter with a cutoff of 70 Hz, and were digitized at 250 Hz with 12-bit resolution over

a 10V range (10 mV nominal relative to the unamplified signals). Each record contains 127,232 samples (slightly less than 8.5 minutes).

(i) **Long Term AF Database** [40] includes 84 long-term ECG recordings of subjects with paroxysmal or sustained atrial fibrillation (AF). Each record contains two simultaneously recorded ECG signals digitized at 128 Hz with 12-bit resolution over a 20 mV range; record durations vary but are typically 24 to 25 hours.

(j) **MIT-BIH Malignant Ventricular Ectopy Database** [34] consists of 22 records of 30 minutes each sampled at 250 Hz with resolution of 12 bits.

The summary of the available datasets for arrhythmia detection using ECG signal is represented in Table 1.7.

Table 1.7 Summary of available ECG arrhythmia detection databases

Database	Number of subject/Data	Sampling Frequency/Range
Physiobank database [34]	ECG signal records=200 Training set= 160; Test set= 40	Not Reported (NR)
MIT-BIH Arrhythmia DB [35]	Number of records=44 Dataset1= 22 (training) Dataset2= 22 (final performance) Ambulatory ECG recordings=48 (half hour each) BIH database (inpatients-60%; outpatients-40% $=$ 23 recordings) Clinically significant arrhythmias= 25 recordings Men= 25 (aged 32 to 89 years) Women=22 (aged 23 to 89 years)	Sampled at 360 Hz Resolution=11 bits, Range= $\pm 10mV$
MIT-BIH Normal Sinus Rhythm DB [34]	Number of significant arrhythmias= 18 subjects Men= 5, aged 26 to 45 years;	Sampled at 128 Hz.

	Women=13, aged 20 to 50 years Training data= from 1 to 2 hours Test data= ECG from hour 13 to 14	
MIT-BIH AF DB[36]	Atrial Fibrillation records=23	NR
PTBDB [34]	Subjects= 290; Records=549 Healthy controls=52; Myocardial Infarction patients=148	Sampled at 1 kHz Resolution=16 bit Range $=\pm16.384\ mV$.
Fantasia database [37]	Young subjects=20 Elderly subjects=20 Continuous supine resting ECG signals obtained = 120 mins	Sampled at 250 Hz
ECG ID database [34]	Total recordings=5066. ECG recordings=310, from 90 persons. 44 men & 46 women Age=13 to 75 years.	Sampled at 500 Hz Resolution= 12 bit Nominal range= $\pm10\ mV$
PCICC2011 DB [34]	Twelve-lead ECG recording=2000	Sampled at 500 samples per second Resolution=16 bit
MIT-BIH SUVT DB [38]	78 two-lead recordings, 30 mins long. Performance evaluation over first 70 records	Sampled at 128 Hz
CUVT DB [39]	Records- 35 of 8 mins each	Sampled at 250 Hz Resolution=12 bit
The MIT-BIH NST DB [34]	ECG recordings=12 half-hour Noise Half-hour recordings = 3	Sampled at 360 Hz
Incart DB [34]	Incart DB=75 recordings > 175000 annotated beats	Sampled at 257 Hz

ECG dataset was obtained from HCM patients and all subjects, ICD patients [41]	HCM patients: No. of patient=221 Total ECG recordings=754 Total heartbeats= 6488 ICD (control): No. of patient= 541 Total ECG recordings=541 Total heartbeats=4442	NR
1631 3-s ECG segments with clinical rhythm annotations. [42]	Obtained from 298 out-of-hospital cardiac arrest patients.	Sampled at 500 Hz Resolution= 16 bit ECG had a resolution of $1.031\mu V$ per least significant bit.
Chinese Cardiovascular Disease Database (CCDD) [43]	Total records=46729 Total ECG labels= 270 12-lead ECG devices from different hospitals. Short-term ECG records=200,000	Sampled at 500 Hz
CinC 2017 A fib database [44]	Total ECG recordings=8528	Sampled at 300 Hz
Mendeley-II dataset [45]	Total= 45 patients, 17 classes 19 females (age: 23 to 89 years) 26 males (age: 32 to 89 years)	Sampling frequency= 360 Hz

*NR: Not Reported

1.6 Evaluation Parameters

Different parameters are used to evaluate the ECG algorithm presented by various researchers. Evaluation parameters provide a mechanism to compare the various presented algorithms. The value Tp is the true positive value shows that model can correctly predict the positive class, Tn is the true negative value tells that model correctly assumes the true negative class, Fp is the false positive outcome says that the model wrongly predicts the positive class and actually it is negative, Fn is the false

negative value shows that model assumes the wrongly negative class and actually it is positive. The performance of detection is estimated by calculating the parameters like Accuracy (*Acc*), Sensitivity (*Sens*), Specificity (*Spec*), Positive predictivity (*ppv*), F1-score value, Error rate, Geometric-mean, MCC value, and Kappa (*k*) value of the system as defined in Eqs. (1.1) − (1.9).

Accuracy (Acc)*:* It calculates proportion of total correctly classified samples, including both normal and abnormal classes in all samples. It reflects the overall performance metrics, shows the efficiency of the model over distinct classes.

$$Acc(\%) = \frac{(Tp + Tn)}{(Tp + Tn + Fp + Fn)} \times 100 \tag{1.1}$$

Sensitivity (Sens)*:* It is also termed as recall or true positive rate. It is the percentage of true positives that are accurately recognised by the model.

$$Sens(\%) = \frac{Tp}{(Tp + Tn)} \times 100 \tag{1.2}$$

Specificity (Spec)*:* It is an estimation of how accurately the model assumes the true negative values. It shows the percentage of true negatives that are correctly identified by the model.

$$Spec (\%) = \frac{Tn}{(Tp + Fp)} \times 100 \tag{1.3}$$

Precision (prec)/ppv*:* It quantifies how many of the instances predicted as positives are actually correct. It can be defined as the ratio of the exactly categorised positive classes to the total count of positive classes.

$$Positive\ Predictivity\ (ppv) = \frac{Tp}{(Tp + Fp)} \tag{1.4}$$

F1-score (F1-sc)*:* It can be explained by the harmonic mean of the precision and recall. It is a statistical measure of the accuracy of the model.

$$F1 - sc = \frac{(2 \times Sensitivity \times positive\ predictivity)}{Sensitivity + positive\ predictivity} \tag{1.5}$$

Error rate*:* It measures the extent of a model's prediction errors relative to the true values or outcomes.

$$Error\ Rate = \frac{(Fp + Fn)}{Total\ beat} \tag{1.6}$$

G-mean*:* It is the representation of the geometric mean evaluated through the square root of the product of specificity and sensitivity in case of binary classification. In multi-classification, G-mean is defined as the higher root of the product of sensitivity of each class.

$$G - mean = \sqrt[n]{x_1, x_2, x_3, \ldots\ldots x_n} \tag{1.7}$$

where *n* is the total number of values to be experimented and *x* represents the sensitivity of each class.

MCC (Matthews Correlation Coefficient)*:* It is the difference between the actual and estimated values on the same categories (class) which is defines as

$$MCC = \frac{(Tp \times Tn - Fn \times Fp)}{\sqrt{(Tp + Fp)(Fp + Tn)(Tp + Fn)(Fn + Tn)}} \tag{1.8}$$

Cohen's kappa*:* It is a metric used to examine the accurate agreement and casual agreement between two raters in accordance to calculate the effectiveness of a predefined classification model.

$$Kappa(k) = \frac{p_o - p_e}{1 - p_e} \tag{1.9}$$

where p_o and p_e are the actual and chance agreement respectively.

As it concerns with the classification of disease, we may define a confusion metrics also known as an error metrics, which describes the performance of an algorithm. The metrics is segregated into predicted and actual classes in rows and columns. It uses four kinds of results as true positive, true negative, false positive and false negative. By analyzing these values, we can compute key performance metrics like accuracy, precision, recall, specificity, and F1-score, allowing the accurate disease detection on test data.

1.7 Motivation to Arrhythmia detection and classification

The early and accurate detection of disease plays a pivotal role in improving patient outcomes. With the growing availability of biomedical data and the evolution of artificial intelligence, there lies a transformative opportunity to revolutionize how diseases are identified.

Cardiovascular diseases remain a leading cause of mortality worldwide, with arrhythmias posing a significant risk due to their sudden onset and potentially fatal consequences. ECG signals serve as a non-invasive, cost-effective, and widely used diagnostic tool for monitoring heart activity. However, the accurate detection and classification of arrhythmias from ECG data remain challenging due to signal complexity, variability among individuals, and noise interference. The motivation to study arrhythmia detection and classification stems from a strong desire to improve early diagnosis and patient care by developing intelligent systems that can automatically and accurately interpret ECG signals.

Detecting arrhythmias early allows timely intervention, helping prevent serious complications such as stroke, heart failure, or sudden cardiac arrest. Arrhythmias, such as AF, ventricular tachycardia (VT), or bradycardia, can disrupt the heart's normal rhythm and impair its ability to pump blood effectively. If left undiagnosed or untreated, these irregularities can lead to dangerous outcomes. To avoid these outcomes, various neural networks for different forms of ECG signal have implemented for early and accurate disease detection. The performance of disease detection degrades due to the dislocation of ECG peaks from its predefined position, which leads to the vague detection of disease. It is necessary to identify the exact location of ECG peaks present in the signal. In the study, this has been done using thresholding techniques and wavelet analysis.

1.8 Thesis Overview

The thesis consists of six chapters, which are organised as follows:

Chapter 1 includes the brief introduction of ECG with waveform, leads, features, and noise or artifacts present in the ECG signal. It includes the idea about occurrence and causes of arrhythmia, the variability in heart rate defines the stage of arrhythmia. The chapter includes the basics of ECG signal acquisition using different datasets, pre-processing, ECG feature extraction, and ECG classification.

Chapter 2 includes the literature review of ECG R-peak detection, ECG signal preprocessing, and ECG classification. The chapter is divided into traditional and modern methods involved in all three sections. The recent literature plays a pivotal

role in monitoring the overall process of classification. Thereafter, the research gaps have been found out and based on those, the research objectives are made.

Chapter 3 includes the ECG R-peak detection using wavelet scattering transform and parallel cluster wavelet analysis over different datasets. This integrated approach enables precise identification and localization of R-peaks within the ECG signal, which is crucial for accurate and effective detection of cardiac conditions. By utilising the strengths of both techniques, the method enhances the robustness and reliability of R-peak detection, thereby supporting improved disease diagnosis.

Chapter 4 focuses on the early detection and multilevel classification of ECG signals by employing advanced signal processing and transformation techniques. The work begins with group sparse mode decomposition, which segments the signal into its constituent modes in different frequency bands, which help in the deeper study of each frequency band. After which, the high resolution superlet transform is imposed over the respective modes. It evaluates the arrhythmia status using time-frequency pattern which is obtained using high resolution transform. The fractional form of superresolution technique is also imposed over distinct forms of ECG signal for validation.

Chapter 5 includes the real-time monitoring of ECG signals which helps in detecting the disease under different phases of subject. It enables the early diagnosis and timely intervention that reduces the need for frequent hospital visits. ECG signals are captured using wearable devices with electrodes placed on the skin. These devices continuously record the electrical impulses generated by the heart. With this, the dynamic modes are generated using decomposition process which is being validated over real-time ECG dataset.

Chapter 6 includes the conclusion and future scope of arrhythmia detection and classification using ECG signals. The work demonstrates that signal processing techniques, such as Wavelet Scattering Transform (WST), Parallel Cluster Wavelet Analysis (PCWA), Superlet transform, and Dynamic Mode Decomposition (DMD), significantly enhance the extraction of informative features from ECG signals. These features, when operate under machine learning and deep learning models, contribute

to the accurate classification of different arrhythmia types, including atrial fibrillation, ventricular tachycardia, and other rhythm irregularities.

Chapter 2

LITERATURE REVIEW

2.1 Literature Review based on ECG Arrhythmia Detection and Classification

For the accurate detection purpose of ECG signal, preprocessing is the primary and crucial step that is to be implemented to eliminate noise, and other artifacts that can distort significant features. Classification plays a pivotal role in identifying whether an ECG signal represents a normal state or an arrhythmia state. By categorising the ECG signal into specific classes, it enables timely diagnosis and appropriate medical intervention. Different machine learning and deep learning algorithms have been implemented for the proper detection and classification of arrhythmia [46]. The literature review summarizes the work related to preprocessing, ECG peak detection, arrhythmia detection and classification using traditional and modern methodologies.

2.1.1 Review on the basis of ECG peak detection

The QRS complex and R-peak detection in ECG signal is critical task, as the features are linked to cardiac abnormalities, involving ventricular arrhythmias, that can result in sudden cardiac death. The difficulty in R-peak detection is noticed by interference of artifacts, noise, and usage of computational resources. In [47], introduced the complete ensemble empirical mode decomposition (CEEMD) for the detection of QRS complexes and P wave. The method eliminates the filtering step, and focus on the QRS complex locations. It worked on the positive and negative amplitudes of ECG signal and an adaptive P wave search approach to detect the true P wave. The QRS detection method shown the *Sens*, *ppv*, and an error rate of 99.96%, 99.9%, and 0.13% over MIT-BIH Arrhythmia DB and QT database. The P wave detection reflects *Sens*, *ppv* of 99.96%, 99.47%, and mean error is less than or equal to one sample ($4\,ms$) on average. In [48], presented a QRS detection method by applying a threshold with noise suppression. Noise suppression is performed by band

pass filter stage followed by a non-linear stage on the basis of particle interaction inside an underdamped monostable potential well. The non-linear stage uses the stochastic resonance, and attained an *F1-sc* that ranges from 98.87% to 99.99% over MIT-BIH Arrhythmia DB, QT DB, European ST-T, and MIT-BIH NST DB. Zou et al. [49], introduced an ASIC design for R-peak detection. The design leads to reduction in overall system energy by utilising a dual-ping-pong-memory architecture. The techniques of coefficients truncation and resource sharing are used for hardware cost reduction. The compression ratio of 10.3 is achieved over MIT-BIH Arrhythmia DB with a root mean square difference of 0.64% under recoding mode. In [50], Warmerdam et al. presented a multichannel hierarchical probabilistic framework for fetal R-peak detection that combines predictive models of ECG waveform and heart rate. The attained average accuracy over set-A of 2013 Physionet /Computing in Cardiology Challenge DB is 99.6%.

Davies et al. [51], introduced a Deep Matched Filter for R-peak detection in wearable ECG. The filter consists of an encoder stage, partially initialised with ECG template and an R-peak classifier stage. The performance is evaluated using leave-one-subject-out cross-validation over 36 subjects with an age range of 18 to 75 years. The model achieved a median *recall* and *prec* of 94.9% and 91.2% respectively. In [52], Deepu et al. introduced an ECG processing technique for joint data compression and QRS detection in wireless wearable sensor. The main aim is to lower the average complexity per task by sharing the computational load among several signal processing tasks needed for wearable devices. Based on the adaptive linear data prediction scheme, the attained compression ratio is 2.286 times the existing technique. The QRS detection algorithm achieved the *Sens* and *ppv* of 99.64% and 99.81% respectively over MIT-BIH Arrhythmia DB. In [53], introduced NEO-CCNN, a robust arrhythmia classification model designed for wearable devices and compatible for implementation over basic microcontrollers. The model precisely identifies the R-peaks utilising an adaptive time-dependent thresholding technique. The model employs an optimized, compact 1D-CNN network with 9701 parameters. To sustain for R-peak location error (RLE), a QRS complex augmentation method is initiated.

The model detects more than 99.79% of R-peaks with RLE of 7.94 ms for MIT-BIH Arrhythmia DB.

In [54], presented a dual self-calibrating system based on a spectral attention kernel independent component analysis (SA-KICA) module and a self-calibrating fetal R-peak detection (SC-FRD) module. The SC-FRD is initiated to use the interior peak information and self-calibrating strategy, includes variance-based fetal R-peak seed selection. A morphological-based channel selector is designed to select the optimal maternal ECG (MECG). The fetal R-peak detection performance enhances after removing MECG. In [55], introduced an adaptive threshold R-peak detection technique on the basis of Brown exponential smoothing model. The model optimizes the smoothing coefficients utilising relative error least square method, therefore, the enhanced threshold is uniform with R-peak detection. The model attained the *prec*, *recall*, and *F1-sc* of 99.6%, 99.7%, and 99.65% respectively over self-maintained ECG dataset.

In [56], introduced a BayeSlope method which is an unsupervised scheme, Bayesian filtering, and random normalisation to upgrade and accurate detection of R-peaks in ECG signal. To avoid the computational complexity introduced by BayeSlope method, introduced an adaptive online design that adjust the complexity according to the embedded systems. The online method attained an *F1-sc* of 99% over five distinct exercise intensities, with energy consumption of 1.55 ± 0.54 mJ. In [57], presented a methodology for R-peak and T-peak detection utilising hierarchical clustering and DWT from ECG signal. T-peaks are determined on the basis of Modulus-Maxima Analysis (MMA) of DWT coefficients. The R-peak detector attained the *Sens, ppv*, and *Acc* of 99.89%, 99.97%, and 99.83% respectively over MIT-BIH Arrhythmia DB. The T-peak detection achieved the *Sens*, and *ppv* of 99.91% and 99.38% respectively.

Peng et al. [58], suggested an enhanced U-net model, named ST-Res U-net for R-peak detection. It consists of three steps, including data preprocessing, ST-Res U-net based on spatiotemporal feature extraction, and a threshold mechanism for locating the R-peaks. The experiment is performed over MIT-BIH Arrhythmia DB and CPSC2019

DB, reflects the detection error rate (DER) of 0.37% and 15.24% respectively. Kumar et al. [59], introduced a combined model on the basis of biorthogonal wavelet transform and run-length encoding for QRS complex detection. Three LPFs with HPF is utilised for biorthogonal wavelet transform. The hardware cost is reduced by 50% using linear phase structure of LPF and HPF. The location of R-peak is identified by comparing the denoised ECG signal with threshold value. The DER of 0.002 is achieved over MIT-BIH Arrhythmia DB. In [60], introduced two deep learning models based on muti-dilated convolutional blocks. First model consists of convolutional blocks and Squeeze-and-Excitation networks and second model (CRNN) includes a hybrid convolutional and recurrent neural network. A five-fold cross validation is performed and achieved an *F1-sc* of 0.9994 and 0.9995 for CNN model and CRNN respectively, over MIT-BIH Arrhythmia DB.

Gabbouj et al. [61], introduced 1D-self organised operational neural networks (Self-ONNs) with generative neurons for R-peak detection. It has an ability of self-organisation since every generative neuron has the ability to create the optimal operator during training. The method achieved an *F1-sc*, *Sens*, and *ppv* of 99.10%, 99.79%, and 98.42% respectively over CPSC dataset for R-peak detection in ECG signal. Jia et al. [62] introduced a high-resolution wavelet packet (HR-WPD) and CNN. HR-WPD splits the ECG signal into multiple signals with distinct frequency bands to provide QRS features. Then, the decomposed signals are fed to CNN for QRS detection. A time-attention module is added to CNN to enhance the robustness. A variable threshold is employed to locate the QRS. The DER is 5.61%, 4.55%, and 0.21% over TELE ECG DB, NSTDB, and MIT-BIH Arrhythmia DB. Varghees et al. [63] introduced a variational mode decomposition, mode selection, first-order derivative, Hilbert transform, and positive zero crossing point for R-peak detection and ECG denoising. Optimized features are selected to eliminate the low and high frequency noises. The average *Sens* and *ppv* of 99.77% and 99.91% is achieved over MIT-BIH Arrhythmia DB.

In [64], introduced fractional Fourier transform with principal component analysis for detecting R-peaks in the presence of different types of noise. The attained *Sens*, *ppv*,

and *Acc* over MIT-BIH Arrhythmia DB is 99.93%, 99.95%, and 99.88% respectively. In [65], Tueche introduced an embedded model on the basis of shape and appearance of the signal. It fetches the information like shape of QRS complex, its slope, and duration between two adjacent QRS complexes. Initially, an adaptive thresholding is implemented to detect the R-peak of ECG signal. Then, the Q and S positions are detected by further tests. The model attained an average *F1-sc* of 99.67%, 99.73%, and 99.83% over MIT-BIH Arrhythmia DB, Pacemaker Rhythm, and NSR DB respectively. The average run time of $16.23\mu s$ per sample is recorded. Habib et al. [66], introduced a domain-agnostic automated post-processing model where a specific RNN based model learns necessary post-processing from the produced outcome from QRS segmenting deep learning model. The RNN based post-processing proves robust over various domain-specific post-processing techniques.

In [67], Nayak et al. introduced an infinite impulse response type digital fractional order differentiator (DFOD) based ECG pre-processor to identify QRS complexes. Initially, an Antlion optimization optimizer is applied to resolve the DFOD design issue. Then, DFOD is applied at pre-processing stage of a threshold independent R-peak detection technique. The attained root mean square error (RMSME) and the average group delay metrics of DFOD is $-38.17db$ and 0.04 samples, respectively. Zahid et al. [68] suggested a 1D-CNN integrated with verification model to minimize the count of false alarms. The structure consisting of encoder-decoder block with sample-wise classification layer to model the 1D segmentation map of R-peaks from ECG signal. The method attained an *F1-sc*, *recall*, and *prec* of 99.30%, 99.69%, and 98.91% respectively over CPSC-DB. The introduced method can reduce the false-positives and false-negatives by more than 54% and 82%, respectively.

Yun et al. [69] introduced a stationary wavelet transform (SWT) with separate convolution. The detail coefficient of level 4 decomposition is done by SWT and first derivative from filtered ECGs were utilised for model inputs. The model achieved *F1-sc* of 0.9994, 0.9985, and 0.9999 over MIT-BIH DB, INCART, and QT databases respectively. After pooling the three databases, the *F1-scs* are 0.9993 and 0.9991 for five-fold cross validation and cross-database validation respectively. In [70],

introduced the variable frequency complex demodulation (VFCDM) method for the detection of QRS complex peaks. The method utilised only the frequency components associated with QRS waveforms by VFCDM decomposition. A position-dependent adaptive thresholds are employed to eliminate false peaks. The achieved *Sens, ppv* value, and DER are 99.94%, 99.95%, and 0.11%, respectively over MIT-BIH Arrhythmia DB. The method proves robustness over various datasets named MIMIC III DB, University of Massachusetts atrial fibrillation data, and SCUBA diving in sea water ECG data.

2.1.2 Review on the basis of Traditional methods (Machine Learning Methods)

Zaunseder et al. [2] revealed about ECG classification that an SFFS algorithm is applied with a new criterion function index based on linear discriminants with classifiers linear discriminant analysis (LDA), *k*-nearest neighbour (*k*NN), and multilayer perceptron (MLP) having an *Acc* of 89%. Different classifiers like decision tree, and quadratic discriminant function (QDF) in a hybrid approach with an *Acc* of 86.3% is introduced by Barni et al. [3]. A time-based encoding using the binning approach with LDA as a classifier having *Sens* of 92% is used by Alvarado et al. [4]. Moran et al. [5] presented reservoir computing with logistic regression attained the *Acc* and *Sens* of 98.4% and 84.85% respectively. Banerjee and Mitra [6] revealed the discrete wavelet transform-based decomposition with *Acc*, *Sens*, and *Spec* of 97.6%, 97.3%, and 98.8%, respectively. Wavelet transform is a very effective technique that results in maximum output. Some techniques like high pass sigma-delta modulator (HPSDM) and chopper-based continuous-time amplifier (CBCTA) as biosignal processors with an *Acc* of 97.25% have been recorded by Lee et al. [7].

Huang and Zhang [8] stated the generalized tensor rank one discriminant analysis (GTR1DA) with a support vector machine (SVM) classifier has an *Acc* of 99.8%. Rahman et al. [11] used the cross-validation with random forest (RF), and SVM with a *Spec* of 0.93. Shadmand and Masoufi [18] presented the ANN and block-based neural network (BBNN) with particle swarm optimization (PSO) algorithm having an *Acc* of 97%. A Gaussian mixture model (GMM) with ANN, LDA, and Quadratic

Discriminant Analysis (QDA) with an *Acc* of 78.5% has been initiated by Eftestol et al. [19]. Oster et al. [20] stated the bayesian filtering with SVM as a classifier has a *Sens* of 99%. Satija et al. [22] used complete modified ensemble empirical mode decomposition (CEEMD) with temporal features having an accuracy of 97.38%. Patro and Kumar [23] stated the cascaded filter with ANN for pattern recognition classifier *Acc* of 98.14%. Li et al. [24] used the generic CNN (GCNN) and tuned dedicated CNN (TDCNN) with an *Acc* of 96.89%. The clustering algorithm has been presented with a *Sens* of 88% by Teijeiro et al. [25]. Ayar and Sabamoniri [26] presented the decision tree approach with a genetic algorithm that used the hybrid model with optimal features having an *Acc* of 2 class and 16 class is 86.76% and 77%, respectively. Gaussian Bernoulli deep belief network with SVM as classifier results in the *Acc* of 99.5% and 99.4% in case of supraventricular and ventricular respectively with the MIT-BIH Arrhythmia DB by Sayanta et al. [27].

In [30], the morphological features are extracted from PQRST wave and ECG segment features are extracted using PCA and dynamic time warping (DTW). The classification between normal beats, supraventricular ectopic beats (SVEB), ventricular ectopic beats (VEB), and fusion of ventricular and normal is performed using SVM and attained an *Acc* of 97.8%. In [71], a local deep field is executed for arrhythmia detection and classification. Adam optimizer with symbolic baseline-corrected approximation (SBCX) approach and multi-perspective CNN (MPCNN) as classifier reflected the *Acc* of 96.4% revealed by Niu et al. [32]. In [33], Lynn et al. introduced a deep recurrent neural network (RNNs) based on Gated Recurrent Unit (GRU) in a bidirectional manner achieving an *Acc* of 98.5%. Here, the 1-D CNN approach and RNN with long short-term memory (LSTM) and GRU have been used for classification. The introduced model was evaluated over ECG ID and MIT-BIH Arrhythmia DB with an *Acc* of 98.6% and 98.4%, respectively.

In [72], introduced a new iterative regeneration method for systematic EMG-noise suppression. The idea of the study is to extract the noise with negligible changes in the signal by temporary neglecting the dominant ECG components. Brophy et al. [73] presented a custom loss function which is capable of denoising electrode motion

33

artefact in ECG signal. The loss function is implemented with CNN to reflect enhanced quality of ECG. The introduced method enhances the level of signal-to-noise ratio (SNR) and maintain the R-wave quality. An improvement of 0.5 db in terms of SNR is observed by mean square error loss function. Finally, an enhancement is noticed in heart rate estimation by 25%. In [74], Ghafari suggested a weighted average cardiac vector, evaluated from denoised signals, and utilised it to rebuild lead signals. The method is relevant to all denoising processes to enhance the denoised limb lead values and minimize the error signals. This post processing achieved an aggregated noise reduction of 28.6% and 10.8% in EMD and wavelet transform respectively. Li et al. [75] suggested an improved VMD denoising algorithm to address the limitations of slow parameter selection and poor generalisation inherent in the traditional VMD approach. The method begins by utilising the EMD algorithm to eliminate low-frequency baseline drift noise. It then applies the adaptive particle swarm optimization (APSO) algorithm to improve the parameter pair (K, α) for VMD.

In [76], introduced a sparse optimization method that accounts for the group sparse characteristics of signals and incorporates a low-pass filter to denoise ECG signals while computing the baseline. The method considers the structural features of ECG signals through building upon the classic total variation denoising approach. It involves a band matrix to model the sparse optimization problem and utilised the majorization-minimization (MM) algorithm to address and adjust the convergence issue. Initially, the method is compared with two total variation denoising methods, and after implementation, it reflects the lower RMSE and higher SNR. In [77], Wang et al. presented an adaptive canceller and singular value decomposition (SVD) algorithm, employed over single-lead capacitive ECG (cECG) for noise reduction. The motive of the work is to compute the feasibility of non-contact ECG measurements using capacitive electrodes for clinical diagnosis. The correlation coefficient between processed cECG and the wet ECG were evaluated with and without the QRS complex as performance metrics. The result depicts high correlation coefficient between cECG and wet ECG for both conditions.

In [78], Wang et.al presented the stacked denoising autoencoders (SDAE) that learned the semantic encoding of heartbeats which helps in the reduction of noise level and correspondingly increases the classification efficiency. Bidirectional LSTM (Bi-LSTM) was employed as a classifier that worked on temporal features. Three databases MIT-BIH arrhythmia DB, MIT-BIH SUVTDB, and MIT-BIH NSTDB have been used and attained an overall *Acc, Spec*, and *Sens* of 98.85%, 99.86%, and 96.32%, respectively. In [79], Bian et al. introduced a task-cognizant sparse signal processing technique for extracting the important information. A correlation-assist compression with adaptive length (CCAL) algorithm-based pattern for detection of ECG signal in compressed domain is generated. The ECG signal is compressed in CCAL algorithm in a fragment-by-fragment way. The varying compression length is computed by evaluating the correlation coefficients between adjacent fragments. The autoregressive coefficients are extracted as features for classification in compressed domain. At last, SVM classifier is utilised to recognise the ECG condition.

In [80], an arrhythmia classification is performed by introducing a multidimensional feature extraction and selection method. To extract image shape features, a multi-interval symmetrized dot pattern method is employed. These features are combined with time-frequency, morphological, and RR interval features to obtain a comprehensive feature set. Then, forming a feature selection method, called WReliefF-GA-SVM, by developing an average-weight-based ReliefF method (WReliefF), and integrated with genetic algorithm and SVM. This hybrid feature selection method is divided into a Filter stage and a Wrapper stage to effectively select the relevant features. The classification is being done using one against all SVM method. The obtained average *Acc, Sens*, and *Spec* is 99.74%, 99.42%, and 99.83% respectively.

Ayar and Sabamoniri [81] introduced the decision tree approach with a genetic algorithm that used the hybrid model with optimal features having an *Acc* of 2 class and 16 class is 86.76% and 77%, respectively. In [82], Saadatnejad et.al presented an architecture consisting of wavelet transform for feature extraction (wavelet and classical features) and multiple LSTM RNNs for classification purposes. It classifies

the heartbeat into VEB and SVEB with an *Acc* of 99.2% and 98.3%, respectively. In [83], an inter-patient-based arrhythmia classification is employed using ensemble learning. It is intended to detect five classes of morphological arrhythmia named Left bundle branch block (LBBB), Right bundle branch block (RBBB), Premature ventricular contraction (PVC), Premature atrial contraction (PAC), and Normal. The evaluation results achieved an average *Acc*, *recall*, *prec*, and *F1-sc* of 87%, 87.4%, 88.4%, and 87% respectively.

Gaussian Bernoulli deep belief network with SVM as classifier results in the *Acc* of 99.5% and 99.4% in case of supraventricular and ventricular respectively over MIT-BIH Arrhythmia DB [84]. In [85], 5-level wavelet decomposition was performed using stop band energy optimal orthogonal wavelet filter. Here, for the classification of heartbeats, noisy data and clean data have been used. Fuzzy entropy, Renyi entropy, and fractal dimension features were extracted for accurate classification. The features are then applied to the *k*-nearest neighbour (*k*NN) classifier that achieved a maximum *Acc, Sens*, and *Spec* of noisy data is 98%, 85.33%, and 98.22, respectively and for clean data, it is 98.1%, 85.63%, and 98.27%, respectively. The *ppv* for noisy and clean data is 94.81% and 94.85% respectively. To assist the clinicians to aid in their diagnosis, this developed system can be used in the intensive care units.

In [86], the Spark Scala tool is used to simplify the machine learning algorithms. It provides the simplest ways to implement classification algorithms like decision trees, random forests, gradient boosted trees (GDB), etc. The presented method is validated on MIT-BIH Arrhythmia DB and MIT-BIH SVDB. For binary classification, the initiated approach achieved an *Acc* of 96.75% and 97.98% using GDB trees and the random forest algorithm, respectively. By using random forest, 98.03% *Acc* is achieved for multi-class classification. Sun et al. [87] presented an ensemble multi-label classification process that involves several classification methods to enhance the performance of the classifier. Based on mutual information, the weights of each classifier are computed. A genetic algorithm is used to calculate the optimum threshold value. CCDD is used with feature extraction for morphological features, time and frequency domain features, and obtained an overall *Acc* of 75.2%. The adaptive *k*-

means clustering algorithm for feature extraction with kNN classifier and visual morphological pattern features is used which shows an overall *Acc* of 97.70% by Yang and Wei [88].

Wang [89] introduced a new method that divides ECG data into four categories according to the channel: electrode shedding, serious and partial noise interference, and high-quality signal. It designed a tree classifier using one-class support vector machine with an overall *Acc* of 98%. In [90], the motive of the study is to adjust the count of hidden layers of extreme machine learning utilising differential evolution algorithm, aids to ECG classification. Pan-Tompkins and DWT approach are implemented and reflects an *Acc* of 98.4% and 97.5% respectively. Lu et al. [91] experimented with 1D-CNN with global average pooling on the Xilinx Zynq ZC706 platform and the z-score process attained *Acc, Sens, Spec*, and *ppv* of 99.10%, 99.13%, 98.59%, and 99.10% respectively. The model is efficient for hardware design in case of wearable healthcare device specially in ECG classification scenario.

Kung et al. [92] presented a feature extraction system based on two delta-sigma modulators and the wave detection algorithm to detect the output of modulators. The *Spec* and *F1-sc* of 99.61% and 99.83%, 81.05% and 97.07% in SVEB and VEB, respectively is achieved. Yang and Wei [16] presented the ensemble classification on the basis of morphological features for detection of atrial and ventricular irregularities. It utilised the discrete wavelet transform approach with an ensemble classifier (KSMAX: kNN, SVM, MLP, AdaBoost, XGBoost) having an overall *Acc* of 98.68%. Ganguly et al. [17] presented a unidirectionally processed multifractal detrended fluctuation analysis (u-MDFA) with Bi-LSTM as a classifier which attained an *Acc* of 97.3% and *Spec* in the case of SVEB and VEB is 99.2% and 98.6% respectively. In [93], a combination of recursive least square algorithm and stationary wavelet transform (SWT) is used for fetal ECG extraction. An enhanced spatially selective noise filtration method or threshold based denoising approach is utilised to upgrade the fetal ECG signal, minimize the noise and artifacts present, and to detect the R-peaks of ECG signal. The efficiency is tested over synthetic and clinical data as well.

The measurements including SNR, QRS complex estimation, and visual inspection are performed. Filtering methods like Butterworth, bandpass filter, wavelet filter, etc. have been implemented with classifiers kNN, ANN, and Naïve Bayes having different algorithms as peak detection algorithms [28], [29], [94].

2.1.3 Review on the basis of modern methodologies over arrhythmia detection and classification

Hou et al. [95], introduced an interpretable deep denoising structure on the basis of sparse representation. To decompose the denoising method into sparse representations as an iterative solution process, the half quadratic splitting algorithm is employed. Furthermore, a new weight distribution module is initiated, which dynamically extracts adaptive hyperparameters based on ECG correlations rather than relying on empirical values. This significantly enhances the efficiency of hyperparameter selection. Ji and Zhu [96], introduced a GRUnet deep learning model, uses CNN to automatically extract the features from ECG signals, thus, improving the feature utilisation and representation capabilities. The gating system of GRU regulates the information flow and aids in capturing long-term dependencies. The introduced method eliminates the issue of manual feature selection, and select appropriate features as compared to previous machine learning methods. An overall classification *Acc* of 99.47% is achieved over European ST-T database.

Hao et al. [97], introduces G2-ResNeXt, an innovative model for inter-patient heartbeat classification. It enhances the original ResNeXt architecture by incorporating a two-fold grouping convolution, enabling more effective automatic feature extraction and classification of ECG signals. It achieved an overall *Acc* of 96.16% and other parameters like *Sens* and *prec* are 97.09% and 95.90% respectively in case of VEB, 80.59% and 82.26% in case of SVEB respectively. It is observed that sometimes, there is an issue of insufficient data for testing. To overcome this issue, a new generative adversarial network-based deep learning method named HeartNet is developed for handling the insufficient data problem [98]. It suggested a deep leaning method which is compressed by a multi-head attention mechanism on CNN architecture. It enhances the overall performance by $5 - 10\%$ on each insufficient data

label category. It achieved an *Acc* of 99.67 ± 0.11 over adversarial data synthesized dataset. In [99], a novel study for inter-patient ECG classification utilising a compact 1D Self-ONN (Operational Neural Network) is introduced by determining morphological and timing information in heart cycles. The temporal features on the basis of RR interval for timing characterization are injected. The model achieved an overall *Acc* of 98.50%.

In [100], the presented methodology includes a Lightweight Custom Convolutional Neural Network (LC-CNN) with only three convolutional layers, alongside a transfer learning model based on the MobileNet-V2 architecture, which utilizes pre-trained features to improve arrhythmia classification. A Butterworth filter is used for noise reduction in data preprocessing. The LC-CNN model achieved an average *Acc* of 99.22% and using MobileNet-V2 model, the *Acc* is 98.69%. In [101], Guan et al. introduced a novel hidden attention residual network (HA-ResNet) for arrhythmia classification. The hidden attention layer combining Squeeze-and-Excitation (SE) block and Bidirectional Convolutional LSTM is utilised to record the deep spatio-temporal features obtained by inserting the two-dimensional images into an embedding layer. The *F1-sc* of 96%, 96.7%, and 87.6% is achieved over $2sec$, $5sec$, and $10sec$ segments respectively.

In [102], EMCNet, an ensemble of multiscale convolutional neural networks is introduced for classifying the single-lead ECG waves acquired by wearable devices. The model has two modules, in which two component classifiers are initially developed, which input the filtered ECG recordings and time-frequency spectrograms, and reflect the prediction probabilities of corresponding categories as output. The overall classification outcome is evaluated through sending the prediction probabilities to an improved weight matrix on the basis of soft voting method. In [103], Yang et al. introduced a multi-view and multi-scale DNN for ECG classification, treating different leads as distinct views to fully leverage the diverse features of a 12-lead ECG. The presented network employs a multi-view strategy to efficiently integrate features from different leads and utilizes a multi-scale CNN architecture to capture temporal features of ECG across various scales. To improve the feature depiction of the network, the

spatial information and channel relationships of ECG features are recorded by coordinate attention.

In [104], introduced a deep learning model for multilabel classification of ECG signals. It can detect up to two labels of an ECG signal including eight rhythms or morphological abnormalities with normal condition. An explainable artificial intelligence structure utilising class activation maps acquired from gradient-weighted class activation mapping technique is introduced in the study. At last, a thresholding is implemented at output probability of softmax layer to get the multilabel classification of ECG signals. The model achieved an *Acc*, *hamming loss*, *precision*, *recall*, and *F1-sc* of $96.2\%, 0.037, 0.986, 0.949$, and 0.967 respectively. Sannino and Pietro [105] stated the ANN approach with a DNN classifier has *Acc, Sens*, and *Spec* of $99.68\%, 99.48\%$, and 99.83% respectively. Adam optimizer with symbolic baseline-corrected approximation (SBCX) approach and MPCNN as classifier shown the *Acc* of 96.4% revealed by Niu et al. [106]. In [107], Lynn et al. introduced a deep recurrent neural network (RNNs) based on Gated Recurrent Unit (GRU) in a bidirectional manner achieving an *Acc* of 98.5%. Here, the 1-D CNN approach and RNN with long short-term memory (LSTM) and GRU have been used for classification. The suggested model was evaluated with ECG ID and MIT-BIH Arrhythmia DB with an *Acc* of 98.6% and 98.4%, respectively.

Li et al. [108] used the generic CNN and tuned dedicated CNN with an accuracy of 96.89%. In [109], Rahhal et.al presented an architecture based on dense convolutional networks for the ECG signal classification. This architecture consists of a generative and discriminative module that one employs the conversion of one-dimensional ECG input to the two-dimensional image so that image can be easily applied to the convolutional neural network and the other employs the classification of the signal. To handle the imbalanced data, introduced the idea to use focal loss that reduces the loss assigned to ECG beats. MIT-BIH Arrhythmia DB, INCART DB, and MIT-BIH SVDB DB have been used for evaluating the method with an overall *Acc* of SVEB is 97% and VEB is 74% respectively. In [110], Huang et al. used two-dimensional (2D) deep CNN for the ECG arrhythmia classification method. By using a short-time Fourier

transform, the time-domain ECG signal is transformed into an image of time–frequency spectrograms, and the outcome is applied as an input to two-dimensional CNN and achieved an *Acc* of 99.0%. It has been observed that with a learning rate of 0.001 and a batch size parameter is 2500, accuracy is reached to a higher level and correspondingly decreases the average loss.

In [111], the spiking neural networks with spike-timing dependent plasticity, and reward- modulated STDP is introduced to train the model weights according to the spike signal timings. For real-time operation, the introduced work is appropriate. The simulation results in energy consumption of 1.78 *µJ* per beat in real-time classification which is 2 to 9 orders of magnitude smaller than another classification method. The method obtained an overall *Acc* of 97.9%. In [112], Wu et al. aimed at multiclass heartbeat recognition in wearable devices where BLSTM and CNN are used to deliver high accuracy with minimal network scale. The weight quantization and parameter precision reduction are adopted as network compression techniques to reduce the storage of parameters for better classification results. The method has shown the *Acc* of 98.6% and 98.3% in VEB and SVEB, respectively. In [113], a novel approach is introduced, comprising two components deep intermediate representation and In-Set Voting Scheme, for representation and classification respectively. MLPNN has been studied that reflects the *Acc* of 99.5%. MIT-BIH Arrhythmia DB and PTBDB have been used.

In [114] Feng et al. presented the probabilistic process neural network for the multi-channel time-varying signal classification problems. Softmax classifier implemented the probabilistic classification of time-varying signals with high efficiency. Specific learning algorithms have been developed that synthesize dynamic time warping, C-means clustering, and Bayesian probability algorithm. CCDD database is used which shows the *Acc* and *Spec* of 84.92% and 84.21%, respectively. Hua et al. [115] introduced a new QRS detection algorithm followed by a deep Boltzmann machine-based classification. A template-based algorithm was used for QRS detection. When the compression ratio (CR) is 40%, it reflects the *Acc* of 90% and 81.88% over MIT-BIH Arrhythmia DB and recorded database respectively, and *Spec* of 95.52% and

94.44% is achieved respectively. Shaker et al. [116], introduced the data augmentation technique using a generative adversarial network (GAN) is an unsupervised method, it consists of two neural networks) to maintain the balance of the dataset. An end-to end approach (directly classifies the heartbeat) and a two-stage hierarchical approach have been used which is based upon deep CNN. The supposed method achieved an overall *Acc, Sens*, and *Spec* of 98.30%, 99.77%, and 99.23% respectively.

In [117], Xu and Liu used the CNN based ECG classification method, explored by computer-aided method. Denoising has been done by wavelet filters and worked upon the MIT-BIH Arrhythmia DB. Overall *Acc* and *Spec* of 99.43% and 99.9%, respectively, is achieved. The *Sens* and *ppv* of VEB and SVEB are 99.2%, 97.5%, and 99.4%, 99.1%, respectively. To monitor long-term ECG data, the initiated system can be directly implemented on wearable devices. Romdhane et al. [118] implemented an optimization step for deep CNN model utilising a novel loss function called focal loss. The system enhanced the classification *Acc, F1-sc, precision*, and *recall* to 98.41%, 98.38%, 98.37%, and 98.41% respectively. It performed the evaluations over MIT-BIH Arrhythmia DB and INCART DB to detect five arrhythmia categories (N, S, V, Q, and F). In [119], the classification of atrial fibrillation and normal sinus rhythm is being performed using CNN. The filtered and non-filtered data reflects the *Acc*, *Spec*, and *Sens* of 99.23% and 99.18%, 98.66% and 99.03%, 99.71% and 99.31% respectively. Song et al. [120] suggested a study to extract the low-level and high-level features of short-term ECG signal. The residual concatenate network through information-theoretic metric learning is used and reflects the *Acc, Sens*, and *Spec* of 88.20%, 80.45%, and 94.81% respectively.

Dokur et al. [121] presented a classification of eleven distinct ECG beat types is performed utilising MIT-BIH Arrhythmia DB through visual inspection of ECG records. The smaller network using Walsh functions with high performance is implemented and achieved an *Acc* of 99.45%. Huang [122] introduced a fast compression residual CNN (FCResNet) for accurate arrhythmia classification. In this model, a fast down-sampling module and various residual block structural units were integrated. The maximal overlap wavelet packet transform gives a time-scale pattern

was used for decomposition of ECG signals and achieved the classification *Acc* of 98.79%. Yan et al. [123] presented a set of inter-patient ECG classification techniques that utilise CNNs and spiking neural networks (SNN), attained the *Acc* of 92% and 91% respectively. SNN is used for energy saving purpose. The average power of a two-class SNN is $0.77\,W$. In [124], two distinct deep learning bagging models are introduced for ECG classification. The CNN-LSTM capture the local features and temporal dynamics whereas RR intervals and higher-order statistics, RRHOS-LSTM model work over classical features. A weighted loss function is used to train the model. The combined models with meta classifier (fusion classifier) on local and classical features attained an *Acc* of 95.81%.

Mahmud et al. [125] presented a wavelet decomposition technique with Deep ArrNet, Pointwise-temporal-pointwise approach on temporal features which attained the *Acc* and *Sens* of 99.28% and 99.13%, respectively. Nurmani et al. [126] introduced the Stacked Convolutional Bi-LSTM model with Bi-LSTM as a classifier and showed an average *Spec, Acc, Sens, prec*, and *F1-sc* of 99.90%, 99.83%, 98.82%, 98.86%, and 98.84% respectively. In [127], Houssein et al. presented a marine predators algorithm with MPA-CNN as a classifier having features like RR interval, 1D local binary pattern, and Higher order statistics (HOS), Hermite basis function (HBF). The model attained an overall *Acc* of 99.76%. In [128], Wang et al. introduced the tri-branch CNN model with a mixup asymmetric tri-training method on morphological features that classify the ECG signal in different beats. Experiments have been performed over MITDB and SVDB in terms of *F1- sc*.

Ahmad et al. [129] presented the multimodal image fusion (MIF) and multimodal feature fusion (MFF) models with SVM, and softmax as classifiers having a precise value of MIF and MFF is 92% and 98%, respectively for ECG heartbeat classification. The input ECG data is being converted into three distinct images utilising Gramian Angular Field (GAF), Recurrence Plot, and Markov Transition Field and applied at the input of models. In [130], Kolhar and Rajeh introduced a dual branch model and AlexNet for ECG classification. The preprocessing includes standardizing, balancing, and reshaping of ECG signals. The AlexNet and dual branch model achieved an *Acc*

of 98.64% and 99% respectively over PTBDB ECG. Several models like *k*NN, SVM classifier [85], [88], ensemble SVM [131], have been used which reflects the high *Acc* but as compared to all models, 2D-ECG image with CNN [29], [110], [116], [119], [121] shows the highest accuracy with least computational complexity. This technique performs best in all other above techniques that represent the maximum accuracy with the least computational complexity.

The layout of machine learning models and deep learning models are illustrated in Fig 2.1., which basically shows that how to build a machine learning and deep learning model using various algorithms. The model is being validated over distinct sets of train and test data. The traditional and modern methods are implemented over 1D time-domain ECG signal and 2D representation of the respective signal for the detection and classification purposes of diseased subject.
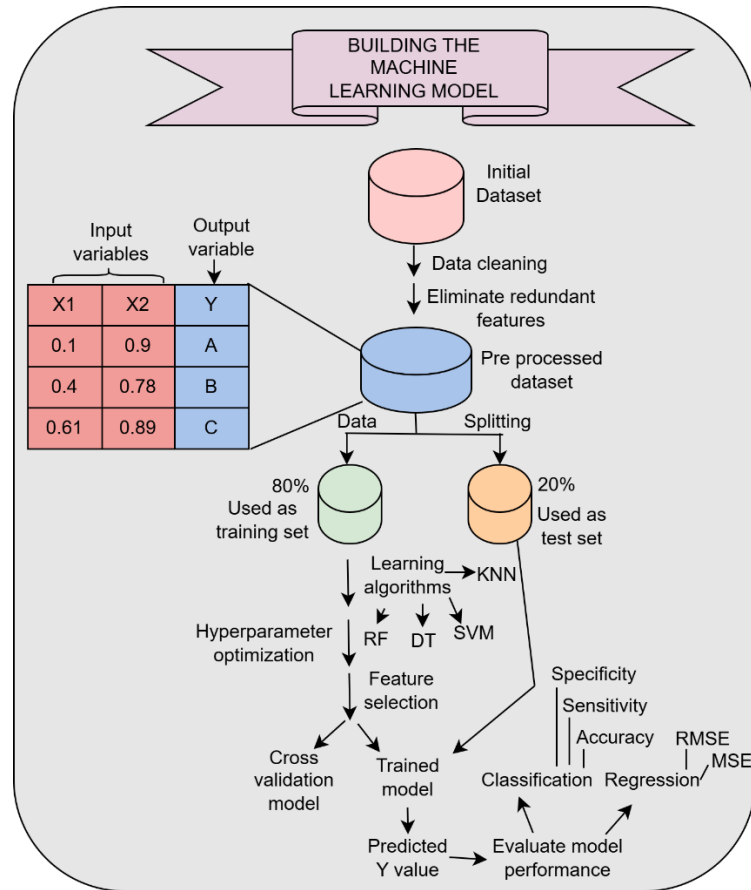
(a) Layout of Machine Learning Model for arrhythmia detection and classification using ECG signal
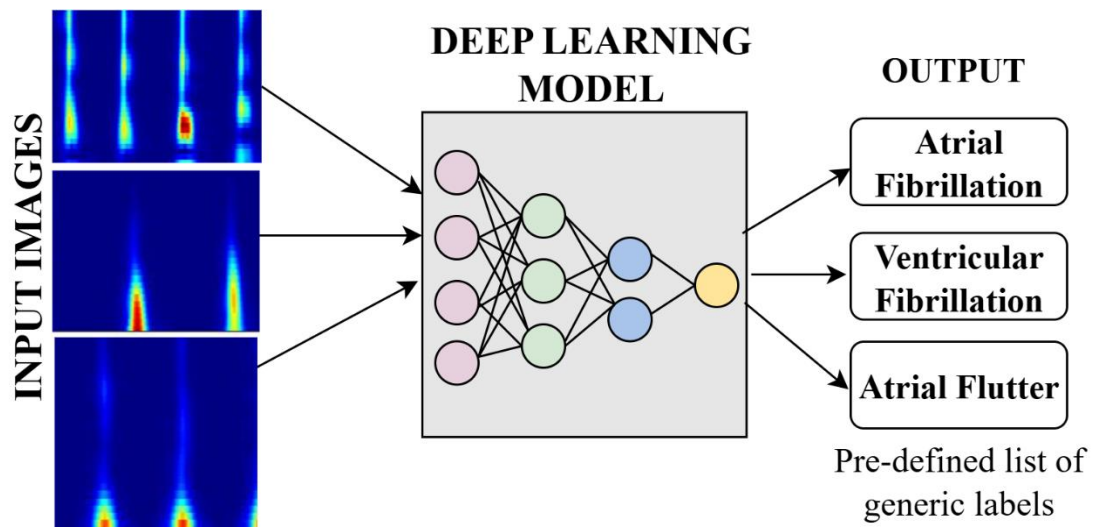
(b) Representation of Deep Learning Model for arrhythmia detection and classification using ECG signal

Fig 2.1 The formation of machine learning and deep learning models for detection and classification of arrhythmia over distinct datasets of ECG signal

2.2 Research gaps

Based on the literature review, ECG classification is an efficient method to classify the signal according to the heart rate and calculate the abnormality which further detects the arrhythmia. Through literature, a few research gaps have been noticed which are underlined as follows:

➢ Interruption of artifacts (Motion artifact, Muscle noise, Electromyographic noise, powerline interference, baseline wander, instrumentation noise, and electrosurgical noise) in the ECG signal causes signal strength degradation, leading to misclassification.

➢ False detection and dislocation of peaks (QRS complex, R peak detection) or peaks can be overlooked causing the misinterpretation of a signal.

➢ Disease classification based on ECG signals frequently yields low accuracy while performing over multiple classes of disease.

➢ Untimely heart strokes lead to demise as continuous monitoring of heart-related signal is required.

2.3 Research Objectives

The challenges involved in the identification of disease, motivate to develop efficient models and frameworks to fulfil the purpose of developing a robust detection and classification system. In order to achieve this, four research objectives are formulated here to handle the practical challenges involved mentioned above, which are as follows:

➤ Design of efficient technique for ECG peak detection.

➤ To propose an efficient technique for early detection of arrhythmia using an ECG signal.

➤ To develop a technique for binary and multiclass heart disease detection and classification.

➤ Design of efficient technique for real-time monitoring of ECG signals and their classification.

Chapter 3

IDENTIFICATION AND LOCALISATION OF R-PEAKS IN ECG SIGNALS

Heart-related disease is one of the pre-eminent origins of mortality across the globe. Early and accurate detection of heart-related disease is essential to avoid an uncertain mishap. Peak detection is a pivotal step for the analysis of different spectral signals. The dislocation of peaks disrupts the detection accuracy of a heart-related disease.

3.1 R-Peak Detection Using Wavelet Scattering Transform for Pre-Term Infant ECG

A precise detection of R-peaks is necessary for recognition of cardiovascular diseases in ECG signals. This work presented a method for accurate R-peak detection of ECG signal, achieved using wavelet scattering transform. It eliminates the artifacts associated to signal with the help of inbuilt filters, proves reliable as it identifies the R-peaks at correct location. The wavelet scattering transform generates rational, instructive, and invariable translation representation of signals. The efficiency of the method for R-peak detection is evaluated over pre-term infant ECG dataset available at physionet. The method outperforms the state-of-the-art methods namely continuous wavelet transform (CWT) and thresholding technique.

The advent of wearable ECG monitors underscores the significance of examining resilient automated R-peak detection in single-lead ECG signals. Although, several methods of R-peak detection have been introduced, it is still an important issue in terms of noise effects, alternative rhythms etc. A typical ECG waveform includes the P wave, QRS complex, and T wave. The QRS complex represents the electrical depolarization of the muscles in the ventricular area of the heart [10], [46]. The HRV assessment are generally influenced by noise level, including artifacts present in the raw ECG signal that makes the R-peak detection complex. Noise sources [9] consists of power-line interference, baseline wandering, and electromyographic noise that affects the ECG

signal in various aspects. It has been observed that R-peak detection is basically split into threshold methods, wavelet analysis method, and deep learning methods. To enhance the adaptive ability of peak detection, a weighted continuous wavelet transform is introduced in [132] that generates spectral peak characteristics in low-scale regions. A brown exponential smoothing model [133] is implemented for an adaptive R-peak detection procedure, achieved precision and recall of 99.6% and 99.7% respectively. The challenge of noise interruption is removed with this implementation and proves well suited for noisy signals. The objective of this work is to detect the R-peak of the pre-term individuals in terms of spectral analysis of the peaks illustrated using scattering transform. The purpose of the study is discussed as follows.

1) The Wavelet Scattering Transform (WST) is utilized for R-peak detection in ECG signals due to its ability to extract robust, time-invariant features while preserving signal structure.

2) By capturing multi-scale and hierarchical signal characteristics, WST enhances the accuracy and reliability of R-peak identification.

3) Examining the wavelet analysis with scattering coefficients generated through WST.

4) The method is implemented over pre-term infant ECG database because these signals are typically noisier and more challenging to analyze due to immature cardiac activity and smaller signal amplitudes. Evaluating the method on such a dataset demonstrates its robustness and effectiveness in detecting R-peaks under difficult conditions.

3.1.1 Wavelet Scattering Transform

The wavelet scattering transform [134], [135] constructs coherent, instructive, and translation-invariant signal depictions. It is rugged to dislocations, and conserves class discriminability that makes it especially efficient for feature extraction and categorisation. The method includes three step iterative signal transformation as wavelet convolution, modulation, and filtering. By using repetitive wavelet decomposition, local averaging, and complex modulus, the features of the signal are extracted. Basically, the high-frequency components of the signal are recognized by the wavelet filter, while the scaling function process the details of the low-frequency signal. With this, the features having low frequency are recovered at each

decomposition step. The stable frequency characteristics are calculated by local averages after evaluating the modulus of the coefficients of high-frequency signals. It has been seen that high-frequency information vanished due to local averaging which can be recovered by initiating the high-frequency wavelet transform. In the end, the stability is maintained between invariance and the discrimination after clearing the signal through different scattering routes [136].

Let the ECG signal analysis is represented by $Y(t)$. To construct the filters that occupy the overall frequencies present in the signal, a low pass filter ϕ and the wavelet function Ψ are designed. $\phi_L(t)$ shows the low pass filter that gives local translation invariant descriptions of Y at a predefined scale T. Let Λ_w be the group of wavelet indices with an octave frequency resolution Q_w. The high pass filter bank is shown by $\{\Psi_{lw}\}_{l_w \in \Lambda_w}$ can be calculated by dilating the wavelet Ψ. The WST is executed with deep convolution network that repeats over classical wavelet transform, complex modulus, and calibrating operators. The convolution $C_o Y(t) = Y * \phi_L(t)$ creates a locally translation invariant feature of Y but that yields in the loss of information having high frequency. The vanished high frequencies can be retrieved by a wavelet modulus transform.

$$|W_1|Y = \left\{ C_o Y(t), \left| Y * \phi_{l_1}(t) \right| \right\}_{l_1 \in \Lambda_1} \tag{3.1}$$

By taking mean of the coefficients of wavelet modulus with ϕ_L, the first order scattering coefficients will be

$$C_1 Y(t) = \left\{ \left| Y * \Psi_{l_1} \right| * \phi_L(t) \right\}_{l_1 \in \Lambda_1} \tag{3.2}$$

Here, the information can be retrieved by averaging, where $C_1 Y(t)$ is noted as low frequency component of $\left| Y * \Psi_{l_1} \right|$, the high frequency coefficients can be extracted by

$$|W_2| \left| Y * \Psi_{l_1} \right| = \left\{ C_1 Y(t), \left| \left| Y * \Psi_{l_1} \right| * \Psi_{l_2}(t) \right| \right\}_{l_2 \in \Lambda_2} \tag{3.3}$$

The second order scattering coefficients is stated as

$$C_2 Y(t) = \left\{ \left| \left| Y * \Psi_{l_1} \right| * \Psi_{l_2} \right| * \phi_L(t) \right\}_{l_i \in \Lambda_i}, i = 1,2. \tag{3.4}$$

Wavelet modulus convolution can be defined by repeating the above process

$$V_m Y(t) = \left\{ \left| \left| \left| Y * \Psi_{l_1} \right| * \ldots \right| * \Psi_{l_m} \right| \right\}_{l_i \in \Lambda_i}, i = 1,2,\ldots,m \qquad (3.5)$$

m-th order scattering coefficients can be estimated by taking mean of $V_m Y(t)$ with ϕ_L.

$$C_m Y(t) = \left\{ \left| \left| \left| Y * \Psi_{l_1} \right| * \ldots \right| * \Psi_{l_m} \right| * \phi_L(t) \right\}_{l_i \in \Lambda_i}, i = 1,2,\ldots,m \qquad (3.6)$$

The endmost scattering matrix is a summation of all scattering coefficients of all orders to discuss the characteristics of the input signal, where n is the order of maximum decomposition,

$$CY(t) = \{C_m Y(t)\}_{0 \leq m \leq n'} \qquad (3.7)$$

Due to the mean operation calculated by the low pass filter, the system is invariable to translations up to the invariance scale, which can be huge enough. The features have a property of deformation stability due to the attributes take over from the wavelet transform. The scattering coefficients are formed that possess a low variance within a group and a high variance between the groups. From the above discussions, it has been reviewed that wavelet scattering notices the minute changes in the duration and amplitude of non-linear information which are difficult to calculate but conveys the state of the heart. Therefore, WST is implemented to generate the rugged formations of ECG heartbeat that decreases the difference in one category of arrhythmia during the maintenance of discriminability between different categories of arrhythmia.

It is to be noted that wavelet scattering is almost similar to CNN except that the filters are not learned, they are defined only, and the features generated from the last layer are the summation of all layers instead of only the last layer. It is visualised that with the increase in the count of the layer, the energy level of scattering coefficients drops suddenly with initial two layers having 99% of the energy. We utilised a second-order scattering network for the extraction of features of ECG signal. It also minimizes the computational complexity by avoiding the calculations of higher order coefficients. The structure of wavelet scattering transform including different scattering coefficient levels is illustrated in Fig 3.1. The wavelet scattering noticed the small variations in time span and dimensions of non-stationary signal which are tough to evaluate but reflects the heart condition.
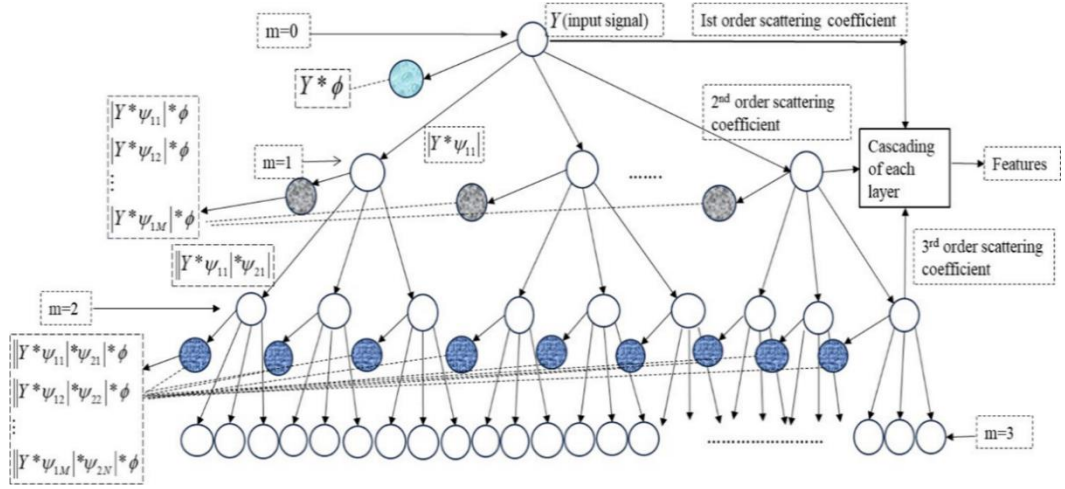
Fig 3.1 Layout of wavelet scattering transform

3.1.2 Pre-Term Infant Dataset Using ECG Signal

The data of ten preterm infant is considered with postconceptional age of $29\frac{3}{7}$ to $34\frac{2}{7}$ weeks (average: $31\frac{1}{7}$ weeks) and weights of 843gm to 2100gm (average: 1468gm) [137], available at physionet which is freely accessible [34].

Table 3.1 Summary of pre-term infant ECG database at physionet

Infants	Age (weeks)	Weight (kg)	Recording Time (hrs)	Mean [SD]	Heart Rate (bpm)	Sampling frequency (Hz)
Inf_1	$29\frac{3}{7}$	1.20	45.6	155	[10]	250
Inf_2	$30\frac{5}{7}$	1.76	43.8	131	[14]	500
Inf_3	$30\frac{5}{7}$	1.71	43.7	131	[13]	500
Inf_4	$30\frac{1}{7}$	0.84	46.8	167	[9]	500
Inf_5	$32\frac{2}{7}$	1.67	48.8	143	[16]	250
Inf_6	$30\frac{1}{7}$	1.14	48.6	137	[8]	500
Inf_7	$30\frac{1}{7}$	1.11	20.3	162	[13]	500
Inf_8	$32\frac{3}{7}$	2.10	24.6	141	[13]	500
Inf_9	$30\frac{4}{7}$	1.23	70.3	150	[13]	500
Inf_10	$34\frac{2}{7}$	1.90	45.1	156	[16]	500

A three-lead ECG signal was recorded for $20 - 70$ hrs per infant of sampling frequency 500Hz. A compound ECG signal was registered at 250 Hz for infant 1 and 5 in the absence of an ECG channel. The remaining recordings are performed at 500 Hz. The whole information of pre-term infant database is summarized in Table 3.1.
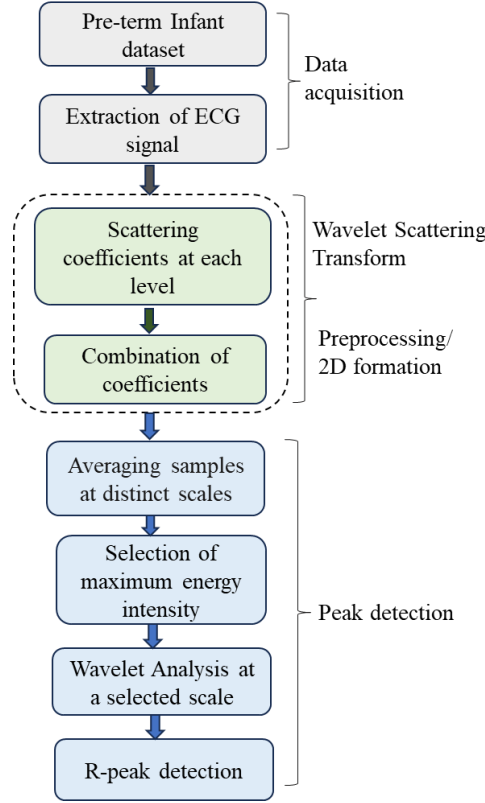
Fig 3.2 The layout of R-peak detection in ECG signal using wavelet scattering transform

3.1.3 Implementation of wavelet scattering transform over pre-term infant ECG dataset

Initially, the ECG signal is extracted from pre-term infant database consisting information of ten infants for different age groups. The extracted signal is normalized for precise and acute processing, to keep the different levels of signal in an appropriate range. WST is implemented over the normalized data, generating coherent, informative, and translation-invariant representation of ECG signals. The benefit of implementing the WST is to utilize the in-built filters. Thus, an extra step of preprocessing is removed by employing this technique. The technique works on both low and high frequency

52

signal at different levels with scattering coefficients. The 2D time-frequency scalogram is generated using WST, represents the amplitude and location of peaks. The energy intensity can be estimated through the formation of peaks, which also separates the noise signal from the original signal. The scattering matrix is generated after combining all scattering coefficients obtained at each level from WST. The matrix obtained after combination is investigated through average of samples at different scales. An automatic selection of scales corresponding to maximum energy intensity is performed. Thus, the maximum wavelet analysis at a selected scale is achieved that helps to notice the R-peak of the ECG signal. The overall process involved in R-peak detection of ECG signal utilizing WST is presented in Fig 3.2, consists of data acquisition, preprocessing using WST, and R-peak detection using wavelet analysis.

3.1.4 Experimental Results

The simulations are executed on MATLAB using GPU: NVIDIA GEFORCE RTX 3070, processor: 11th Gen Intel(R) Core (TM) i7-11370H@3.30GHz, and memory of 128 GB with software: Win 10, 64-bit operating system.

Initially, the ECG records are fetched from pre-term infant database for R-peak detection. The input signal, *Inf_1* consisting 2500 samples is normalized and applied to the WST. The scalogram generated from WST conveys the spectral analysis of the respective signal. It represents the energy intensity of the specified peaks through which the R-peak detection of ECG signal is achieved. From WST, a resultant scattering coefficient matrix is produced which is analysed at different samples. Finally, the averaging of these sample value reflects the selected time-scale. Thereafter, localized the R-peaks in the given range of samples.

The results obtained through implementation of WST over pre-term infant dataset is illustrated in Fig 3.3, represents the normalized ECG signal, the combined form of scattering coefficients, and the corresponding 2D scalogram representation, respectively. A random selection of samples is made and correspondingly, the detection accuracy of R-peaks is calculated using WST implementation, discussed in Table 3.2. The evaluation parameters named as accuracy and specificity are calculated and compared with the existing techniques for R-peak detection.

53
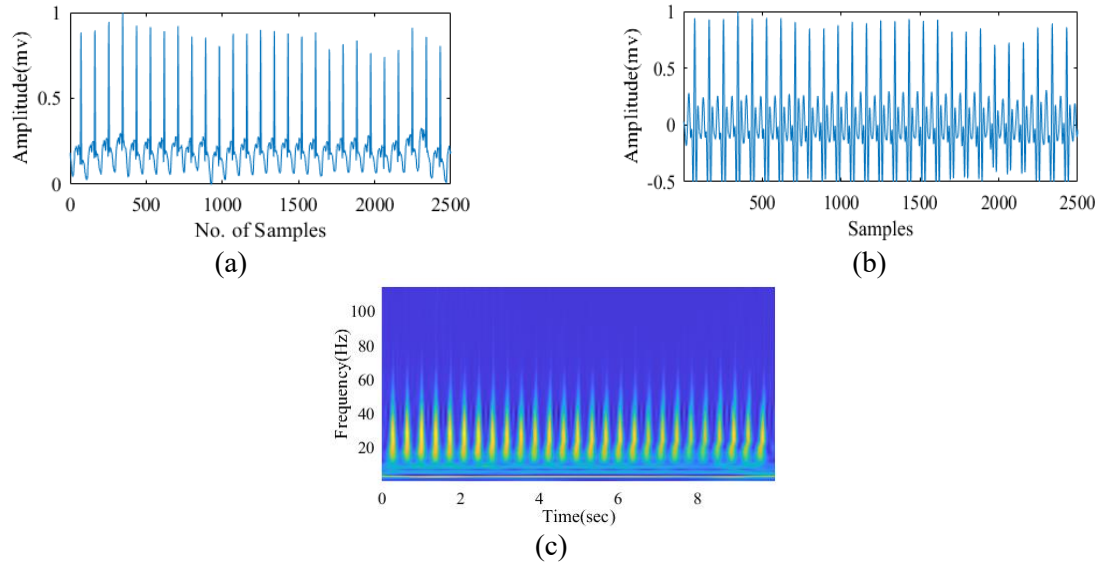
Fig 3.3 (a) ECG signal of infant *Inf_1* from pre-term infant dataset (b) Result obtained through different combinations of WST coefficients (c) The corresponding scalogram generated through WST for detection of R-peaks.

Table 3.2 Summary of detection accuracy using WST at different samples of infants

Infants	Samples	Total no. of Peaks given	Detected Peaks using WST	Detection accuracy (%)
Inf_1	3600	27	27	100
Inf_2	2500	23	23	100
Inf_2_17	4000	28	28	100
Inf_3	2300	10	9	90.0
Inf_4	1800	15	15	100
Inf_5	1300	12	12	100
Inf_5_9	3200	24	24	100
Inf_6	1000	8	8	100
Inf_7	1000	9	9	100
Inf_8	1200	11	11	100
Inf_8_11	1400	12	12	100
Inf_9	1700	16	16	100
Inf_10	2200	21	21	100

The presented method is compared with existing methods to assess performance in terms of accuracy and specificity. Other methods such as continuous wavelet transform performed well but somehow lags in computational time which is an important parameter while handling a diseased subject. Few existing methods are compared with executed method discussed in Table 3.3.

Table 3.3 Summary of comparison between executed method with existing methods for R-peak detection using ECG signals.

Year	Database	Method	Performance (%)
(2024) [51]	Real-time 36 subjects with an age range of 18-75 years	Deep Matched Filter	*recall*: 94.9 *prec*: 91.2
(2023) [54]	CinC 2013 Set-A ADFECG dataset [138]	Spectral Attention Kernel Independent Component Analysis	*ppv*: 99.6, *F1-sc*: 99.5
			ppv: 97.6, *F1-sc*: 98.0
(2023) [139]	MIT-BIH Arrhythmia DB	ST-Res U-net	*Sens:* 99.76
	CPSC2019		*Sens:* 90.01
(2022) [140]	MIT-BIH ST	SWT and Separable Convolution	*F1-sc*: 0.9995
	European ST-T		*F1-sc:* 0.9988
	TELE		*F1-sc:* 0.9790
(2022) [141]	MIT-BIH Arrhythmia DB	CWT + U-Net3 model	*Acc:* 98
(2016) [142]	MIT-BIH Arrhythmia DB, PTBDB, Fantasia DB	Wavelet Transform (scale 4)	Overall *Spec*: 99.98
(2024) [143]	Pre-term Infant ECG DB	Wavelet Scattering Transform	*Acc*: 99.23 *Spec*: 99.86

3.1.5 Discussions

The R-peak detection of ECG signal is a crucial step in diagnosing an arrhythmia disease. The dislocation of peaks from their original position disrupts the heart status, correspondingly decrease the detection accuracy of the respective disease. In this work, executed an R-peak detection algorithm based on the wavelet scattering transform.

Computational complexity of wavelet scattering transform

The Wavelet Scattering Transform (WST) performs cascaded wavelet convolutions and modulus nonlinearities across multiple orders; if P is the number of band-pass filters at the first order and M is the maximum scattering order, then the number of convolutions grows approximately as $\sum_{m=0}^{M} P^m$. Using FFT-based convolution, the cost scales as $O(N \log N \cdot \sum_{m=0}^{M} P^m)$.

3.1.6 Summary of identification of R-peaks using WST over pre-term infant ECG signals

The core of this work is to detect the peak status on the basis of sample and scale group. The method deals with the coefficients generated though WST, where wavelet analysis is utilized to detect the level of the obtained peaks. The verification of detected R-peaks of ECG signal with the original number of peaks is performed using a combined form of scattering coefficients, which is being averaged over different samples. The presented methodology is tested over the preterm infant dataset and achieved an average *Acc* and *Spec* of 99.23%, 99.86% respectively. The computed average computational time of presented method is 13 seconds.

Table 3.4 Illustration of the hyperparameters of WST for R-peak detection

Method	Hyper-parameter	Description	Typical Values
WST (Wavelet Scattering Transform)	Number of scattering paths	Depth of scattering cascade (0th, 1st, 2nd order)	2–3 layers
	Number of scales	Log-spaced wavelet scales	6–10
	Wavelet type	Morlet (default in WST)	Morlet
	Quality factor	Filters per octave	1–8

	Invariance scale	Time-scale for averaging / low-pass	32–128 samples
	Oversampling factor	Degree of redundancy	1–2
	Sampling rate	Signal frequency	Dataset-dependent

3.2 PARALLEL CLUSTER WAVELET ANANLYSIS WITH MULTI-SPOT GAUSSIAN OVER LOW-QUALITY ECG SIGNALS FOR MULTI-PEAK DETECTION

The low-quality ECG signals fetched from noisy devices can undermine the accuracy and robustness of R-peak detection models. While most of the techniques addressed the challenge of R-peak detection, a remarkable performance gap remains, when dealing with low-quality ECG signals with the location of peaks. The time or frequency resolution in STFT is constrained through window width function which cannot be modify at the same time. This limitation is overcome by using wavelets. The new multi-scale CWT technique addresses the peak finding objective with its location by examining peaks at various scales, significantly enhancing detection accuracy. In this work, the Parallel Cluster Wavelet Analysis with Multi-Spot Gaussian (PCWA-MSG) is used to identify the R-peak of single and multi-peaks of low-quality ECG signals with its location. The significance of methodology is based on the wavelet analysis utilizing Ricker wavelet with multiple Gaussian functions to identify the R-peaks. The methodology recognized the restricted events from the original ECG data, aids to exclude the preprocessing step that makes it time efficient process.

3.2.1 Introduction

A clear understanding of the QRS complex depends heavily on the precise detection of the R-peak, which is a critical feature for identifying various cardiac abnormalities. The thresholding-based algorithm introduced by Pan and Tompkins (P&T) [144] is one of the most widely used methods for R-peak detection and has served as a benchmark for over three decades. However, its performance deteriorates in the

presence of noise, baseline drift, and signal artifacts, leading to increased detection errors. Additionally, the method is computationally intensive, requiring significant processing resources. A combination of hierarchical clustering and Discrete wavelet transform is implemented [145] to detect the R-peak and T-peak of ECG signals. The DWT coefficients are computed and achieved an *Acc* of 99.83% over MIT-BIH Arrhythmia database for single-peak ECG signals. In [146], bilateral threshold technique is introduced to detect the R-peaks for wearable ECG sensors and reflects high detection error rate. The recurrent neural network (RNN) based model [147] with post-processing step is introduced on a specific domain for QRS detection. The post-processing step reflects superiority over domain-specific cases and lags behind over other cases with an approximate value of 2%. It mentioned the efficacy attained through RNN but did not consider the computational complexity. In [148], the Brown's exponential smoothing model is suggested for an adaptive R-peak detection. Morphological features have been selected and used the relative error square method to optimize the smoothing coefficients over single peak noisy ECG signal. In [149], the high-resolution wavelet packet decomposition (HR-WPD) with time-attention CNN is introduced. The QRS features are extracted using the decomposition of ECG signal. It reflects the high error rate of 5.61%, 4.55% over TELEDB (Telehealth database) and NSTDB respectively. A few R-peak detection techniques with its location are discussed in [47], [48], [49], [50], [51], [52].

Literature suggests that peak detection methods are generally compatible with wearable devices and tend to perform well on high-quality, noise-free ECG signals. However, they often lack robustness in noisy environments. In particular, conventional QRS detection methods struggle with low-quality ECG signals that exhibit multiple peaks. The key contributions of this work are outlined as follows:

1. The technique, PCWA-MSG effectively combines robust R-peak detection with accurate identification of low-quality, multi-peak ECG signals. It leverages custom-designed wavelets to locate R-peaks based on the energy intensity associated with each peak.

2. An unsupervised technique is initiated with Ricker wavelet, reflects the greater number of cluster sets that calculate parallelly by evaluating the distance values.

3. A Multi-Spot Gaussian (MSG) wavelet is constructed by summing N Gaussian functions, each separated by a scale parameter sc, and bordered on both sides by negatively skewed peaks.

4. To validate the effectiveness of the methodology for R-peak detection, the following PhysioNet datasets are utilized: Pre-term Infant ECG, MIT-BIH Atrial Fibrillation, MIT-BIH Malignant Ventricular, and MIT-BIH Arrhythmia.

3.2.2 Mathematical modelling of Parallel Cluster Wavelet Analysis Using Ricker Wavelet

We present a flexible signal processing approach designed for the unsupervised recognition of single-channel signals. This methodology harnesses the highly parallel and multi-scale strengths of continuous wavelet transform (CWT) analysis, effectively tackling key challenges such as accuracy, execution speed, and computational complexity, making it well-suited for real-time signal recognition applications. The approach demonstrates the effectiveness of the Parallel Cluster Wavelet Analysis (PCWA) [150] in accurately detecting R-peaks within low-quality ECG signals along with its location where R-peaks are identified, highlighting its advantages in both computational efficiency and processing time. By leveraging custom-designed wavelets, the presented technique achieves over a four-fold improvement in R-peak detection rates and a six-fold reduction in error compared to previously adopted methodologies.

The Continuous Wavelet Transform (CWT) operates by comparing the signal $y(\mathbb{t})$ to a temporal pattern defined by the mother wavelet $\psi(\mathbb{t})$, aiming to identify points in time where this wavelet pattern appears as actual events within the signal.

$$CWT(\mathbb{t}, sc) = \langle \mathbb{f}, \psi_{\mathbb{t}, sc} \rangle = \int_{-}^{+} \mathbb{f}(\mathbb{t}') \,{1}/{\sqrt{sc}}\, \psi^* \left(\frac{\mathbb{t} - \mathbb{t}'}{sc} \right) dt' \qquad (3.8)$$

The scaling factor $sc > 0$ adjusts the wavelet pattern, allowing it to stretch or compress over time. The relationship between the true signal and the shifted, dilated basis function can be represented in a 2D map of the signal's equivalent coefficients,

59

$CWT(\mathbb{t}, sc)$. The presence of a specific pattern is indicated by local maxima in this 2D map, and by varying the scaling factor, the search for the same pattern is extended across multiple scales. The multi-scale nature of CWT analysis in the $(\mathbb{t}, sc)$ domain provides a revealing advantage by offering additional information through the assignment of events at different scale values, upgrading the interpretation of signal. The 2D CWT transform of the ECG signal is calculated using a Ricker wavelet, which is a zero-phase wavelet specified by a central peak and two smaller side lobes. The features of the Ricker wavelet are determined by its peak frequency, denoted as "$\mathbb{f}$," which makes it suitable for several areas. The width of the Ricker wavelet corresponds to the time interval between the centres of the two side lobes and is defined as the reciprocal of its peak frequency.

$$\psi(\mathbb{t}) = \frac{2}{\sqrt{3\sigma}\pi^{1/4}}\left(1 - \left(\mathbb{t}/\sigma\right)^2\right)e^{-\mathbb{t}^2/2\sigma^2} \tag{3.9}$$

CWT algorithms initially identify accurate points using the ridge methodology, which starts from the maxima at the highest scale value [151], [152]. Typically, ridges are formed by detecting the maxima in the subsequent scaled rows that are within a predefined distance on the CWT map. Once the ridges are formed, the time locations of the refined ridges with a SNR above a certain threshold are marked as peak locations. However, this process is computationally slow and resource-intensive, as the algorithm is executed serially. Furthermore, it is not highly efficient for detecting peak locations.

A modified approach is introduced to gather additional information about peak location and width by using ridges derived from zero crossings and local minima in the 2D CWT plot [153]. This method is more effective than direct ridge analysis, but it requires significantly more memory. To address this, an adaptive, robust, and memory-efficient methodology is presented for cluster analysis in real-time CWT experiments. The process begins by discussing macro-clusters (MC) of CWT maxima, which are separated by gaps along the time axis that exceed a predefined threshold. All sets are then analysed in parallel by evaluating the distance values around the local maxima with the highest $Clstr(\mathbb{t}, sc)$ value, which is typically associated with a

detected peak. The overlap of these maxima within the same set is then assessed and discussed.

$$Overlap(m, z) = sgn((r_m + r_z)^2 - \mathbb{D}^2(m, z)) \qquad (3.10)$$

$$\mathbb{D}^2(m, z) = (\mathbb{t}_m - \mathbb{t}_z)^2 + (sc_m - sc_z)^2 \qquad (3.11)$$

$$r_m = \frac{uvN_{p_m}sc_m\sqrt{C'_m}}{\sqrt{u^2N_{p_m}^2 sin^2\theta_m + v^2 cos^2\theta_m}} \qquad (3.12)$$

$$C'_m = \frac{C_m - min(C)}{max(C) - min(C)} \qquad (3.13)$$

$$r_z = \frac{uvN_{p_z}sc_z}{\sqrt{u^2N_{p_m}^2 sin^2\theta_m + v^2 cos^2\theta_m}} \qquad (3.14)$$

where r shows the ellipse radius, $\mathbb{D}$ is the Euclidean distance, u and v are the adaptable spreading conditions defines the refinement sensitivity in time and scale respectively. N is the total count of peaks utilized. The $(r_m + r_z)^2$ represents the sum of normalized CWT coefficients assist to identify weak intensity peaks near high intensity peaks. If the connected points to the centroid is greater than a mentioned value, is termed as micro cluster, may be stated as the identification of an original peak. The separate points frame a new, small macro cluster where a new centroid is formed. The experiment proceeds iteratively until no additional clusters can be formed that meet the user-defined minimum number of peaks. It is visualized that the presented methodology has $O(M)$ complexity, where M represents the number of data points. The organization of presented methodology is structured in Fig 3.4, shows the flow of implementing the idea. An algorithm specifies the procedure followed using PCWA-MSG is depicted in Algorithm 3.1.
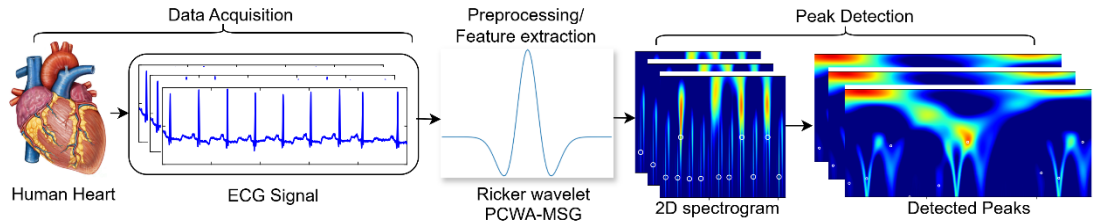
Fig 3.4 The layout of presented methodology for R-peak detection

Algorithm 3.1*: Parallel Cluster Wavelet with Multi-Spot Gaussian analysis for R-peak detection*

Inputs and Definitions
•   Load 1 minute ECG segment
• $x(\mathbb{t}) \rightarrow$ input signal
• $\psi(\mathbb{t}) \rightarrow$ Wavelet function
Output
•   Local maxima
•   Overlapping length
•   Clusters formation
•   R-peak detection

Step1: (i) Execute CWT using Ricker wavelet on ECG segment

$Ricker(t) = (1 - 2\pi^2 \mathbb{f}^2 \mathbb{t}^2) e^{(-\pi^2 \mathbb{f}^2 \mathbb{t}^2)}$

(ii) Convolution of scaled and dilated version of mother wavelet with raw ECG, noted the CWT coefficients.

$$CWT(sc, b) = \int_{-\infty}^{\infty} x(t) . \frac{1}{\sqrt{sc}} \psi\left(\frac{\mathbb{t} - b}{sc}\right) dt$$

$sc \rightarrow$ scale parameter, controls the width of wavelet.

$b \rightarrow$ dilation parameter, controls the position of the wavelet.

Step2: Marked the local maxima using CWT coefficients obtained.

(i)   Apply clustering algorithm.

➤   Initialize randomly k cluster centroids in same space.

➤   Assign the data points to the nearest cluster centroid.

$C_i = \{x_p : \|x_p - c_i\| \leq \|x_p - c_j\|\}$ for all j.

C_i depicts the cluster assigned to centroid c_i.

➤   Based on the mean of data points given to each cluster, estimate the centroids.

$$c_i = \frac{1}{|C_i|} \sum_{x_j \in C_i} x_j$$

Clustering aims to minimize the within cluster sum of squares,

$$\sum_{i=1}^{k} \sum_{x_j \in C_i} \|x_j - c_i\|^2$$

(ii)   Calculate the Euclidean distance for positioning ellipses around local maxima

$$\mathbb{D}^2(m, z) = (\mathbb{t}_m - \mathbb{t}_z)^2 + (sc_m - sc_z)^2$$

$m \; and \; z$ are the maximum and initial points.

(iii)   Overlapping of an ellipse with center generates a link.

$$Overlap(m, z) = sgn((r_m + r_z)^2 - \mathbb{D}^2(m, z))$$

Step3: For each macro cluster in **MACROCLUSTER**:

    if len (MACROCLUSTER) > scale:

        Calculate overlapping length and arrange

    else:

        Go to macrocluster

    End

    if len (overlapping length) > scale:

        mention micro cluster

    else

        delete overlap length of (MACROCLUSTER)

    end

    end

Step4: Identify the respective peaks associated with the micro cluster.

3.2.2.1 Clustered Inspection of multi-peak signals using Multi-Spot Gaussian (MSG) Wavelet

Multi-peak signals provide substantial benefits for practical sensor approaches. By incorporating repetition and modelling into the data, enhance the authentic detection of events amidst corrupted surroundings that suggests single peaks. Additionally, multi-peak signals facilitate multiple detection, as various targets may generate distinct signal structure. This capability is essentially valuable for biomedical applications. Here, executed the multi-spot gaussian (MSG) wavelet evaluated by the addition of N gaussians segregated by scale a and encompass by two negative skewed peaks which are explained as

$$\psi_N(\mathbb{t}, sc) = \sum_{n=0}^{N-1} exp\left(\frac{-\left[\mathbb{t}-\left(n-\frac{N-1}{2}\right)sc\right]^2}{2sc^2\sigma_+^2}\right) -$$

$$\sum_{k=\pm1} \frac{2c}{sc\sigma_-} \phi\left(\frac{\mathbb{t}+k\left(\sigma_-m_z-\frac{N}{2}\right)sc}{sc\sigma_-}\right)\Phi\left(k\alpha\frac{\mathbb{t}+k\left(\sigma_-m_z-\frac{N}{2}\right)sc}{sc\sigma_-}\right) \qquad (3.15)$$

Few parameters of skewed Gaussian functions are described as follows.

$$\phi(t) = \frac{1}{(2\pi)^{\frac{1}{2}}} exp\left(\frac{-t^2}{2}\right) \qquad (3.16)$$

$$\Phi(t) = \int_{-\infty}^{t} \phi(un)dun = \frac{1}{2}\left[1 + erf\left(\frac{t}{\sqrt{2}}\right)\right] \qquad (3.17)$$

$$m_z(\alpha) \approx \mu_z - \frac{\gamma_1 \sigma_z}{2} - \frac{sgn(\alpha)}{2} exp\left(\frac{-2\pi}{|\alpha|}\right) \tag{3.18}$$

$$\delta = \frac{\alpha}{\sqrt{1+\alpha^2}} \tag{3.19}$$

$$\mu_z = \sqrt{2/\pi} \tag{3.20}$$

$$\sigma_z = \sqrt{1 - \mu_z^2} \tag{3.21}$$

For positive peaks, the parameter σ_+ is structured to those considered from multi-peak signals calibrated to scale sc. To obtain optimal compactness and sensitivity, the parameters c and σ_- are evaluated according to the positive peaks. For acquiring high sensitivity of the wavelet to data points, the maximum point of gaussian functions at both ends are fixed at scale, sc. The zero mean state is applicable shown by the negative side peaks of the respective wavelet which is scaled for square norm of one. The peaks are identified according to the threshold value set. The weaker strength of peaks is also marked with stronger peaks convey the identification of low-quality ECG peaks. The location of the R-peak is identified by the high energy intensity of the peaks formed after converting to 2D format.

3.2.3 Distinct Datasets utilised for R-Peak Detection using PCWA-MSG

This section elaborates on the four datasets (Pre-term infant ECG [137], MIT-BIH Atrial fibrillation [36], MIT-BIH Malignant ventricular [34], and MIT-BIH Arrhythmia [35]) used for experimental calculation of R-peak detection using presented methodology. The records of the respective datasets are captured in Table 3.4.

Table 3.5 Description of datasets used for R-peak detection

Database	Total Duration (hrs)	Records	Labels	Episodes	Duration (hr:min:sec)	Sampling freq.
Preterm Infant Cardio-Respiratory Signals [137]	11:59:59:888	Infant_1	Normal	1	00:56:44.660	500 Hz
			Bradycardia	17	11:03:15.228	
	11:59:59.608	Infant_5	Normal	1	01:37:21.148	
			Bradycardia	13	10:22:38.460	
	11:59:59.910	Infant_7	Normal	1	00:33:29.170	
			Bradycardia	25	11:26:30.740	
	11:59:59.976		Normal	1	00:09:29.522	

		Infant_10	Bradycardia	14	11:50:30.454	
MIT-BIH Atrial Fibrillation Database [36]	10:13:43	06995	Normal	3	5:24:13	250 Hz
			Afib	6	4:49:18	
			AFL	2	0:13	
		08219	Normal	40	8:01:14	
			AFIB	39	2:12:29	
		08455	Normal	2	3:09:12	
			Afib	2	7:04:31	
		04908	Normal	5	9:18:07	
			AFIB	8	51:22	
			AFL	4	4:14	
MIT-BIH Malignant Ventricular Ectopy [34]	35:00	418	Normal	61	30:54	250 Hz
			VFL	60	4:06	
	34:37.192	429	VT	3	0:10	
			VFL	2	1:32	
			BI	12	30:08	
			Noise	6	3:10	
	31:48.304	610	Normal	12	22:35	
			VT	1	0:06	
			HGEA	11	10:57	
			Noise	2	0:25	
	33:38:536	615	VT	5	0:35	
			AFIB	6	34:25	
MIT-BIH Arrhythmia [35]	30:04.936	203	VT	21	0:33	360 Hz
			AFIB	21	24:15	
			AFL	2	5:14	
	30:04.997	207	SVTA	1	0:52	
			VT	2	0:28	
			VFL	6	2:24	
	30:04.828	217	VT	1	0:02	
			AFIB	24	4:12	
			B	9	0:42	
			P	33	25:10	
	30:05.164	222	N	32	15:57	
			SVTA	4	0:08	
			AFIB	24	1:44	
			AFL	42	7:03	

3.2.4 Experimental Results with computational complexity for R-peak Detection

The experimental setup utilized for detecting the R-peak is discussed. A comprehensive series of peak detection experiments and comparative evaluations over state-of-the-art methods are conducted for all datasets.

3.2.4.1 Time-scale characterization of ECG records using PCWA-MSG

The isolated capability of the PCWA-MSG methodology to identify both single and multi-peak ECG signals utilizing customized wavelets presents the primary outcome of the script. The direct way to identify the peaks is utilizing the threshold of peak counts above the background. The 2D formation is evaluated using a Ricker wavelet and experimented on multiple ECG databases to prove the robustness of the presented methodology which will be helpful in detecting the corresponding heart disease. The PCWA-MSG is implemented over pre-term infant ECG dataset of duration 1 $minute$ 8 $seconds$ depicted in Fig 3.5(a), results in the 2D representation of time-scale pattern, identifies the high intensity peaks according to the threshold value set. The ECG signal is framed as bright streaks and the scaled locations with the highest CWT coefficient associated to true peaks which are marked with white circles in Fig 3.5(b). To demonstrate deeply, select an ECG segment of 10 seconds in Fig 3.5(c), pointed the local maxima with white dots in the 2D map is detected at each scale with the traditional peak detecting procedure shown in Fig 3.5(d). The macro clusters are formed which are separated by gaps along the time axis by greater than some default value. $\mathbb{D}$ and r are the Euclidean distance and radius of the ellipses respectively. Fig 3.5(e) depicts the micro-clusters identification, represents the number of points connected to the centroid is higher than a preset value.
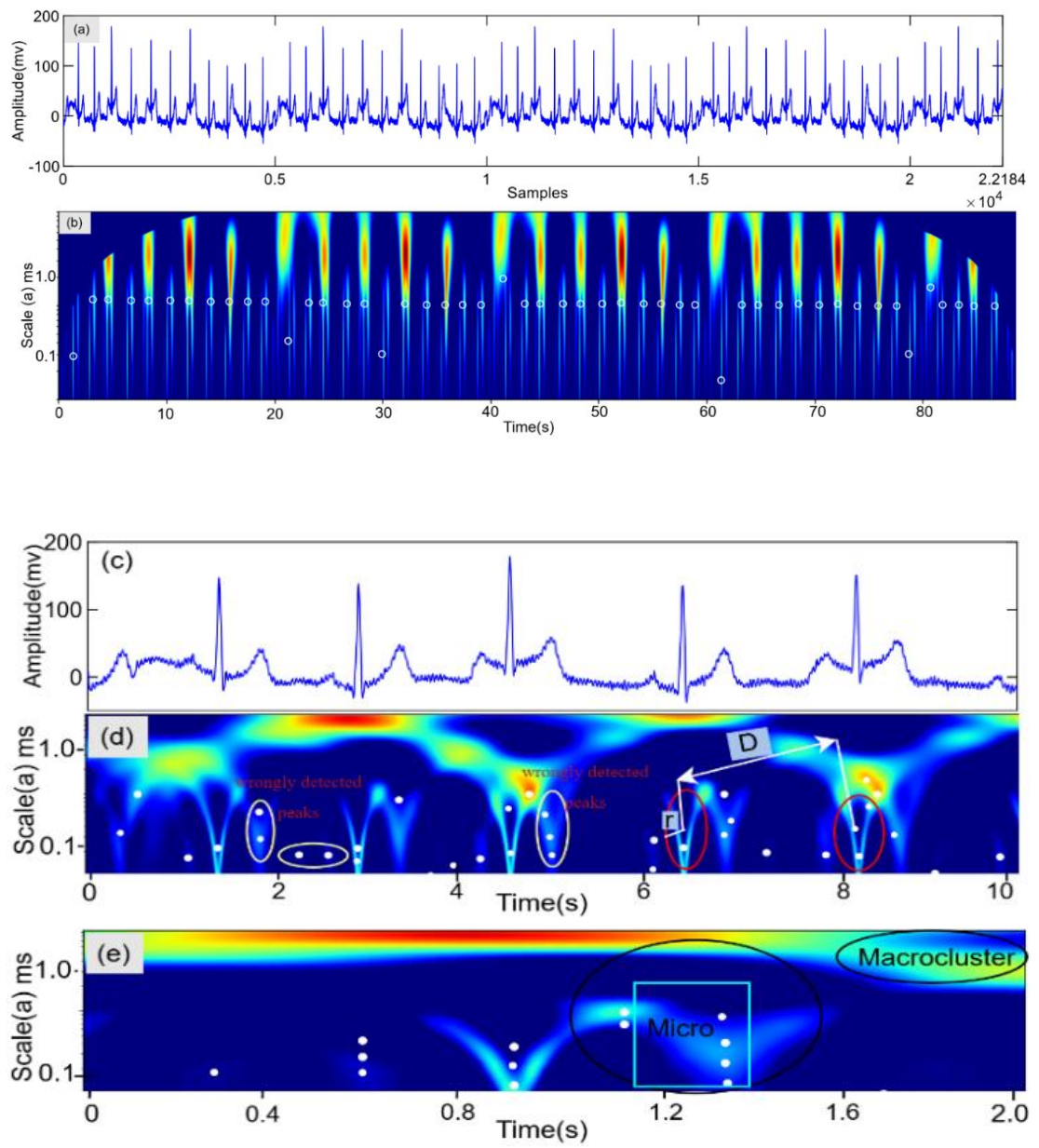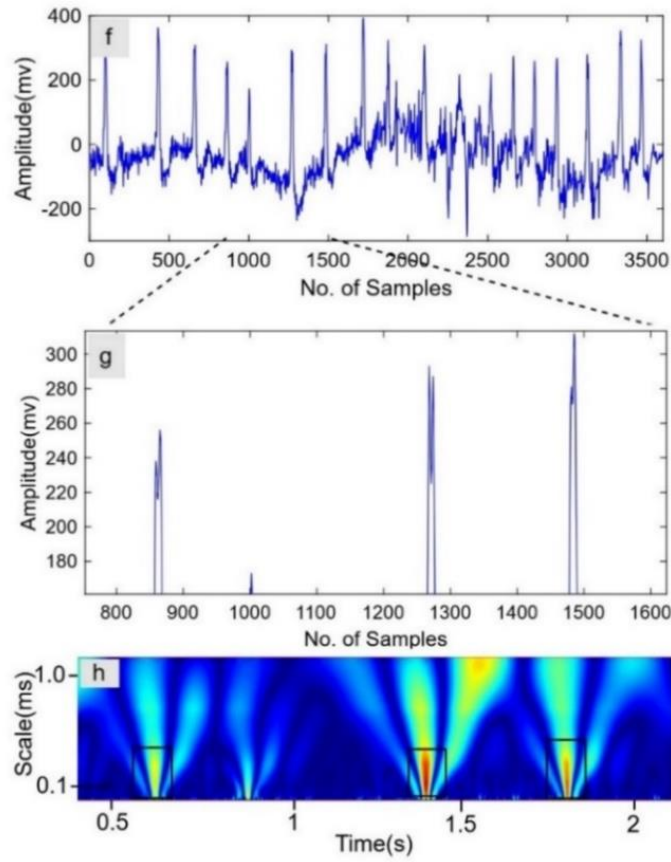
Fig 3.5 (a) ECG data of Pre-term infant *(inf_5)* of duration 1min 8sec (b) Time-scale representation indicates the preferred local maxima points marked with the circles detected through the implementation of PCWA-MSG methodology. The circles determine the high intensity peaks according to the threshold value set (c) A duration of 10 sec ECG segment is fetched from the *(inf_5)* ECG dataset. (d) The local maxima points are mentioned. The clustering process employs Euclidean distance between ellipses, positioning them around each local maximum to identify potential links. A link is an overlap of an ellipse with the centroid point (e) The macro and micro clusters are noticed with black and light blue color respectively. (f) Multi-peak ECG signal of MIT-BIH_203 record. (g) The zoomed ECG multi-peaks depicted. (h) Reflects the single predominant bright spot, illustrate the coherent peak detection and outstanding localization on time scale axes, proportional to accurate identification of peaks with intensity.

The MIT-BIH ECG signal (record 203) of 10sec duration is presented in Fig 3.5(f) from which a 2sec ECG segment is selected, and represents the multi-peaks in Fig 3.5(g). Fig 3.5(h) depicts the CWT map acquired from the custom MSG mother

wavelet. It shows a single dominant red spot that elaborates on the acute detection and localization on both the time and scale axes, proportional to the correct identification of the R-peaks with intensity. A high accuracy is noticed using the PCWA-MSG methodology, approximately 4.3% more peaks are detected as compared to conventional techniques, seemed faster and accurate than other techniques. The implementation is performed on Python with 100 logarithmic scale values on 11th Gen Intel® Core™ i7-11370H@3.30GHz. The remarkable capability of the presented methodology to identify multi-peak signals utilizing customized wavelets portrays the distinctive outcome of the methodology. Table 3.5 depicts the R-peak detection performance over four utilized distinct ECG database. From the results, it is visualized that PCWA-MSG attained the topmost accomplishment on Pre-term infant dataset with an *Acc* and *F1-sc* of 99.99% and 99.75% respectively. The main objective of implementing the presented methodology is to detect the R-peaks from a low-quality ECG signal is achieved. It remarkably misses less than 1% of the total arrhythmic beats present. The capability of accurately identifying these irregular events, which can be indicators of underlying cardiac conditions, is a crucial strength of methodology, setting it apart from other state-of-the-art methods that may fail to identify arrhythmia events. The detection error rate helps to find the identification rate of true R-peak in ECG signal. The performance of particular methodology can be scrutinized over detection error rate achieved in that case.

The methodology reduced the FPs and FNs by more than 67% and 91% respectively. This shows the detection of real peaks over such low-quality ECG signal. The ability to reliably locate the peaks of these irregular beats is essential for fulfilling the ultimate goal of an automated ECG analysis and diagnosis of potential arrhythmic conditions. The computation time is the time required to implement a specific method over ECG signals. A significant improvement in computational time for identifying R-peaks, compared to existing methods, is observed in Table 3.6.

Table 3.6 Performance analysis of PCWA-MSG over distinct dataset for R-peak detection.

Data set	Record No.	Total peaks	TP	FN	FP	Sens (%)	Prec (%)	F1-sc (%)	Acc (%)	DER
Pre-term Infant Ectopy DB	Infant1_ecg	10799972	10799734	238	383	99.78	99.64	99.70	99.99	0.01
	Infant5_ecg	10799902	10799535	367	421	99.63	99.58	99.60	99.84	0.16
	Infant7_ecg	21599955	21599526	429	687	99.62	99.39	99.50	99.89	0.11
	Infant10_ecg	21599988	21599716	272	524	99.74	99.51	99.62	99.78	0.22
MIT-BIH Atrial Fibrillation DB	AFIB_06995	6274349	6273476	873	1012	99.98	99.82	99.89	99.98	0.20
	AFIB_08219	6086765	6085492	1273	7251	99.97	99.89	99.91	99.86	0.14
	AFIB_08455	2850351	2847889	2462	9342	99.91	99.67	99.78	99.58	0.42
	AFIB_04908	8797787	8792160	5627	12370	99.93	99.85	99.90	99.79	0.21
MIT-BIH Malignant Ventricular DB	Malign_418	401423	401106	317	869	99.92	99.78	99.84	99.70	0.3
	Malign_429	519298	518695	603	1293	99.87	99.75	99.80	99.63	0.37
	Malign_610	477076	476543	533	952	99.86	99.80	99.82	99.68	0.32
	Malign_615	504634	504048	586	1048	99.88	99.79	99.83	99.67	0.33
MIT-BIH Arrhythmia DB	203	649777	649671	106	137	99.79	99.76	99.71	99.84	0.16
	207	649799	649706	93	118	99.83	99.81	99.79	99.82	0.18
	208	649935	649823	112	133	99.80	99.78	99.76	99.87	0.13
	212	649945	649819	126	148	99.81	99.84	99.75	99.81	0.19

Table 3.7. Summary of comparison between executed method and existing methods over different datasets.

Year	Dataset	Methodology	TP	FP	FN	Sens (%)	Prec (%)	Acc (%)	DER	Computation Time
(2021) [154]	MIT-BIH Arrhythmia DB	Adaptive Threshold	3037	9	13	99.65	99.69	NR	NR	NR
(2022) [53]		NEO-CCNN	109342	112	152	99.87	99.90	99.77	0.23	6.44 sec for 30 min ECG
(2023) [58]		ST-Res U-net	49592	64	120	99.76	99.87	99.63	0.37	360 ms for 30 min ECG
(2022) [155]		1D-CNN	109,304	182	171	99.85	99.82	NR	NR	202 msec for 20 sec ECG
(2022) [156]		FrFT + PCA	1,10,084	FN+FP= 138		99.93	99.95	99.88	0.12	NR
(2022) [157]		SWT	109,403	90	78	99.93	99.92	NR	NR	NR
(2023) [158]		VMD + HT	109,496	86	289	99.77	99.91	99.68	0.32	NR
(2021) [159]		Moving average + Adaptive Threshold	109,258	238	708	99.36	99.78	99.14	0.86	NR
(2022) [160]		Fuzzy clustering	109303	125	191	99.81	99.88	NR	NR	4.07 sec without VF
Presented work		PCWA-MSG	638943	148	117	99.83	99.78	99.91	0.09	103 ms for 30 min ECG
	Pre-term		10799734	383	238	99.78	99.64	99.99	0.01	270 ms for 30 min ECG
	AF DB		6085492	3254	649	99.97	99.89	99.86	0.14	193 ms for 30 min ECG
	Malignant DB		401106	869	317	99.92	99.78	99.74	0.26	117 ms for 30 min ECG

71

3.2.4.2 Computation Time evaluated over implementation of PCWA-MSG

The executed methodology is implemented using Python and Visual Studio Code. The evaluation is noted in the manuscript accomplished on NVIDIA GeForce RTX 3070 Graphic Card. The validation of model is prepared by CUDA kernels. For overall verification and testing, it utilized about 9 msec for 1 minute ECG fragment, whereas P&T model utilized around 71 msec to perform on an ECG fragment of the same length. The predominant feature and merits of the presented methodology is its fast processing for R-peak identification. The same process is verified over single-CPU, shows the total time for 1 minute ECG fragment to detect the peak locations is about 549 msec which reflects an approximate 50 times of the real time speed.

3.2.5 Ablation Study

An ablation study concerns with conducting number of experiments by consistently modifying or removing different components of a model and correspondingly noticed the performance at each observation.

3.2.5.1 Implementation of Shift Multiply Algorithm for R-peak detection

Earlier, the multi-peak signals are identified for multiplex detection utilizing a shift-multiply algorithm. Depending upon the recursive shift of a selected multipeak event by scale sc and multiplying an altered information with each other. The augmented outcome results in remarkable SNR refinement in comparison to purely threshold-based technique. FDR is the false discovery rate, shows the ratio of false positives to the total of false positives and true positives. Table 3.7 explains the performance comparison of evaluated methods with presented methodology.
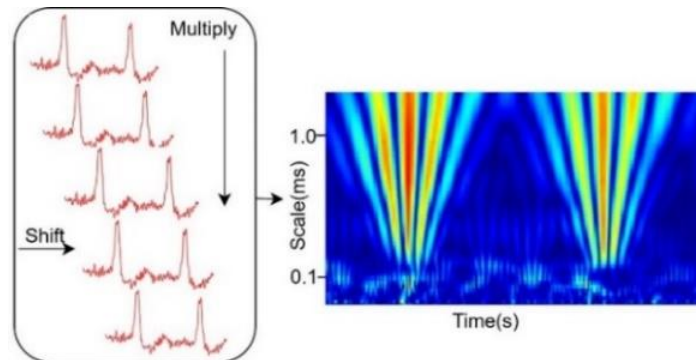
Fig 3.6 Shift-multiply algorithm analysis

3.2.5.2 Execution of Haar wavelet for R-peak detection

The demonstration is improved over shift-multiply algorithm by utilizing a customized wavelet. The implementation of Haar wavelet over MIT-BIH 203 record is performed. The pattern formation gets blurred because of noisy data and therefore, the lobes information is unable to detect the R-peaks. Hence, it is not possible to achieve the desired outcome with Haar wavelet over low-quality ECG signals.

Fig 3.7 PCWA-Haar wavelet analysis

3.2.5.3 Execution of Morlet wavelet for R-peak detection

The improvement over the Haar wavelet is proved with the implementation of Morlet wavelet, commonly used in CWT analysis, results in multiple red spots over multi-peak ECG signal. Therefore, a precise information is unable to achieve as the information is scattered in different lobes in case of multi-peak ECG signal.
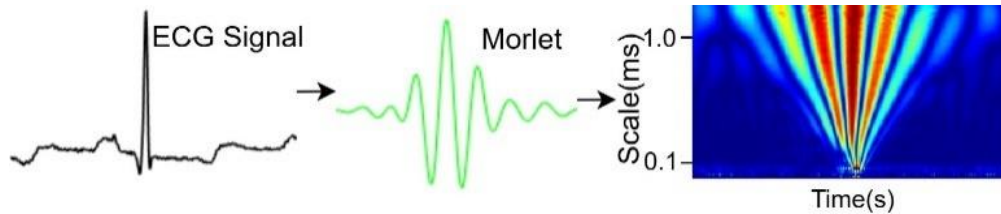
Fig 3.8 PCWA-Morlet analysis over ECG signal

The best part of it is to gather the peak identification status from a single point but reduces the low-quality ECG peak identification.

Table 3.7. Summary of performance comparison using different wavelets for R-peak detection

	Shift-Multiply	PCWA-Haar	PCWA-Morlet	PCWA-MSG
Total detected peaks	32	63	179	257
TPR	0.123	0.242	0.688	0.988
FDR	0.025	0.013	0.017	0.003
Accuracy (%)	58.7	33.6	76.3	98.6

3.2.6 Discussions

We performed a shift-multiply algorithm over MIT-BIH 203 record represents the multi-peak ECG signal, reflects the scattered wavelet pattern identifies the multiple spots with distracted information of identified peaks. The accuracy achieved in identifying the ECG peaks is 89%.

Computational complexity of Ricker wavelet

The Ricker wavelet in parallel cluster wavelet analysis itself is just a mathematical function: $\psi(t) = (1 - \frac{t^2}{\sigma^2})e^{-t^2/(2\sigma^2)}$

Computing this function at a single time sample is O(1) (constant complexity). The Ricker wavelet alone has O(1) per-sample cost, but when used in a CWT its computational complexity is O(NS²) for time-domain convolution and O(NS log N) with FFT-based convolution, where N and S represents the number of samples and number of scales respectively.

3.2.7 Summary for the detection of R-peaks using PCWA-MSG

The work presents a novel methodology (PCWA-MSG) using Ricker wavelet for R-peak detection over low-quality time-domain ECG signal, which shows the prominent peaks in an ECG signal depicting ventricular contractions of the heart. It is an unsupervised methodology that works parallelly over multiple signals at a time. The methodology is constructive for low-quality multi-peak ECG signals. The R-peak detection is considered as a 1D segmentation task. The requirement of post-processing step is eliminated with the executed methodology. It demonstrates superior performance by reducing the FPs and FNs, when compared to the state-of-the-art methods for R-peak detection. The substantial reduction in false negatives presents the undetected beats, is a critical improvement offered by PCWA-MSG methodology.

Chapter 4

ECG-BASED EARLY DETECTION AND MULTICLASSIFICATION OF ARRHYTHMIA

Early detection of heart related disease plays a pivotal role in human life. Having an idea about the heart disease at an early stage can save someone's life and avoid the mishappening that can occur in future. Cardiac arrhythmia is caused due to the irregularity of the heartbeat, and heart rhythm, which increases the complications leading to the risk of heart strokes [46]. Several artifacts are present in ECG signal, such as power line interference, baseline wander, and others, that deteriorate the performance of overall system; therefore, some denoising techniques can be implemented to minimize the effect and upgrade the efficacy of the system.

The proposed technique GSMD is utilised for decomposition of time-domain signal into different frequency bandwidths. The technique is novel as it works over fixed number of decomposition levels instead of adaptive number of levels. It is used to decompose the time-domain signal into different frequency bandwidths which helps to provide all the information related to that particular segment. It is advantageous because it works over fixed number of frequency bands whereas the existing methods of decomposition works over the adaptive number of frequency levels.

The term SLT is being performed over the frequency bands obtained using GSMD and attained the high resolution of R-peaks that helps to detect the irregularity in the ECG signal. The combined form GSMD+SLT provides the high resolution 2D images with sharp, and acute peaks which is necessary for detection of disease at an early stage to avoid any mishap.

4.1 Group Sparse Mode Decomposition and High-Resolution-Based Technique for Multilevel Classification of Cardiac Arrhythmia

Atrial fibrillation and ventricular fibrillation are the most prevalent cardiac arrhythmia. Timely and precise detection of arrhythmia reduces mortality rates which are essential

to prevent various heart diseases. The work utilizes the Group Sparse Mode Decomposition technique for decomposing the non-stationary ECG signals into the intrinsic mode functions (IMFs). Then, the super-resolution technique is applied to obtain time-frequency spectrograms corresponding to IMFs generated using GSMD. The spectrogram conveys the information related to transient events or the sudden changes in frequency. Basically, it provides the energy intensity of the particular event when occurs. The SLT is a high-resolution technique used to reshape the 1D ECG signal into a 2D pattern. The spectrograms obtained through SLT, are fed to the deep neural networks for arrhythmia classification. The classification is done between healthy heart, atrial fibrillation, and ventricular fibrillation.

4.1.1 Introduction

A decomposition technique is useful in arrhythmia classification as it helps in analysing and extracting meaningful features from complex and often noisy ECG signals. The most prevalent method is empirical mode decomposition (EMD), used to decompose the ECG signal into IMFs [161] resulting in the recursive sifting scheme. There is an issue of mode mixing or mode splitting in EMD, which causes uncertainty in explaining the acquired modes. To deteriorate the effects of mode mixing or mode splitting and end effects, compact EMD (CEMD) is introduced in [162]. The technique includes two parts (i) the highest frequency sampling to produce pseudo extrema for unique detection of upper and lower envelopes (ii) a cluster of 2N algebraic equations for identifying the maximum envelope at every decomposition step. Somehow, the above technique lags behind in finding the precise value while implementing over corrupted signals. The limitation of CEMD tried to overcome with use of successive variational mode decomposition (SVMD) [163] that results in the extraction of extra signals that leads to the generation of excess noise, due to which SVMD suffers from mode splitting of wideband modes. Above all, to analyse the nonlinear data, a set of a small number of band-limited Fourier intrinsic band functions (FIBFs) are generated by a Fourier decomposition method (FDM) [164]. A detailed discussion of decomposition techniques for nonlinear ECG signals is given in [161], [162], [163],

76

[164]. As Fourier analysis is not the best method for decomposition, so, for accurate results, the GSMD technique [165] is evolved, where IMFs are estimated utilizing a set of ideal filters in the frequency domain. The idea of this article comes with the development of research in the detection and classification of arrhythmia is as follows:

1) The GSMD technique is employed to decompose the nonstationary ECG signal into a set of basic function, IMFs and employs a set of ideal filters with the weighted l_0 norm as a penalty term to develop an efficient model.

2) A high-resolution technique, superlet transform (SLT) is applied for denoising purposes, detection of QRS complexes, and to transform the nonlinear data into 2-D time–frequency (TF) representation that will be useful for arrhythmia detection and classification.

3) A combination of GSMD with SLT over Physionet and the combined dataset (Physionet + Mendeley-II) is initiated to categorize the ECG data into healthy heart, CU ventricular, and atrial fibrillation (AF) classes.

4) Deep neural network (VGG19, RESNET 18, GoogleNet, and AlexNet) are implemented on transformed signals for arrhythmia classification.

4.1.2 Mathematical modelling of Group Sparse Mode Decomposition

A method based on the decomposition of non-linear signals is utilized, resulting in the generation of IMFs, which have a smaller bandwidth, and the frequency bands of IMFs are displaced from each other. It has been initiated to calculate the IMFs using a set of ideal filters and utilizing the weighted penalty l_0-norm. On the basis of energy detection over short windows, weighting parameters and regularization parameters are calculated. A non-linear signal $z(t)$ is represented in this script [165] utilizing the equation

$$z(t) = p(t) + q(t), \qquad t = 1, \dots. N \tag{4.1}$$

Here, N denotes the count of samples, $q(t)$ shows the additive white noise with variance σ_v^2 having zero mean, and $p(t)$ is a non-linear signal comprised of a set of F basis functions, termed as intrinsic mode function [166], IMFs represented by

$$\{h_f(t)\}_{f=1}^F, \text{i.e } p(t) = \sum_{f=1}^F h_f(t), \qquad t = 1, \dots. N \tag{4.2}$$

Here, $\tau(.)$ has been chosen as the Discrete Cosine Transform (DCT) [167]. DCT is used due to a property of energy compaction and deals with reflective boundary conditions that help to remove the artifacts during the analysis of the signal as compared to the DFT [168]. The coefficients of DCT are real-valued as compared to DFT which is normally complex. Mentioning $\tau(.)$, a linear transformation on eq. (4.1) and (4.2), we obtain the corresponding calculation in the frequency domain,

$$d_z = d_p + d_q = \sum_{f=1}^{F} d_{h_f} + d_q \qquad (4.3)$$

where the DCT coefficients of d_z, d_p, d_q, and d_{h_f} are $d_z \in S^N, d_p \in S^N, d_q \in S^N$, and $d_{h_f} \in S^N$ respectively. Referring $R_f \subset [1, N]$ as a support to d_{h_f} represent the indices of non-zero entries and the total of indices in R_f is shown by $|R_f|$. The mode $h_f(t)$ is primarily estimated as

$$\widehat{h_f}(t) = \tau^{-1}(r_f \circ d_z), f = 1, \dots F, \qquad (4.4)$$

where $\circ$ shows the Hadamard product (multiplication of element to element) and the DCT coefficient vector of an ideal filter is r_f mentioned as $r_f[i] = \begin{cases} 1, & i \in R_f \\ 0, & \text{otherwise} \end{cases}$

From eq. (4.3) and (4.4), the estimated value of d_p is discussed as

$$\widehat{d_p} = \sum_{f=1}^{F} d_{h_f} = \sum_{f=1}^{F} d_z \circ r_f = d_z \circ r \qquad (4.5)$$

where $r := \sum_{f=1}^{F} r_f = \begin{cases} 1, & i \in R_f \\ 0, & \text{otherwise} \end{cases}$ and the support of d_p is $R := \cup_{f=1}^{F} R_f$.

It is recommended to calculate the estimated value of the general filter r as an ideal filter which reduces

$\left\| d_z - \widehat{d_p} \right\|_2^2 = \| d_z - d_z \circ r \|_2^2$ with the limitation that r is an on-off group sparse vector that comprises zeros and ones, where ones tend to focus in clusters. Every single filter r_f can be approximated as a category of contiguous samples in r, in total, they are equal to one. With this, an estimated number of modes F can be done directly with the number of groups r and the bandwidth of each filter r_f is modified accordingly. By resolving the optimum value, it is recommended to evaluate the ideal filter bank r, is defined as

$$\hat{r} = arg \min_r \tau(r) := \| d_z - d_z \circ r \|_2^2 + \lambda \| r \|_{o,w} \qquad (4.6)$$

where λ denotes the regularization parameter, that limits the trade-off between accuracy of the regular data, recorded by $(\|d_z - d_z \circ r\|_2^2)$ and the on-off group sparsity of the filter bank calculated by the weighted l_0 norm, $(\|r\|_{o,w} := \sum_{i=1}^{N} w_i \pi_{\{r_i\}})$ and a group of positive weighting conditions is denoted by $\{w_i\}$. The value of λ is chosen wisely for attaining the desired outcome of the filtered signal.

Some of the key features of GSMD are discussed.

1) To observe the presence of IMFs in the frequency domain, the opinion of group sparsity was applied.

2) To strengthen the on-off group sparsity of the ideal filters, utilized the weighted $l0$-norm as a penalty term.

3) Based on the energy concentration of every single IMF, bandwidth is automatically modified by selecting the weighting parameters.

4.1.3 High-Resolution Superlet Transform

A superlet transform [169] can be defined by a Morlet wavelet representing the multiplication of plane waves with a Gaussian envelope. The normalization constant of the Morlet wavelet is used to remove its mean and becomes negligible when the wavelet is broad. An improved Morlet wavelet is defined as

$$\Psi_{f,r}(t) = \frac{1}{B_r \sqrt{2\pi}} e^{\frac{-t^2}{2B_r^2}} e^{j2\pi ft} \tag{4.7}$$

$$B_r = {}^{r}\!/_{kf} \tag{4.8}$$

where f represents the central frequency, r shows the no. of cycles, and the time spread parameter, B_r is inversely proportional to the variation in frequency. k and r are the design parameters. Wavelet normalization is the salient feature to study as it calculates the capability of the time-scale characterization to demonstrate the distinct properties of data. It is suggested to merge Fourier-based spectrograms acquired with the varying lengths of the window, and this technique was named "Super-resolution" because it can localize oscillation packets in both time and frequency simultaneously [169]. To upgrade the resolution, various spectrograms are merged by calculating their Geometric Mean which is analogous to the Minimum Mean Cross-Entropy (MMCE). The Morlet method can be described as follows:

With the rise in the central frequency of the wavelet, the Morlet with a fixed number of cycles gives multiscale standard sense with constant relative temporal resolution but decreases the frequency resolution. On raising the time spread parameter (more cycles), the frequency resolution increases while decreasing the temporal resolution. The resolution can be increased by combining the short wavelets having high temporal resolution with the long wavelets having a high-frequency resolution. The main objective of the Superlet transform is to utilize multiple wavelets with fixed centre frequency occupying a range of different cycles [169] defined by

$$SL_{f,o} = \{\Psi_{f,r} | r = r_1, r_2, \dots r_o\} \tag{4.9}$$

where o represents the order shows the number of wavelets having central frequency f; $r_1, r_2, \dots. r_o$ is the number of cycles in the set that varies from 1 to o. The different additive or multiplicative ways, help to choose the number of cycles which defines the wavelet. In additive Superlet, $r_i = r_1 + i - 1$ for $i = 2,3, \dots. o$. In multiplicative, $r_i = i. r_1$. The response of the Superlet is defined as the Geometric Mean of the individual responses of the wavelets.

$$R[SL_{f,o}] = \sqrt[o]{\prod_{i=1}^{o} R[\Psi_{f,r_i}]} = \sqrt[o]{\prod_{i=1}^{o} \left| \sqrt{2} \frac{1}{a} \int_{-\infty}^{\infty} s(\tau) \Psi_{f,r_i} * \left(\frac{\tau - t}{a}\right) d\tau \right|} \tag{4.10}$$

where $R[\Psi_{f,r_i}]$ is the response to the signal from i_{th} wavelet which is the magnitude of the complex convoluted wavelets is defined in eq (4.11),

$$R[\Psi_{f,r_i}] = s(t) * \Psi_{f,r_i}(t) = \frac{1}{a} \int_{-\infty}^{\infty} s(\tau) \Psi_{f,r_i} * \left(\frac{\tau - t}{a}\right) d\tau \tag{4.11}$$

The wavelet $\Psi_{ri}(t)$ of i_{th} order in an SL is shown,

$$\Psi_{r_i}(t) = \frac{kf}{r.i.\sqrt{2\pi}} e^{\frac{-1}{2}\left[\frac{kft}{r.i}\right]^2} e^{j2\pi ft} \tag{4.12}$$

At the central frequency f, the SL evaluates the presence of oscillation packets in the signal. The order 1 of SL indicates CWT and signal representation is sharp for higher-order SLT.

Adaptive SLs: Adaptive Superlet is an altered form that changes its order to the central frequency to compensate for the higher wavelet bandwidth with higher frequency. The

low frequencies can be estimated by fixing the order low of ASLT. The order of ASLT, which is dependent on the frequency, increases to attain the exact TF resolution shown in eq (4.13), SLT is used for narrowband frequency range whereas ASLT is used for wide frequency range.

$$ASLT_f = SL_{f,o} = a(f) \qquad (4.13)$$

4.1.4 Implementation of GSMD for decomposition of ECG signal

Here, the GSMD algorithm is utilized to segment the non-stationary ECG signals into IMFs, which have finite bandwidth and the frequency bands are disjoint. IMFs are calculated using a set of ideal filters with a weighted penalty term. The two datasets are used in the study to demonstrate the robustness, reliability, and efficiency of the presented algorithm. The first dataset is fetched from the physionet and the second dataset is the combination of the physionet and the Mendeley-II dataset. The data is categorized into three classes, Healthy (MIT-BIH Arrhythmia DB), AF (MIT-BIH AF DB), and VF (MIT-BIH Ventricular Fibrillation DB). Initially, segmentation is performed on the records of both the datasets and segmented into a 10-second duration to increase the quantity of ECG data. The segmented ECG signal is then applied to the GSMD algorithm that generates several decomposition levels. Various combinations are made on these levels to obtain the noiseless data which is used further for transforming the time domain signal into a time-frequency (TF) energy spectrogram. A high-resolution technique, Superlet transform is applied which is a combination of Fourier-based spectrograms acquired with a long and short window, or with a set of windows of different sizes. It is used to convert the 1D ECG signals into 2D energy plots and the resolution of an obtained image is increased after combining the multiple spectrograms by calculating their geometric mean, which is identical to the minimum mean cross entropy. With these representations, the details on time, frequency, and energy characterization related to arrhythmia diseases are evaluated. The obtained spectrograms are then fed to the deep neural network for arrhythmia detection and classification. A multilevel classification is performed which classifies the data into multiple classes, Healthy, AF, and VF. A few points are mentioned as follows.

(i) The requirement of an extra denoising step of pre-processing is eliminated by the

use of SLT after decomposition by GSMD. The noise including the baseline drift, electrode motion artifacts, and powerline interference is suppressed which reduces the overall complexity and increases the efficiency.

(ii) The dislocation of ECG peaks is recovered, thus, the detection of QRS complexes is fulfilled by the use of Superlet transform.

The implementation of GSMD+SLT generates the spectrograms from calculated IMFs is described in Algorithm 4.1.

Algorithm 4.1: Implementation of GSMD +SLT for decomposition and denoising of ECG signal

START program; LOAD ECG data
INITIALISE function GSMD
For $k = 1: k_{max}$
Calculate $g = \frac{1}{B_t} \sum_{t-b_t^k}^{t+b_t^k} d_z^2[\tau]$ where $B_t = 2b_t^k + 1$
Evaluate $\lambda = \left(\frac{2\widehat{\sigma_v}^2}{B_t}\right) \Gamma^{-1}\left(\frac{B_t}{2}, \alpha\Gamma\left(\frac{B_t}{2}\right)\right)$
Update $r_t^k := \begin{cases} g > \lambda, r_t^k = 1 \\ r_t^k = 0, otherwise \end{cases}$
Update $k: k_t = kurtosis\left(d_z[t - b_t^k : t + b_t^k]\right)$
Adjust $r^k, d_z^2, \widehat{\sigma_v}^2, \alpha$
CONSTRUCT the f ideal filter r_f; Set $r_f = 0$, update $r_f = 1$
Construct the DCT coefficient vector of $\widehat{h_f}(t)$: $\widehat{d_{h_f}} = r_f \circ d_z$
FORMULATE the matrix of IMFs
$H \in S^{\hat{f} \times N}: H = [\widehat{h_1}(t); \widehat{h_2}(t); \ldots ; \widehat{h_{\hat{f}}}(t)]$
CONSTRUCT the denoised signal: $\hat{p}(t) = \sum_{f=1}^{\hat{f}} \widehat{h_f}(t)$
INITIALISE function SLT.
Calculate the response of SL, $R[SL_{f,o}] = \sqrt[o]{\prod_{i=1}^{o} R[\Psi_{f,s_i}]}$
INITIALISE frequency resolution ranges from [10 to 90]
CALCULATE Geometric Mean and the wavelet coefficient of the revised spectrogram of individual wavelets.

4.1.5 Computational complexity of GSMD and SLT

The computational complexity of the method describes the number of resources required to run it. The time complexity of the methods is discussed in Table 4.1.

Table 4.1 The Computational Complexity of GSMD and SLT

(i) Kurtosis: $\text{TC}(k\bar{v}) = 4nADD + 2nMUL + 2DIVI$

n → number of samples, k→ number of iterations.

ADD → Addition; MUL→ Multiplication

DIVI→ Division; COMP → Comparison

Variance: $TC(\widehat{\sigma_v^2}) = 3nADD + nMUL + 2DIVI$

(ii) Total time-complexity of GSMD

$\cong [11k + 4\hat{J} + 4 + (7M_l + 12L_{max} + 20).k_{max}).n]$

$TC \cong (7M_l + 12L_{max} + 20).k_{max}.n$

k_{max}→ the maximum number of iterations

L_{max} → maximum number of blocks used in filter bank.

$\hat{J}$ → the number of estimated IMFs,

$M_l := 2m_l + 1$, where m_l is the largest value of m.

Time-complexity of SLT:

(i) Morlet wavelet complexity:

$TC = (4n + 6)MUL + (4n + 2)ADD$,

n→ the shaping factor in Morlet wavelet.

The various steps involved in arrhythmia classification are represented in Fig 4.1 which shows the data acquisition, segmentation of ECG records, implementation of GSMD+SLT followed by the classification using deep neural networks. From the literature, it is noted that the non-linear ECG signal shows the occurrence of noisy data mixed with the original signal, due to which there are more chances of missing out of QRS peaks. To verify the existence of several peaks at specific points, a frequency spectrum is calculated of every individual intrinsic mode function. From the above characterization, it has been shown that GSMD with SLT demonstrates a better result that can be seen in a 2D image in all the cases. The various steps involved in the overall process of classification are represented in Fig 4.2.
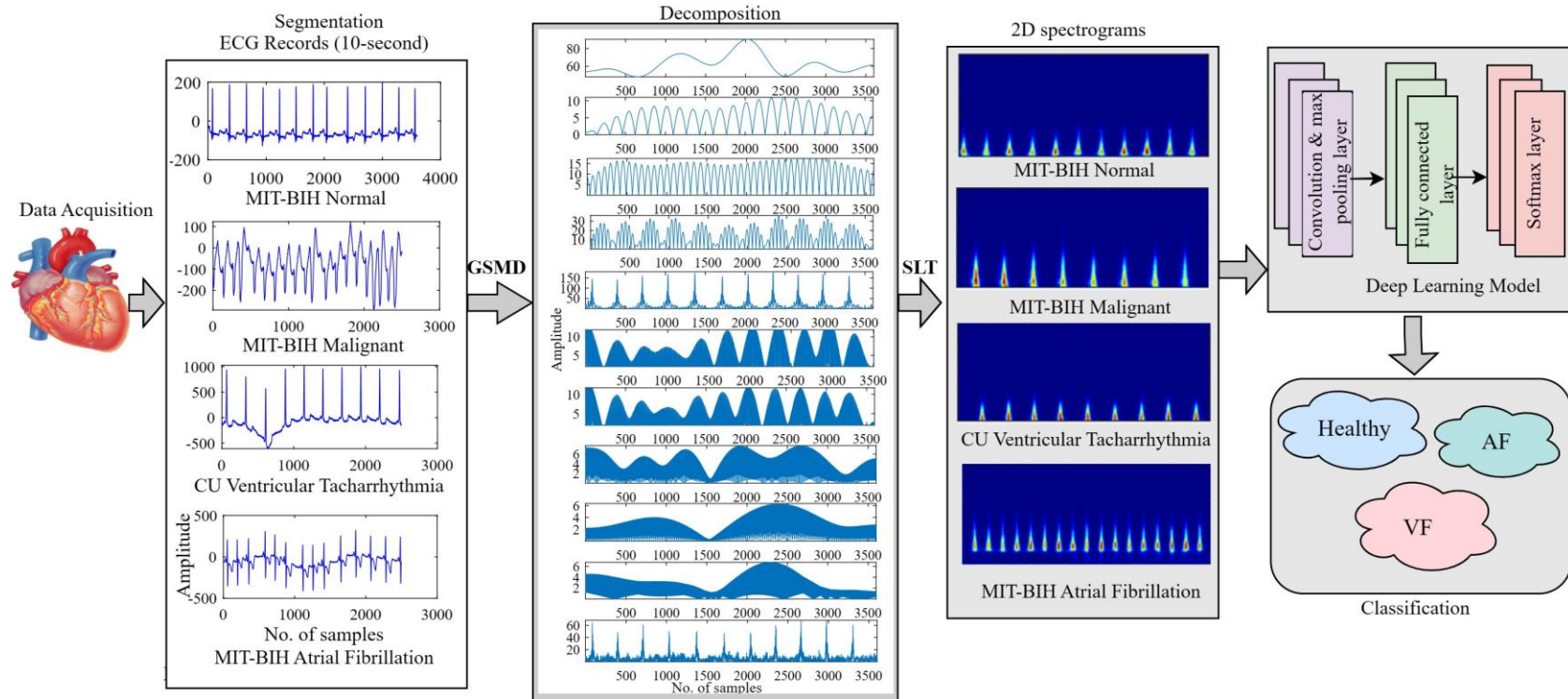
Fig 4.1 The presented methodology GSMD+SLT for arrhythmia detection and classification using deep neural network

(a) MIT-BIH arrhythmia of record 100

(b) Decomposition levels obtained by GSMD

(c) Representation of IMFs in 3D

(d) Denoised signal after combination of decomposition levels

(e) Spectrogram generated using SLT
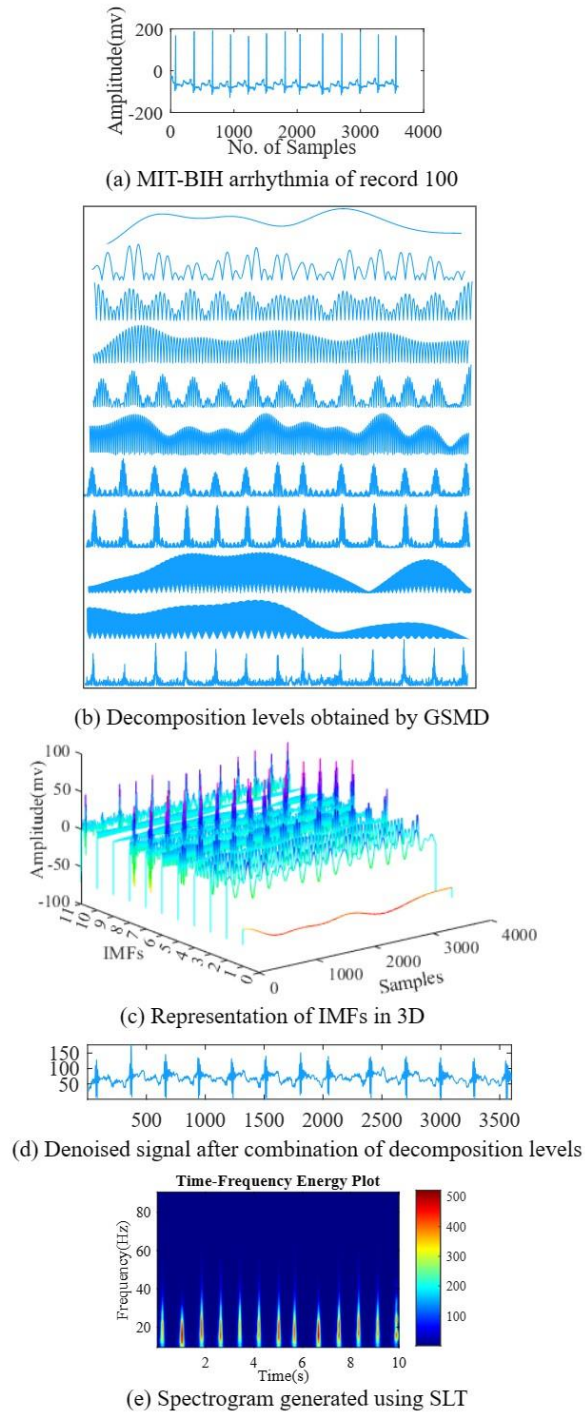
Fig 4.2 (a) The uppermost panel reflects the noisy ECG signal of record 100 from MIT-BIH arrhythmia database. (b) Depicts the IMFs generated from GSMD. (c) A 3D view of IMFs is shown. (d) Depicts a denoised signal estimated from different combinations of IMFs. (e) 2D spectrogram generated from SLT.

4.1.6 Classification Techniques used for arrhythmia classification over GSMD+SLT data

VGG19: A convolution neural network, CNN commenced in 2014 by Simonyan and Zisserman [170], comprises 19 layers in which 16 convolutional layers are adequate to extricate the features with three fully connected layers, used to label the images into 1000 object classes and infused on the database of ImageNet [171]. It is an appropriate method for image classification by utilising 3×3 kernels and a stride size of 1 pixel in each convolutional layer, shown in Fig 4.3. The five max-pooling layers are placed between the 16 feature layers which are divided into different groups and the final layer is equivalent to a SoftMax layer. To identify the image, an RGB input image of size 224×224 is applied to the model, shows the matrix of shape ($224 \times 224 \times 3$).
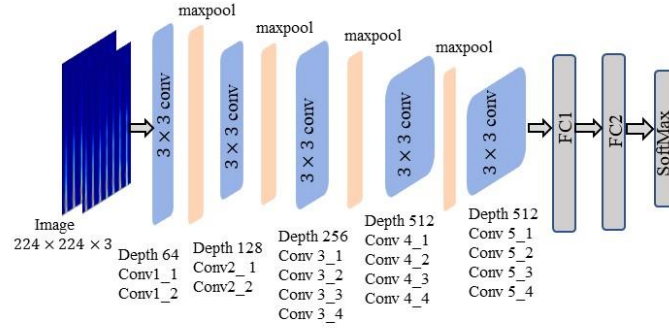
Fig 4.3 Representation of VGG19 architecture

RESNET-18: The CNN emphasizes millions of images from the ImageNet database. The input image of 224×224 size is applied at the input terminal, and a skip connection is maintained after the first layer [172].
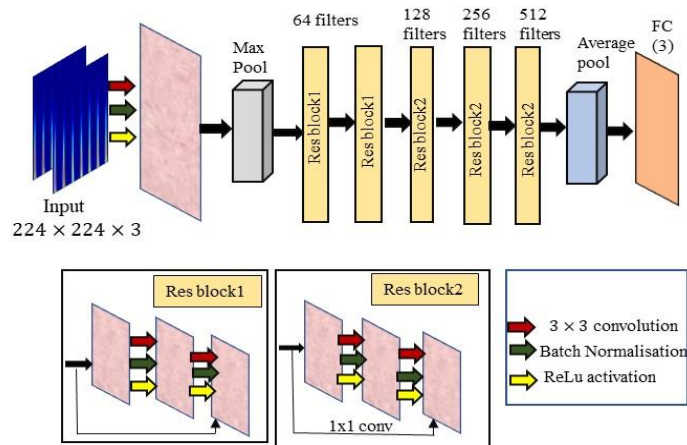
Fig 4.4. Representation of RESNET-18 architecture

The connection between input and output is obtained by two convolutional sheets each of 64 kernels with size 3 × 3, showing the first residual block is shown in Fig 4.4. The third block consists of the output of the second block through a skip connection and the output of two convolutional layers with a 3x3 filter size and 256 filters. The final block includes the 512 filters with convolutional layer output through a skip connection. In the last stage, average pooling is executed on the output, applied the fully connected layers followed by the SoftMax layer to attain the desired outcome.

GoogleNet: It is a 22-layered structure based upon the Inception architecture [173]. It utilizes distinct techniques like global average pooling and 1x1 pooling to enhance the architecture. The deep CNN, Inception is introduced at the 2014 ImageNet Large Scale Visual Recognition Challenge (ILSVRC14). The auxiliary classifiers used in training have an average pooling layer of 5 × 5 filter size and a stride of 3. The input is passed through the normalization layer, max pooling layer to reach the second convolutional layer. The same procedure is followed by the remaining layers and the output is obtained from SoftMax layer. The structure of GoogleNet deep neural network is shown in Fig 4.5.
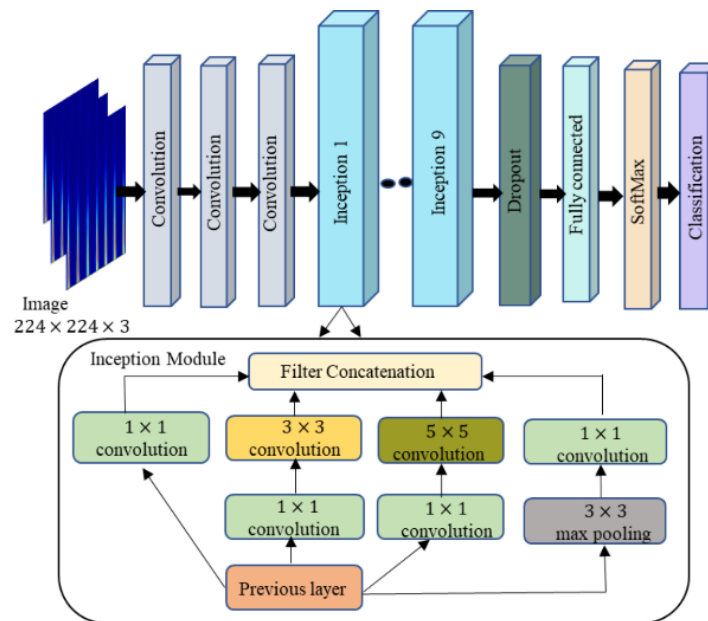
Fig 4.5 Representation of GoogleNet architecture

AlexNet: The CNN is designed to categorize 1.2 million images in the ImageNet LSVRC-2010 into 1000 different classes [174]. The architecture consists of five convolutional layers followed by two fully connected layers and a SoftMax layer of

1000 as an object as output. The size of an input image is $227 \times 227 \times 3$ applied to the input of the convolutional layer with a stride of four.

4.1.7 Experimental Results

Arrhythmia classification is being performed and categorized into three distinct classes, Healthy, AF, and VF, by utilizing the Physionet dataset and the combined dataset (Physionet+Mendeley-II). The evaluation parameters like accuracy, sensitivity, specificity, precision, and F1-score are evaluated.

(a)   (b)   (c)
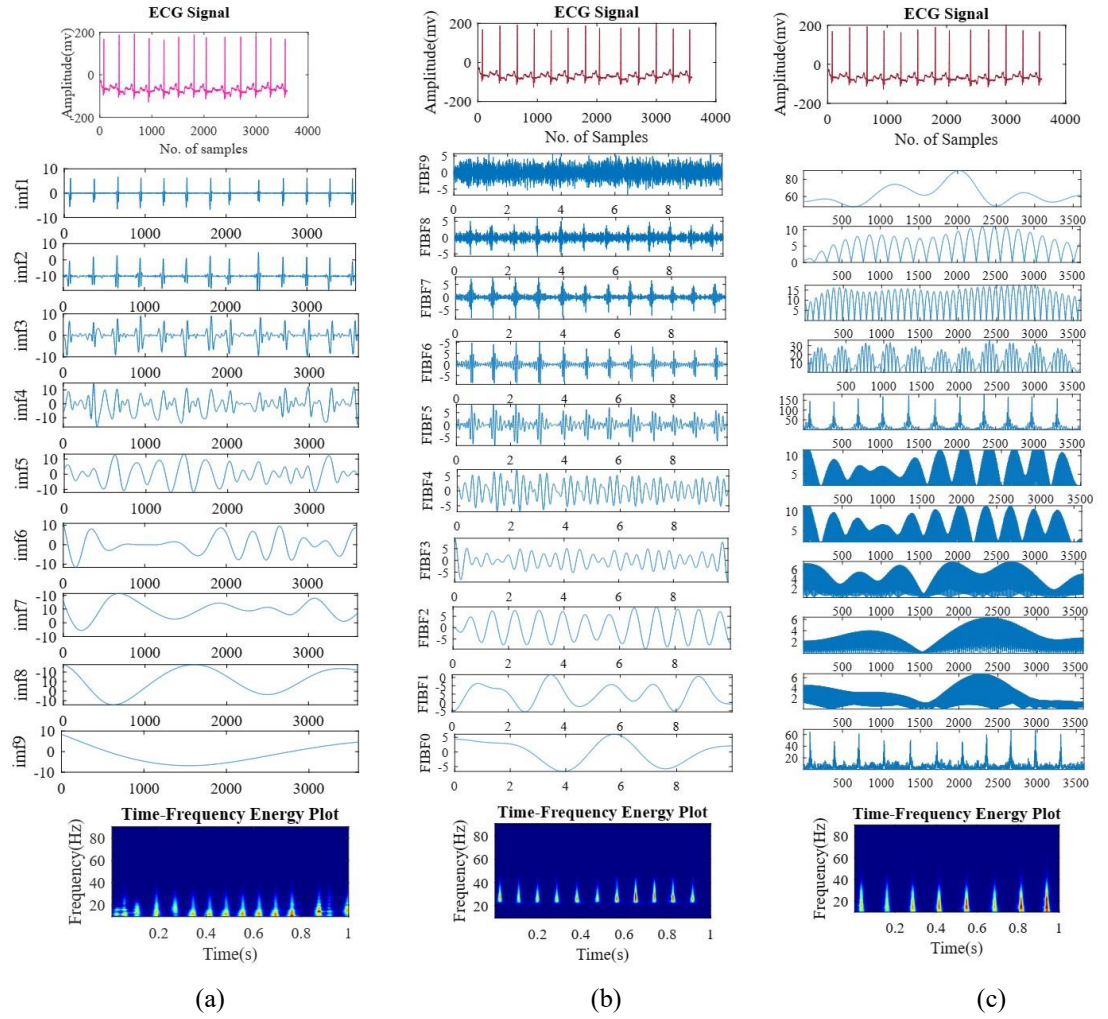
Fig 4.6 (a) The decomposition levels with the corresponding spectrogram are shown by implementing EMD and SLT on MIT-BIH Arrhythmia record-100 (b) Application of FDM over ECG signal generates the perfect oriented intrinsic band functions, FIBFs, and correspondingly energy graph is plotted. (c) The GSMD technique reflects the different intrinsic mode functions with high-resolution 2D image transformed by SLT.

Here, the existing decomposition methods (EMD and FDM) using SLT are compared with the presented method GSMD+SLT and depicted in Fig 4.6. The count of 2214 images using physionet dataset is generated from SLT where each class contains 738 images of which 15% is used for validation. For testing purposes, a set of 147 images is preserved separately. The count of 615 images is generated using combined dataset (Physionet+Mendeley-II) where each class has 165 training images and 40 images are used for testing purposes. The tuning of hyperparameters (optimizer, learning rate, number of epochs, mini-batch size) of deep learning models is performed to attain the higher classification results. It has been observed that best results of arrhythmia classification acquired from VGG19 with an *Acc* of 98.2% using Stochastic gradient descent optimizer under 60 epochs with learning rate 10^{-5} having a loss of 0.07 and a batch size of 32. The generated 2D pattern is fed to the deep neural networks, VGG19, RESNET-18, GoogleNet, and AlexNet for the acute classification results, out of which VGG19 and RESNET-18 shown the best results for physionet dataset whereas the method GSMD+SLT using GoogleNet shows the highest accuracy over combined dataset. As per the size of necessity of the model, the images of the dataset are rescaled to $224 \times 224 \times 3$.

The confusion metrics allow the visualization of the performance of an algorithm for classification. The confusion metrices of validation and testing records using VGG19 on physionet dataset is shown in Fig 4.7.

Fig 4.7 (a) The confusion metrics obtained over validation dataset using VGG19 for multiclassification of arrhythmia (b) The confusion metrics obtained over test dataset using VGG19 on the physionet dataset for multiclassification of arrhythmia

It is noticed that 142 images corresponding to 32.3% are correctly classified as AF, whereas 3 images of Healthy section are wrongly named as AF. The 144 and 146 images are accurately categorized as Healthy and VF respectively.

The next model RESNET-18 achieved the validation and testing *Acc* of 95.1% and 98% respectively on physionet dataset shown in Fig 4.8. It is noted that 141 images are accurately classified as AF signifies to 32%, and 2 images of Healthy class are wrongly categorized as AF. A count of 145 images is perfectly classified as Healthy and AF both. The multiclassification is performed on the combined dataset using various deep learning models (RESNET-18, AlexNet, VGG19, and GoogleNet) out of which GoogleNet performed best with validation and testing *Acc* of 98.0% and 99.2% respectively.

Fig 4.8 (a) The confusion metrics obtained over validation dataset using RESNET-18 for arrhythmia classification (b) The confusion metrics obtained over test dataset using RESNET-18 on physionet dataset for arrhythmia classification

The comparison between the method GSMD+SLT on both datasets (Physionet and combined dataset) and the existing decomposition methods of non-linear signals are reported in Table 4.2 that achieved the *Acc, Sens*, and *Spec* of 98.2%, 98.1%, and 99.09%, respectively using VGG19 on physionet dataset. The performance is also measured on the combined dataset using GoogleNet, attained an *Acc* of 99.2%. The FDM+SLT shows an *Acc* of 97.3% over VGG19 which is better than the existing FDM technique.

Table 4.2 Summary of existing decomposition techniques with the presented method (GSMD+SLT) on both datasets (Physionet and combined dataset) for arrhythmia classification.

Year	Dataset	Method	Class	Acc (%)	Sen (%)	Spec (%)
(2022) [175]	Physionet dataset	EMD+SMOTE+ 1D CNN	2	91.8	91	92.6
(2024) [176]		EMD+SLT	3	93.2	92.8	93
(2020) [177]		FDM+SVM	2	99.5	NR	NR
(2024) [176]		FDM + SLT	3	97.3	97.1	98
		GSMD + SLT + VGG19	3	98.2	98.1	99.09
	(Physionet+ Mendeley-II)	GSMD+SLT+ GoogleNet	3	99.2	98.6	99

Table 4.3 The performance comparison between the presented method with existing methods for Atrial Fibrillation on physionet dataset.

Year	Method	Acc (%)	Sen (%)	Spec (%)	Prec (%)	F1-sc (%)
(2022) [178]	SLT+ DenseNet – 201	97.1	100	95.7	92.1	95.8
(2021)[179]	Recurrent plot + CNN	86.97	86.79	NR	73.61	79.65
(2020) [180]	Patch-based lead + CNN	93.1	93.1	93.4	NR	NR
(2019) [181]	CNN-BLSTM	96.59	99.93	97.03	NR	NR
(2018) [182]	MS-CNN	97.19	80.26	98.84	87.14	88.78
(2024) [176]	GSMD+SLT+ VGG19	98.18	97.93	98.30	96.59	97.32
	GSMD+SLT+ RESNET-18	98.18	98.60	97.97	95.91	97.21
	GSMD+ SLT+ GoogleNet	93.63	95.41	92.88	85.03	89.89
	GSMD+ SLT+ AlexNet	98.18	100	97.34	94.55	97.20

A performance comparison of Atrial Fibrillation is reported between the presented method and the existing methods on the physionet dataset discussed in Table 4.3. The highest *Acc* of 98.18% is achieved on VGG19, RESNET-18, and AlexNet. The other evaluation parameters (sensitivity, specificity, precision, and F1-score) are also mentioned. Table 4.4 represents the comparison of the executed method with the existing ones for the detection of Ventricular Fibrillation on physionet dataset. The value of *Spec* is 100%, 99.6%, 98.9% and 100% obtained using VGG19, RESNET-18, GoogleNet, and AlexNet respectively. The AlexNet and GoogleNet performed better in terms of precision.

Table 4.4 Comparison of the presented method with existing methods for Ventricular Fibrillation on physionet dataset for multiclassification of arrhythmia

Year	Method	Acc (%)	Sens (%)	Spec (%)	Prec (%)	F1-sc (%)
(2022) [178]	SLT+ DenseNet-201	97.1	92.8	99.2	NR	95.6
(2022) [183]	Ensemble method	97.02	92.71	NR	NR	NR
(2022) [184]	Sampling vector RF	98.2	NR	NR	NR	NR
(2022) [185]	Gabor Tr + DL features	98.75	98.18	99	NR	NR
(2024) [176]	GSMD+ SLT+VGG19	98.8	96.6	100	100	98.3
	GSMD+SLT+ RESNET18	98.4	96.02	99.6	99.3	97.6
	GSMD+ SLT+ GoogleNet	94.31	86.6	98.9	97.9	91.93
	GSMD+ SLT+ AlexNet	97.72	93.58	100	100	96.68

The simulation results of presented method using VGG19 and RESNET-18 on physionet dataset are listed in Table 4.5. The highest value of *Sens* is recorded as 100% in case of healthy class. Table 4.6 represents the comparison in multilevel classification between the presented and the existing methods. The highest *Acc* of 98% and 99.2% is achieved with GSMD+SLT+VGG19 over physionet dataset and GSMD+SLT+GoogleNet over combined dataset respectively.

Table 4.5 Simulation results of GSMD+SLT method using VGG19 and RESNET18 over physionet dataset

Class	Acc (%)		Sen (%)		Spec (%)		Precision (%)		F1-sc (%)	
	VGG 19	RESNET 18	VGG 19	RESNET 18	VGG 19	RESNET 18	VGG 19	RESNET 18	VGG 19	RESNET 18
AF	98.18	98.18	97.93	98.60	98.30	97.97	96.59	95.91	97.32	97.21
Healthy	98.86	99.31	100	99.31	98.98	99.31	97.95	98.63	98.98	98.98
VF	98.86	98.40	96.68	96.02	100	99.65	100	99.31	98.32	97.64

Table 4.6 Comparison of the executed method (GSMD+SLT) with existing techniques for multilevel classification

Year	Dataset	Method	Class	Acc. (%)
(2022) [178]	AF termination challenge, CUVT, MIT-BIH MV, MIT-BIH Arrhythmia DB.	SLT+ AlexNet	3	92.9
		SLT+ GoogleNet		93.8
(2021) [186]	Zheng et al dataset	HIT pattern + SVM	7	92.95
(2012) [187]	MAHB	LDC+ EMCA	3	95.42
(2022) [188]	MIT-BIH Arrhythmia DB	CNN-LSTM + RRHOS-LSTM	4	95.81
(2024) [176]	MIT-BIH AF, CUVT, Malignant Ventricular Ectopy, MIT-BIH Arrhythmia DB	GSMD+ SLT+ AlexNet	3	97.7
		GSMD+SLT+VGG19		98.2
		GSMD+ SLT+ RESNET-18		98.0
		GSMD+ SLT+ GoogleNet		94.5
	Combined dataset (Physionet + Mendeley II)	GSMD+SLT+VGG19	3	94.3
		GSMD+SLT+GoogleNet		99.2
		GSMD+SLT+AlexNet		93.4
		GSMD+SLT+RESNET-18		96.7

The performance of the method GSMD+SLT on both datasets using deep learning models is represented by histogram in Fig 4.9.
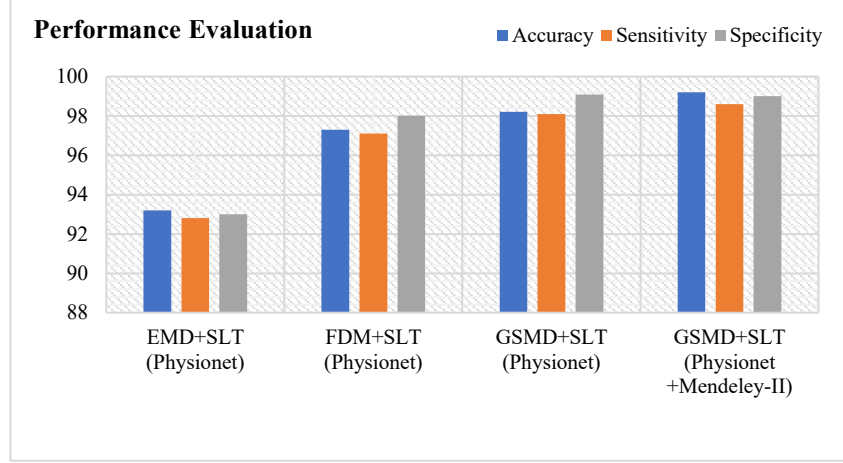
Fig 4.9 Histogram representing the performance of the presented method (GSMD+SLT) on both datasets with existing methods

4.1.8 Discussions

The value of *Spec* is 100%, 99.6%, 98.9% and 100% obtained using VGG19, RESNET-18, GoogleNet, and AlexNet respectively. The AlexNet and GoogleNet performed better in terms of precision. The highest *Acc* of 98% and 99.2% is achieved with GSMD+SLT+VGG19 over physionet dataset and GSMD+SLT+GoogleNet over combined dataset respectively.

Computational complexity of GSMD and SLT

The Superlet is used for converting the 1D time-domain signal into 2D spectrograms reflects the energy intensity of the respective peaks. The computational complexity is represented as: $\mathbf{FLOPs = 5N\log_2(N) \cdot F \cdot K}$

Where *N* represents the number of samples, *F* shows the frequency of the signal, and *K* represents the count of cycles. Approximately *4.7 million FLOPs* are utilised for superlet transform.

$$\mathbf{\textit{GSMD} \approx 4.2 \times 10^7 \textit{ FLOPs}}.$$

4.1.9 Summary of GSMD+SLT multiclassification of arrhythmia

We initiated a method that shows a combined technique of GSMD and high-resolution, SLT, to detect and perform the multilevel classification which categorizes the cardiac arrhythmia into Healthy, AF, and VF classes using ECG signal. The GSMD technique decomposes the complex ECG signal into a set of intrinsic mode functions, assuming

an IMF has a finite bandwidth and the frequency bands of several IMFs are disjoint. By grouping them in several combinations, the denoised signal is acquired with the use of filters integrated with GSMD. The high-resolution technique, SLT, is employed that transformed the obtained signal from GSMD into a 2D spectrogram which is then fed to the deep neural networks for arrhythmia classification. The models, VGG19, RESNET-18, GoogleNet, and Alexnet are utilized for classifying the ECG signal and achieved an Acc of $98.2\%, 98\%, 94.5\%,$ and 97.7% respectively over physionet dataset. The combined dataset (Physionet+Mendeley-II), attained an Acc of $94.3\%, 94.3\%, 99.2\%,$ and 93.4% respectively from the above deep learning models. The results show that the executed method (GSMD+SLT) is reliable and efficient for arrhythmia classification.

4.2 FRACTIONAL ORDER-BASED HIGH RESOLUTION SPECTRAL ANALYSIS FOR ARRHYTHMIA DETECTION AND CLASSIFICATION

The elimination of artifacts, peak dislocation, and unattended weaker neighbouring packets with strong spectral neighbours usually pose a challenge during the process of arrhythmia detection. To deal with these challenges, the work exploits the Fractional Superlet spectral analysis (FSSA) that smooth out the variation in time-frequency resolution as a function of frequency by allowing fractional order of wavelets and hence makes the signal noise-free and ensures proper placement of peaks. The clear depiction of time-frequency pattern enhances the accuracy of heart rate estimation. It also presents a deep learning-based model employing a time-frequency energy representation of the signal to detect and classify multiple classes of arrhythmia. This provides enough information to make preferable use of CNN performance thus eliminating the need for artefact removal and feature extraction steps.

The term FASLT refers to the fractional superlet transform in which the order is used in the fractional form. The elimination of artefacts, peak dislocation, and unattended weaker neighbouring packets with strong spectral neighbours usually pose a challenge during the process of arrhythmia detection. To deal with these challenges, exploits the

Fractional Superlet transform that smooth out the variation in time-frequency resolution as a function of frequency by allowing fractional order of wavelets and hence makes the signal noise-free and ensures proper placement of peaks. As the frequency rises, ASLT introduces banding in the TF characterization due to the distinct hops of the order of SLT. Therefore, an effective technique named, FASLT is utilized where the order is in the fractional form generated by weighted Geometric Mean in the SLT formula which provides a sharp illustration of the frequency domain.

4.2.1 Introduction

To recognize CVD, health informatics demands the collection and processing of data, and analysis of the health status of the cardiovascular system. This requires the upgradation of biomedical informatics, with the fervor on (i) the expansion of the screening tool with maximum susceptivity and (ii) risk analysis methods with higher specificity for correct and early diagnosis of people at CVDs risk [9]. Some restrained monitoring devices have been outlined to gain physiological signals for real-time applications. Through accurate and absolute training, this distinctive ability prepares them a unique tool for several engineering programs for 2D signals such as images and video recordings. For the analysis and processing of non-stationary data, there exist several methods that enhance the efficacy of the system such as the Short Time Fourier Transform (STFT), CWT, EMD, Compact Empirical Mode Decomposition (CEMD), and FDM.

The STFT is an instinctive method of time-frequency representation that evaluates the Fourier Spectra on consecutive sliding windows. For a specific window size, the frequency resolution of STFT is unvarying but its temporal precision degrades with an increase in frequency. This creates an issue in the analysis of scale-free signals that have oscillation bursts that are self-similar across frequencies. There is a tradeoff in time and frequency in STFT, thereafter, a multiresolution technique named CWT is initiated that produces a superior temporal resolution at higher frequencies but, at the same time, also deteriorates the frequency resolution at the same parameters. By compressing/dilating a mother wavelet according to frequency, the CWT enables precise relative temporal localization. These TF uncertainty restrictions hinder the

analysis of TF-containing ECG signals. This shows that both STFT and CWT share the same inbuilt limitations. The main idea of the presented work over arrhythmia detection is underlined as:

1) The challenge of noise interruption in ECG signal, peak displacement, and avoidance of weak neighboring spectral peaks from dominating spectral peaks, is resolved with "Fractional Adaptive Super-resolution" technique.

2) The presented technique leads to the detection of QRS complexes consisting of short-term oscillations and also removes the extra denoising step by providing high intensity energy peaks that help in the classification of disease.

3) The 1D data is reshaped to a 2D format by utilizing the fractional order, as ASLT suffers from banding while altering the order to get the high-resolution peaks.

4) The high-resolution time-frequency pattern is used to predict the heart rate using FASLT which eliminates the need for pre-processing.

4.2.2 Fractional Adaptive Superlet Transform

To overcome the above explained restrictions for TF analysis, a Morlet wavelet is utilised which is defined as a multiplication of plane waves with a Gaussian envelope.

Adaptive SLs: Adaptive Superlet [169] [176] is an altered form that changes its order to the central frequency to compensate for the higher wavelet bandwidth with higher frequency. The low frequencies can be estimated by fixing the order low of ASLT. The order of ASLT, which is dependent on the frequency, increases to attain the exact TF resolution. SLT is used for narrowband frequency range whereas ASLT is used for wide frequency range.

Fractional Adaptive Superlet: As the frequency rises, ASLT introduces banding in the TF characterization due to the distinct hops of the order of SLT. Therefore, an effective technique named, FASLT is utilized where the order is in the fractional form generated by weighted Geometric Mean in the SLT formula which provides a sharp illustration of the frequency domain. It is considered that the integer part of each wavelet weighs 1, whereas the last wavelet represents the fractional weight. The fractional order can be defined as:

$$o_{fr} = o_{in} + \beta \tag{4.14}$$

where o_{fr} and o_{in} is the fractional order and integer order respectively, where $o_{in} \geq$ 1, and a fractional part, $\beta \in [0,1)$. The FASLT is defined as:

$$FASLT_{s,r_1,o_{fr}}(t,f) = \left[R_s(r_1[o_{in}+1]; t,f)^\beta \prod_{i=1}^{o_{in}} R_s(r_1.i; t,f) \right]^{1/o_{fr}} \qquad (4.15)$$

FASLT comprises a factor to the Geometric Mean and is measured with the fractional part of the order. When β is 0, it is similar to SLT. The restriction of using an integer in ASLT is removed in FASLT.

$$o_{fr} = o_{min} + \left[(o_{max} - o_{min}) \left(\frac{f - f_{min}}{f_{max} - f_{min}} \right) \right] \qquad (4.16)$$

where o_{min} and o_{max} are the orders proportional to the smallest and largest central frequency f_{min} and f_{max} respectively.

4.2.3 Implementation of Fractional Adaptive Superlet Transform

The 1D ECG input data is reshaped to 2D time-frequency energy representation for getting information on the time, frequency, and energy of arrhythmia diseases. The obtained images are fed to various deep-learning models for the detection and multi-classification of arrhythmia. The distinct databases are involved in implementation to increase the number of ECG recordings that are fetched using the leads of every database. The data is segmented into small packets of ten-second duration of every recording. After segmentation, the application of FASLT on segmented data reconstructs the data into 2D format. A sharper and more intriguing time-frequency spectrogram is generated after combining the responses of wavelets geometrically in the executed technique. Few points are stated as follows:

(i) The greater denoising capability of FASLT eliminates the noisy ECG signal, without the use of additional filters. With additional artifacts including baseline drift, electrode motion artifact, and powerline interference, FASLT performs efficiently in terms of complexity and accuracy. Hence, this removes the need of denoising step in pre-processing.

(ii) Detection of QRS complexes of ECG signal is initiated with presented FASLT. For averaged TF spectra, conventional techniques (STFT and CWT) may be unable to show the genuine TF structure within a particular band if strong spectral neighbours

exist, as the latter's depiction leaks into the band of interest, affecting its estimation. Powerful oscillation packets can theoretically be found using a variety of techniques.

Due to the TF concentration of spectral power, FASLTs offer a reliable and exquisite solution to this issue by reducing cross-band contamination during spectral estimation. The flow diagram of the presented method constitutes the different stages of arrhythmia classification is shown in Fig 4.10 which clearly defines the formation of respective spectrograms and feeding those to the deep learning models. The FASLT is represented by algorithm 4.2 which conveys the required steps involved to calculate the geometric mean of the responses of wavelets. The data of 3200 images is utilized using the FASLT technique which is associated with MI-BIH AF [36], MIT-BIH SUVT [39] , MIT-BIH Arrhythmia DB [35], and MIT-BIH malignant ventricular[34]. A count of 800 images is selected from every dataset, out of which 120 images are used for validation and 160 from each dataset is used for testing purposes in arrhythmia classification process. The time-frequency energy diagrams generated from FASLT are employed to classify the arrhythmia effectively into four classes that are Normal, Malignant, Atrial Fibrillation, and Supraventricular. The datasets are initiated from physionet [34] on which application of various techniques is done to reform the data from 1D to 2D image.

A comparison of energy diagrams is made between the techniques STFT, CWT, ASLT, and FASLT which clarifies the acuteness, and sharpness of the peaks under the respective classes to give a clear picture of the data in Fig 4.11. Deep learning-based CNN are used according to the input data provided to enhance the efficacy of the system with some variations in hyper-parameters depending upon the model. The learning rate, batch size, optimizer, validation frequency, and number of epochs are modified to obtain the pre-eminent arrhythmia categorization outcomes.
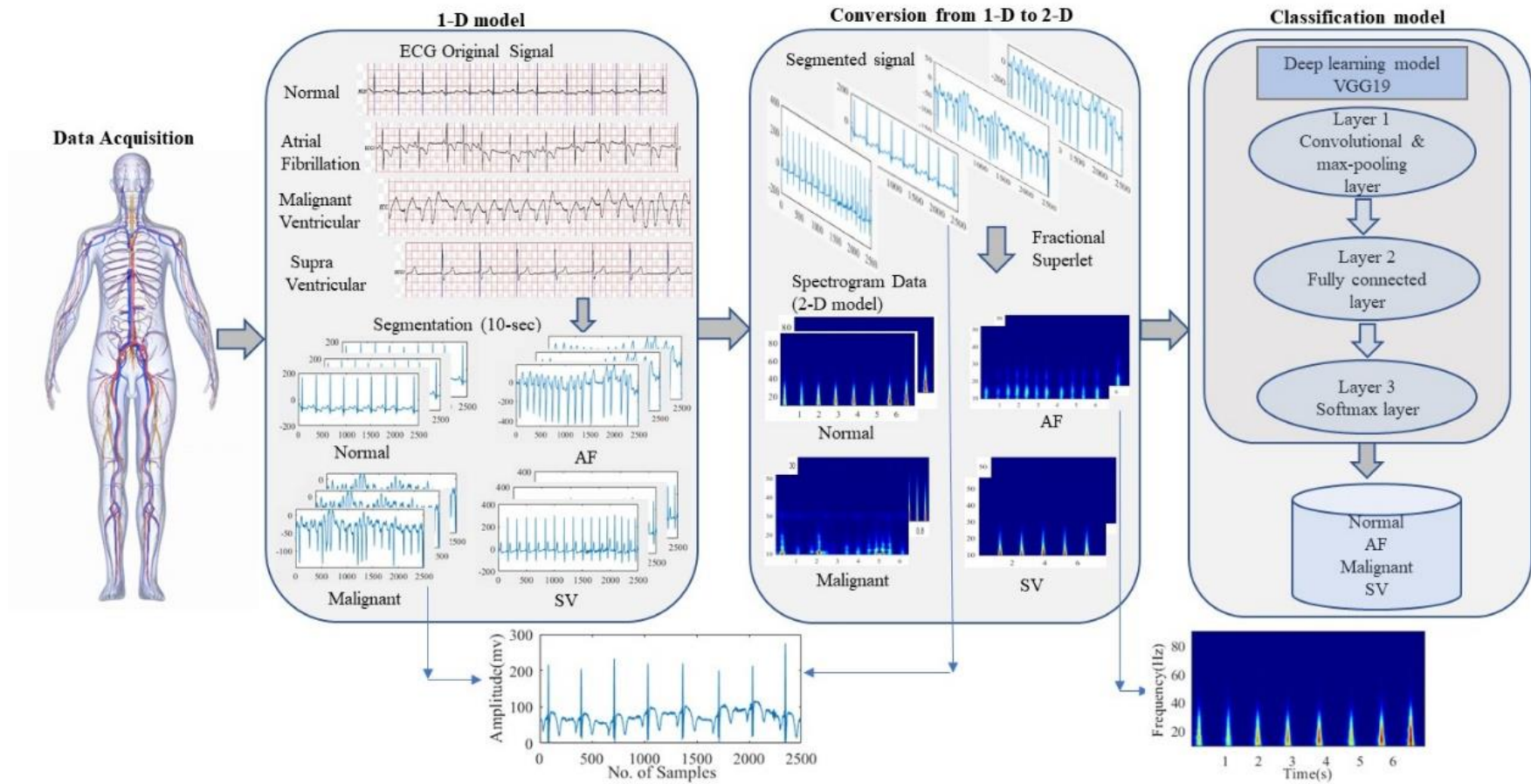
Fig 4.10 Illustration of multilevel modelling of cardiovascular systems with arrhythmia classification using deep neural network

ALGORITHM 4.2: Fractional Adaptive Superlet Transform implementation over ECG Signal

INITIALISE Input: $s\rightarrow$ 10 second ECG signal

$Fs\rightarrow$ Sampling frequency

$Fi\rightarrow$ Frequency interval

$Nf\rightarrow$ Samples

$o\rightarrow$ [1 × 2] interval of super-resolution order

$o_{fr}\rightarrow$ fractional order

$r\rightarrow$ Number of cycles

$c1\rightarrow$ initial wavelet cycles

Output: A superlet spectrum

wtresult$\rightarrow$ [frequency × samples]

Step 1: Compute and Initialize frequency parameter

  if $(Fi(1) > Fi(2))$; $i\rightarrow$ Ranges from (1 to Nf) samples

    $F\rightarrow$ Range between $\big(Fi(1), Fi(2)\big)$ with samples Nf

  end

Step 2: Initialize the fractional order parameter having a range over samples Nf

$$o_{fr} = o_{min} + \left[(o_{max} - o_{min})\left(\frac{f - f_{min}}{f_{max} - f_{min}}\right)\right]$$

where o_{max} and o_{min} represent the max and min value of the order.

Step 3: Assign the number of cycles by additive rule using relation

$$SL_{f,o} = \{\Psi_{f,r}|r = r_1, r_2, \dots r_o\}$$

Step 4: Evaluate the fractional adaptive superlet transform utilizing the relation

$$FASLT_{s,r_1,o_{fr}}(t,f) = \left[R_s(r_1[o_{in} + 1]; t, f)^{\beta} \prod_{i=1}^{o_{in}} R_s(r_1.i; t, f)\right]^{1/o_{fr}}$$

Step 5: Calculate the Geometric mean and the wavelet coefficient of the revised spectrogram of individual wavelets.
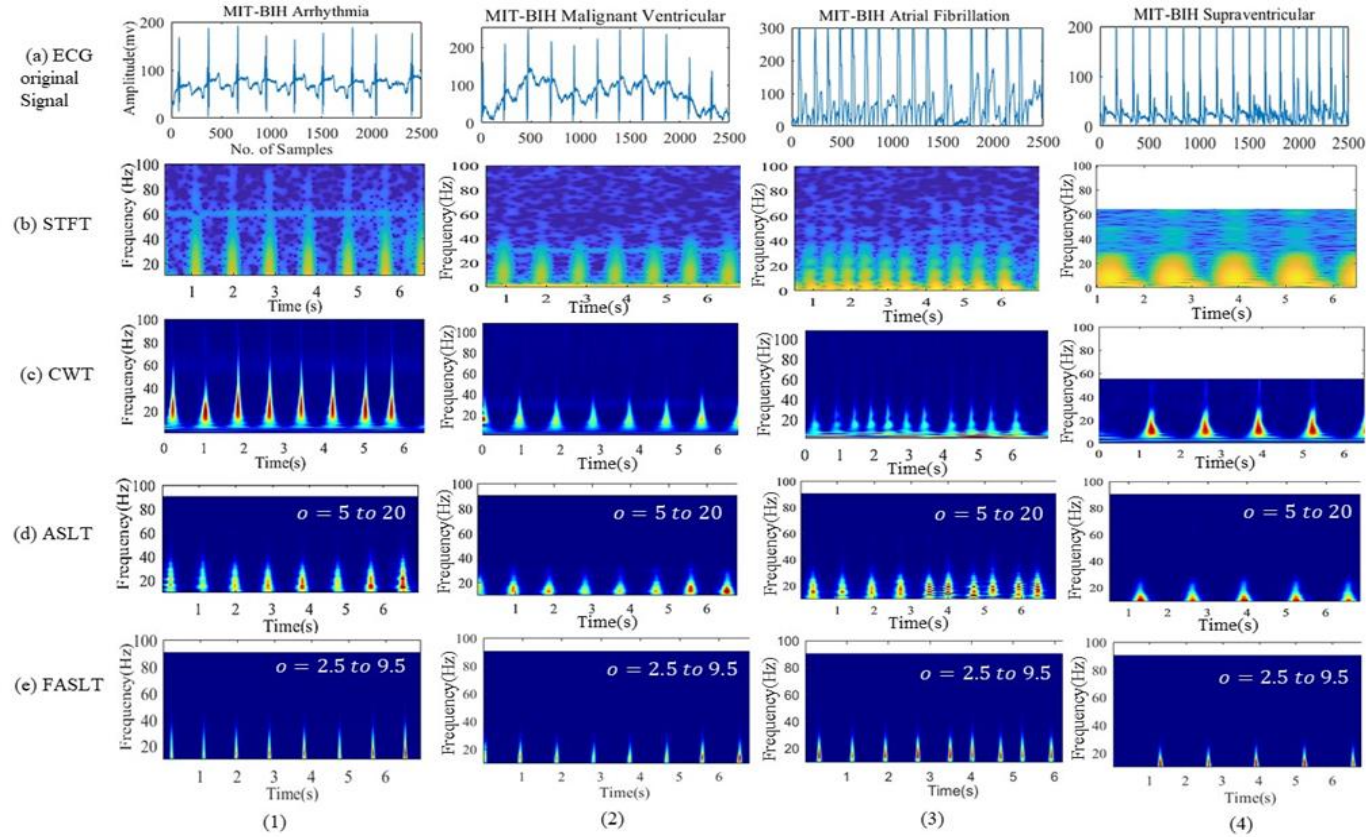
Fig 4.11 Estimation of time-frequency resolution of various classes. (a) Test records containing cardiovascular diseases having sampling frequencies of $360Hz, 250Hz, 250Hz$ and $128Hz$ respectively. (b) Time-frequency energy representation of the test signal using STFT produces the spectrograms. (c) Consistent to STFT but with the application of CWT reflects the scalograms. (d) Using ASLT with order ranges from $o = 5$ to 20 having a number of base cycles $r = 3$ (e) Identical to STFT, CWT, and ASLT but measured using FASLT with order ranges from $o = 2.5$ to 9.5 in fractional form and number of base cycles $r = 5$.

4.2.3.1 Time-Frequency Representation of ECG Signal Using FASLT

The high-resolution technique FASLT has an outstanding proficiency to divulge high-frequency fragments in every individual trial. With increasing order, the FASLTs mainly focus on frequency resolution that exhibits very sharp and limited bandwidth. The FASLTs are quite good at detecting high-frequency bursts in a single attempt. In this, the normalization of wavelets controls the excess of time-frequency presentation and also assists in the detection of instantaneous power at a scale-independent frequency. For averaged TF spectra, conventional techniques (STFT and CWT) may be unable to show the genuine TF structure within a particular band if strong spectral neighbors exist, as the latter's depiction leaks into the band of interest, affecting its estimation. Powerful oscillation packets can theoretically be found using a variety of techniques. However, calculating neighboring, weaker packets turns out to be challenging for conventional methods, including those relying on the directionally filtered WVD, which may impede the creation of significant findings about the simultaneous coordination of rhythms across nearby bands. Due to the TF concentration of spectral power, FASLTs offer a reliable and exquisite solution to this issue by reducing cross-band contamination during spectral estimation [189]. Detection of QRS complexes in the overall classification process plays a supreme role as it helps to determine the accuracy of the system, represented in Fig 4.12 under distinct examples.

(i)   (ii)

| (iii) | (iv) |
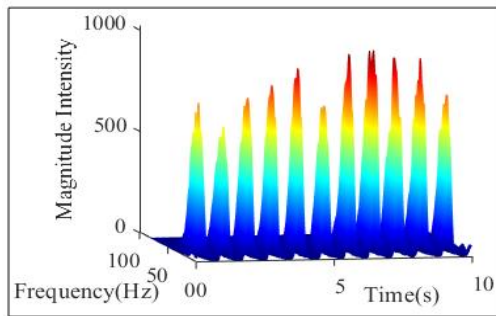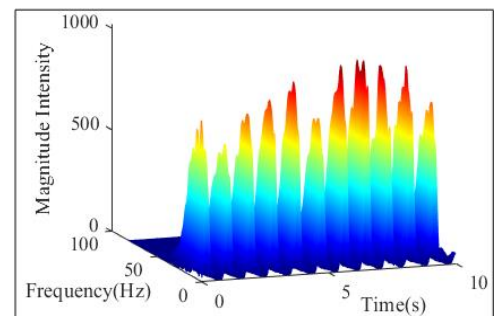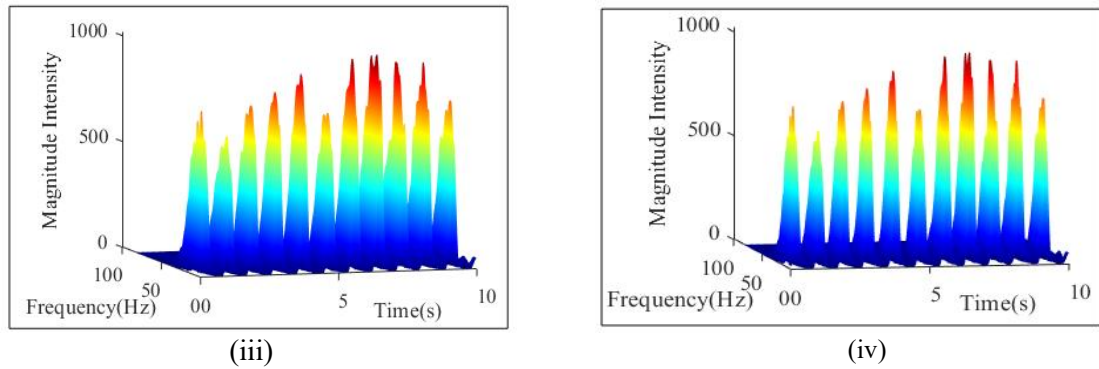
Fig 4.12 Representation of detected peaks with variation in detection parameters of MIT-BIH Arrhythmia record-101. (i) $r = 3, f = 1Hz$, and $k = 1.3$ (ii) $r = 5, f = 2Hz$ and $k = 0.75$ (iii) $r = 6, f = 3Hz$ and $k = 0.40$ (iv) $r = 9, f = 4Hz$ and $k = 0.30$

Table 4.7 implies the number of peaks detected at the original and at a different location under some detection parameters with standard deviation k, count of base cycles r, and center frequency f. The QRS peaks at specific location can be determined with number of cycles, central frequency, and standard deviation. With variations in count of cycles, the QRS peaks can be find out at different locations. The deep learning models VGG19 [190] and RESNET-18 [172] are utilized for the detection and classification of arrhythmia.

Table 4.7 Representation of peaks at different base cycles and central frequency with detection parameters at MIT-BIH Arrhythmia record-101.

Standard Deviation (k)	Base cycles (r)	Centre frequency (f)	Time spread parameter	QRS peaks at correct location	QRS peaks at Different location
1.3	3	1	2.3	7	4
0.75	5	2	3.3	9	2
0.40	6	3	5	10	1
0.30	9	4	7.5	11	0

4.2.4 Experimental Results

The simulations are executed with NVIDIA GEFORCE RTX 3070, 11th Gen Intel core i7-11370H processor @ 3.30 GHz, 64-bit Windows system. The confusion metrics gives the detailed data of classification results according to the real and estimated category. It is used to estimate the performance of the classification model for the measured set of test data. The performance parameters consisting Accuracy, Sensitivity, Specificity, Precision, and F1-score are evaluated. The deep learning models, (VGG19, and RESNET-18) are utilized that withdraw features from the images and classify accordingly. Segregating the training and validation data is the foremost step in the process and is separated by 85% and 15% respectively. 20% of data (160 images from each dataset) are used for testing purposes for classification. A separate set of 640 images is used to classify them into different classes. The testing and validation confusion metrics of VGG19 is shown in Fig 4.13, represents that 154 images are accurately categorized as AF and seven images of Malignant are wrongly classified as AF. The RESNET-18 model, performed with a net testing and validation accuracy of 96.7% and 93.2% respectively.

(i)

Confusion Matrix

(ii)

Fig. 4.13 (i) Confusion metrics obtained over test dataset using VGG19 for multilevel arrhythmia classification (ii) Confusion metrics obtained over validation data using VGG19 for multilevel arrhythmia classification.

The evaluation parameters comprising accuracy, sensitivity, specificity, precision, and F1-score are calculated using VGG19 and RESNET 18 and represented in Table 4.8.

Table 4.8 Summary of evaluation parameters over test dataset with executed technique FASLT and CNN models (VGG19 and RESNET-18)

	Acc. (%)		Sens. (%)		Spec. (%)		Prec. (%)		F1-sc (%)	
Class	VGG 19	RESNET-18	VGG 19	RESNET-18	VGG 19	RESNET-18	VGG 19	RESNET-18	VGG 19	RESNET-18
AF	97.96	97.65	95.65	96.17	98.74	98.13	96.25	94.30	95.95	95.32
Malignant	98.28	96.73	97.4	92.63	98.55	98.12	95.6	94.32	96.52	93.52
Normal	100	99.06	100	98.12	100	99.3	100	98.12	100	98.12
SV	99.68	100	98.76	100	100	100	100	100	99.37	100

Training loss and validation loss are the two important metrics assist to track how well the model performs over training data and unseen data respectively. The loss curve is depicted in Fig 4.14. The figure represents the training loss and validation loss curves over 30 epochs. For the first 10 epochs, both training and validation loss decreases sharply shows the learning stage of the model. After 10 epochs, the loss values stabilize at lower values.
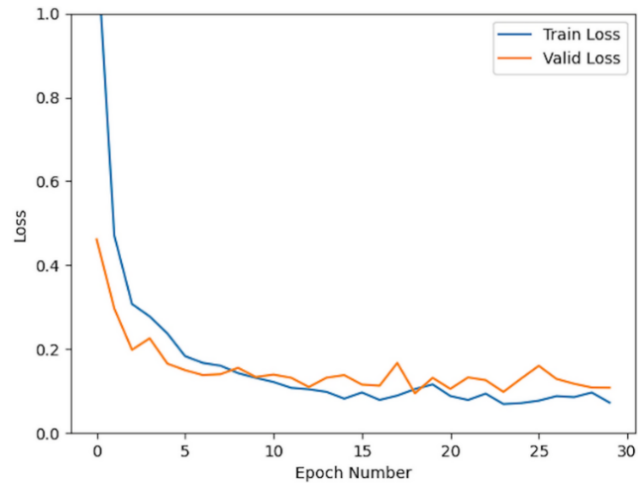
Fig 4.14 The training and validation loss curve over 30 epochs employing FASLT using VGG19 for multilevel arrhythmia classification

The Receiver Operating Curve (ROC) is a graphical representation used to compute the performance of binary classifier and multilevel classifier. It says how well the model separates the positive cases from the negative cases. A multi-class ROC curve using deep learning model VGG19 is visualized and depicted in Fig 4.15.
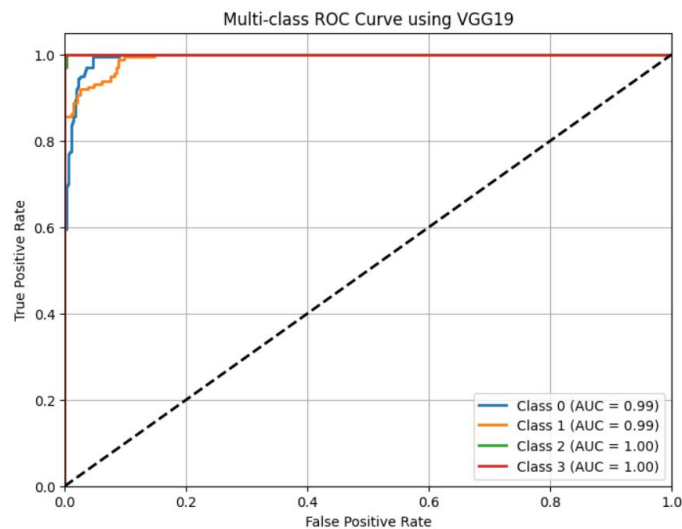
Fig 4.15 The multiclass ROC curve using VGG19 for arrhythmia classification
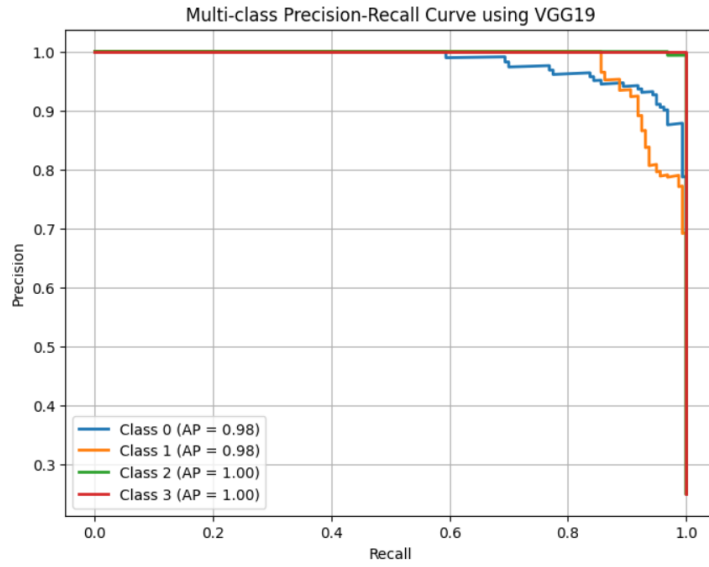
Fig 4.16 The curve representing Precision-Recall relationship employing FASLT using VGG19

The precision-recall curve is a graphical representation that assist to understand the accuracy of the binary or multiclass classification model when the input data is especially imbalanced. The respective curve is depicted in Fig 4.16. Class 0 represents "Atrial Fibrillation (AF class)", class 1 reflects the "Malignant class", class 2 shows the "Normal class", whereas class 3 represents the "Supraventricular class (SV)" respectively. From the simulation results, it is observed that VGG19 is best suited for the multilevel classification as the testing accuracy reached to 98.0% and attained a validation accuracy of 97.7% in comparison to RESNET-18.

4.2.5 DISCUSSIONS

The multilevel arrhythmia classification is performed by implementing the FASLT+Deep neural networks (VGG19 and RESNET-18) on segmented ECG data fetched from physionet. The VGG19 and RESNET-18 model attained an *Acc* of 98.0% and 96.7%, respectively. It is scrutinized that a few evaluation parameters of RESNET-18 shown better results as compared to VGG19. The highest value of *Spec* is recorded as 100% and 98.13% in VGG19 and RESNET-18, respectively. A comparison is made between the presented model and the existing ones on the same dataset based on the performance of the detection of Atrial Fibrillation, listed in Table 4.9. Few methods alongwith their performance is displayed in Table 4.10, conveys an arrhythmia classification using different number of classes. For the diagnosis of Supraventricular

disease, existing applied methods with the presented methods are discussed in Table 4.11 showing the value of accuracy 100% with RESNET-18 deep learning model is achieved. Few merits of presented technique is discussed.

➤ The presented FASLT technique eliminates the noisy ECG signal, demonstrating better denoising capabilities without the use of additional filters.

➤ Detection of QRS complexes in the overall classification process plays a supreme role as it helps to determine the accuracy of the system. FASLT identifies the QRS complex peaks available in given records.

➤ Due to TF concentration of spectral power, FASLTs offer a reliable and exquisite solution to the issue of calculating neighboring weaker packets by reducing cross-band contamination during spectral estimation.

The challenge of noise interruption in ECG signal, peak displacement, and avoidance of weak neighbouring spectral peaks from dominating spectral peaks, is resolved with FASLT.

Computational complexity of FASLT:

The Superlet is used for converting the 1D time-domain signal into 2D spectrograms reflects the energy intensity of the respective peaks. The computational complexity is represented as:

$$\text{FLOPs} = 5N\log_2(N) \cdot F \cdot K$$

Where N represents the number of samples, F shows the frequency of the signal, and K represents the count of cycles. Approximately *4.7 million FLOPs* are utilised for superlet transform.

Table 4.9. Illustration of hyper-parameters of FASLT

Method	Hyper-parameter	Description	Typical Values
FASLT (Fractional Adaptive Superlet Transform)	Number of base cycles	Base cycle count for lowest order superlet	2–5
	Superlet order	Number of wavelets averaged per frequency	3–7
	Fractional order	Fractional tuning of cycles for adaptive resolution	0.1–1.0

	Frequency range	TF decomposition frequencies	e.g., 0.5–40 Hz (ECG)
	Frequency resolution	Number of frequency bins	100–300
	Time-spread parameter	Controls support of wavelet	Derived from cycles

Table 4.10 The analogy of the operation of presented technique FASLT with existing ones for the detection of Atrial Fibrillation.

Year	Dataset	Method	Acc (%)	Sens (%)	Spec (%)	Prec (%)	F1-sc (%)
(2024) [191]	MIT-BIH AFIB	Sequential neural network	98.6	97.9	99.2	98.1	98.0
(2022) [192]		Resnet+ SE block+ Bi-LSTM	99.35	NR	NR	NR	92.86
(2019) [193]		CNN-BLSTM	96.59	99.93	97.03	NR	NR
(2020) [194]		FDM+KNN	94.43	95.16	92.46	NR	NR
(2022) [195]		CNN+LSTM	95.97	96.84	95.76	NR	NR
(2025) [196]		FASLT+ VGG19	97.96	97.95	98.74	97.24	97.95
		FASLT+ RESNET-18	97.65	96.17	98.13	94.30	95.32

Table 4.11 Representation of existing techniques with the executed technique for the detection of multi-level arrhythmia classification.

Author	Model	Class	Datasets	Performance (%)
(2024) [100]	LC-CNN (AC-GAN)	4	MIT-BIH Arrhythmia (N, S, V, F)	Acc: 99.22, Sens: 94.2, Prec:98.2, F1-sc: 96.2
	MobileNet-V2			Acc: 98.69, Sens: 86.2, Prec: 95.8, F1-sc: 90.8
(2020) [135]	WSN-KNN (N, S, V, F)	4	MIT-BIH Arrhythmia	Acc: 99.30, Sens: 99.5, Spec: 98.8, Prec: 99.6
(2021) [197]	MRFO-SVM (N, S, V, F, Q)	5	MIT-BIH Arrhythmia	Acc: 98.26, Sens: 97.43
(2023) [99]	1D Self-ONN	3	MIT-BIH Arrhythmia	Sens: 99.10, Prec: 99.21, F1-sc: 99.15
			SVEBs	Sens: 82.50, Prec: 82.19, F1-sc: 82.34
			VEBs	Sens: 96.1, Prec: 94.4, F1-sc: 95.2
(2022) [124]	CNN-LSTM + RRHOS-LSTM(N, S, V, F)	4	MIT-BIH Arrhythmia	Acc: 95.8, Sens: 69.2, Spec: 94.5, Pre: 74.9, F1-sc: 71.0
(2021) [198]	CQ-NSGT +AlexNet	3	BIDMC CHF, Arrhythmia, NSR	Acc: 98.82, Sens: 98.87, Spec: 99.21, Prec: 99.20
(2020) [199]	BaROA + DCNN	5	MIT-BIH Arrhythmia	Acc: 93.1, Sens: 93.9, Spec: 95.0
(2020) [118]	DCNN	5	MIT-BIH Arrhythmia, INCART	Acc: 98.41, Sens: 98.41, Prec: 98.37, F1-sc: 98.38
(2025) [196]	FASLT+VGG19	4	MIT-BIH Arrhythmia, AF, MIT-BIH MV, SUVT	Acc: 98.0, Sen: 97.95, Spe: 99.3, Prec: 97.9, F1-sc: 97.93
	FASLT+ RESNET-18	4	MIT-BIH Arrhythmia, AF, MIT-BIH MV, SUVT	Acc: 96.7, Sens: 96.71, Spec: 98.90, Prec: 96.7, F1-sc: 96.7

Table 4.12 Summary of comparison between the presented technique with existing ones for the detection of Supraventricular disease.

Year	Dataset	Method		Acc. (%)	Sens(%)	Spec (%)	Prec (%)	F1-sc (%)
(2023) [200]	MIT-BIH SVDB	Sequential AFE	SVEB	NR	82.54	NR	78.44	80.46
			VEB	NR	93.17	NR	97.12	95.10
(2018) [201]		Statistical features + SVM		92.23	79.43	81.44	NR	NR
(2016) [202]		Atrial-based detection + Tree scheme		93.29	83.21	95.80	NR	NR
(2022) [203]		1D Self-ONNs		98	NR	NR	NR	76.6
(2025) [196]		FASLT+ VGG19		99.68	98.76	100	100	99.37
		FASLT+RESNET-18		100	100	100	100	100

4.2.6 Summary for the multilevel arrhythmia classification using FASLT with deep neural network

In this work, a multi-level classification of arrhythmia with FASLT technique using ECG signal is presented. It transforms the 1D ECG signal into a 2D time-frequency energy representation with high resolution which is directly applied to the 2D CNN (VGG19 and RESNET-18) for multilevel classification. The noise is a source of deformity of the ECG signal that disrupts the characteristics badly which needs to be removed at any cost. With the implementation of FASLT, the extra steps of noise suppression are eliminated and detection of QRS peaks is successfully fulfilled which directly reduces the computational complexity. Using FASLT, the deep neural network VGG19 achieved an overall testing and validation *Acc* of 98.0% and 97.7% respectively. The work is scrutinized over arrhythmia datasets which shows the generalized capability of the peak-assisted process to monitor the heart rate that signifies the regularity of the heart. The presented technique will be scrutinized in different domains of real-time scenarios to analyse the effective results in specific domain application.

CHAPTER 5

SPATIOTEMPORAL-BASED ARRHYTHMIA
CLASSIFICATION OVER REAL-TIME ECG SIGNAL

An instantaneous monitoring of electrocardiogram signals is an efficacious process for
the early detection and prevention of arrhythmia. To prevent untimely demise, the
evolution of cardiovascular health information system requires acquiring the data,
processing, and scrutiny of the cardiovascular system to obviate from CVDs in a
premature state. This development is beneficial for early detection, timely projection,
early identification, and corresponding treatment of CVDs.

5.1 Introduction

To calculate the ECG, some unobtrusive controlling devices can be executed to obtain
the physiological conditions of the heart. The gadgets can be executed in a few ways:
installing the sensors into ornaments, like earrings, rings, etc., and fixing the sensors
in daily used objects like tables, chairs, etc. These sensors can transmit the calculated
health information to the remote-control center through wireless communication
technology. The above method can help in the regular monitoring of CVD patients
outside the hospitals in daily life. Sometimes, the recording and measurements carried
outside the hospital are more efficient for the timely and accurate detection of CVD.

    The work focuses on the spatial–temporal modes generated through dynamic mode
decomposition (DMD) technique implementing on the ECG signals. Then, the wavelet
scattering transform (WST) is employed to extract the features of the DMD modes that
yields an outcome of translation-invariant and deformation-stable characteristics by
using wavelet convolutions. Several machine learning models SVM, kNN, Boosted
Tree, Bagged Tree, Weighted Tree, Linear Tree, Quadratic Discriminant Analysis
(QDA), and LDA are implemented over the extracted features for arrhythmia
classification. Here, the process of arrhythmia classification is evaluated by utilizing
three datasets that consist of the physionet dataset [34] (dataset I), the Mendeley-II
dataset [45] (dataset II), and the real-time dataset (dataset III, recorded with iWorx

LabScribe data recording device and analysis software).

The ensemble empirical mode decomposition [204] is introduced where white noise is added to the signal in many variants. It also reduces the time-scale separation problem of EMD. For multichannel data analysis, multivariate EMD can be employed [205]. Variational Mode Decomposition is also an enhanced formation of EMD that decomposes the non-linear signal into a set of bandlimited amplitude and frequency-modulated waves termed modes [206]. To overcome the limitations of these techniques, the FDM is introduced which produces a small set of bandlimited Fourier Intrinsic Band Functions (FIBFs) that are adaptive, orthogonal, and unconnected from a manufacturing perspective [164][177]. In FDM, cut-off frequencies are required to generate the FIBFs at every level. It has been noted from well-developed research that Fourier-based methods are the appropriate tools for spectrum analysis. In this work, DMD, the dimensionality reduction technique, is initiated to analyze the combined features of principal component analysis (PCA) in space and power spectral analysis in time. The main contribution is as follows:

1. The dynamic mode decomposition technique is imposed on the quasi-stationary ECG signal that decomposes the raw data into different frequency components representing the spatial and temporal modes.

2. The modes obtained from DMD are fed to the wavelet scattering transform for feature extraction and exhibiting the scattering coefficients with filter banks.

3. The work is used to perform the detection and multiclassification of arrhythmia using ECG signals from physionet dataset, Mendeley-II dataset, and real-time ECG dataset (recorded through iWorx LabScribe data recording device and analysis software).
Here, a combined approach based on DMD+WST is presented on the available standard dataset and real-time dataset recorded using a traditional medical grade ECG acquisition device for arrhythmia classification.

5.2 Dynamic Mode Decomposition

DMD is an efficient technique used for the decomposition of non-stationary signals into dynamic modes. It is able to record the consistent spatial-temporal structure from non-

linear information by considering that the dimensions of the projected information at every single time point is specified by a direct fusion of spatial structures at earlier time points. This technique utilizes the principal component analysis for spatial and temporal modes generation. To begin with, this technique was initially executed for the inspection of fluid flows, where it can break down the high dimensional data into spatial-temporal modes [207]. It includes the capability of both spectral analysis (to compute the forward and backward vibrating occurrences belonging to those inherent modes) and Singular Value Decomposition (to retrieve fundamental modes from complex data). Due to these factors, the high-dimensional and dynamic physiological signals as well as public health information, including brain-related signals, along with other information, have lately been analyzed using DMD. It is seen that the DMD technique is associated with the Koopman spectral analysis, inspiring its functionality in identifying the dynamics of complex systems. DMD has the capability to decompose the time-domain signal into a set of modes that carry the spatial-temporal patterns [208].

5.3 Implementation of DMD over ECG Signal

Let us assume two $r \times (s-1)$ data matrices Y and Y^T, whose rows and columns show the leads and sampling points of ECG signals, respectively. Here, r represents the number of leads taken for the detection of any signal. The matrix can be formed by calculating the observations from s sampling time points mentioned below.

$$Y = \begin{pmatrix} y_{11} & \cdots & y_{1(s-1)} \\ \vdots & \ddots & \vdots \\ y_{r1} & \cdots & y_{r(s-1)} \end{pmatrix} = [m_1 \ldots \ldots m_{s-1}] \tag{5.1}$$

$$Y^T = \begin{pmatrix} y_{12} & \cdots & y_{1s} \\ \vdots & \ddots & \vdots \\ y_{r2} & \cdots & y_{rs} \end{pmatrix} = [m_2 \ldots . m_s] \tag{5.2}$$

where columns of Y^T are acquired by adjusting those in Y by a single time point, implying the overlapping of information in these matrices. A temporal succession from Y to Y^T is led by the linear operator Z, which fulfils the given relationship:

$$Y^T = ZY \tag{5.3}$$

Linear regression of the complex dynamics in these successive data matrices, i.e. Y and Y^T is estimated by evaluating the eigen decomposition of the operator Z based on a single feasible method, which is used to compute the pseudo inverse of Y using its SVD. It is assumed that the transition matrix Z having size $(r \times r)$ is a high dimensional matrix if the estimates r of an image are larger than the total count of images, $s - 1$. To evaluate the eigen decomposition of Z, the DMD technique utilized a reduced matrix $\tilde{Z}$ given by projecting Z onto the leading singular vectors of Y implementing the following procedure.

Eventually, the detected information can be roughly formulated as the simple dynamic model $\widehat{Y}(t)$:

$$Y(t) \approx \hat{Y}(t) = \phi \exp(\Omega t) \, b \tag{5.4}$$

where $\Omega = log \frac{\Lambda}{\Delta t}$, a diagonal matrix comprising eigenvalues in regular time, t shows the time and the time difference between two successive points represented by Δt. The value b introduce a vector consisting of a set of weights to combine the starting time point measured, such that $b = \Phi^{-1} m_1$.

The different dynamic modes (DMs) and their eigenvalues can be represented as follows:

$$\Phi = [\Phi^U, \Phi^S] \Leftrightarrow \Lambda = \begin{bmatrix} \Lambda^U & 0 \\ 0 & \Lambda^S \end{bmatrix} \tag{5.5}$$

where Φ^U shows the matrix having unstable DMs, and Λ^U reflects the diagonal matrix having eigenvalues as follows:

$$\Phi^U = [\phi_1^U, \dots, \phi_d^U, \dots, \phi_D^U] \tag{5.6}$$

In relation to discrete linear systems, the stability of the system is represented by the magnitude of the eigenvalue $|\lambda_I|$, which shows the stability of the system depending upon the value. If $|\lambda_I| > 1$, reflects the instability of the system and vice versa. Therefore, the eigenvalue specifies the stability and frequency of an individual mode. The essential attribute of the algorithm is that it decomposes the data, into a set of coupled spatial-temporal modes. It is important to note that the decomposition of spatial-temporal behaves as a fusion of static mode extraction by PCA in the spatial domain and spectral transformation in the frequency domain. The DMD algorithm implementing over ECG signal is discussed in algorithm 5.1.

Algorithm 5.1: DMD Algorithm for Quasi-Stationary ECG Signal Decomposition

INITIALISE Input: Load eight second ECG segment

$Y \rightarrow$ Raw data matrix of $r \times (s - 1)$

$r \rightarrow$ Number of leads

$s \rightarrow$ Sampling time point

$Y^T \rightarrow$ Matrix whose columns are acquired by shifting those in Y by one time point.

$Z \rightarrow$ Linear operator deals with temporal succession from Y to Y^T.

Output: $\Phi \rightarrow$ Dynamic modes

Step1: Calculate the SVD of first data matrix, $Y = U\Sigma V^*$

$U \rightarrow$ Left singular vector

$V \rightarrow$ Right singular vector

$\Sigma \rightarrow$ Singular values

Find the SVD of Y^T by substituting Y into Y^T.

Step2: Evaluate the pseudo inverse of Y to obtain the matrix Z.

$$Z = Y^T Y^{-1} = Y^T V \Sigma^{-1} U^*$$

Step 3: Predict Z onto the orthogonal decomposition modes of U to determine the value of $\tilde{Z}$ which signifies $\tilde{Z} = U^* Z U = U^* Y^T V \Sigma^{-1}$

Step 4: Evaluate the eigen decomposition of $\tilde{Z}$, implies $\tilde{Z} N = N\Lambda$

$N \rightarrow$ Matrix where columns of N are the eigenvectors of $\tilde{Z}$.

$\Lambda \rightarrow$ Diagonal matrix representing the eigenvalues of matrix Z.

Step 5: Enumerate the dynamic modes of utilizing the eigenvectors N and time-shifted snapshot matrix Y^T, $\Phi = Y^T V \Sigma^{-1} N$

Step 6: It is visualized that dynamic mode Φ shows the eigenvectors of the multi-dimensional operator Z, where each dynamic mode ϕ_a is proportional to the eigenvalue λ_a given by Λ.

$$\Lambda^U = \begin{bmatrix} \lambda_1^U & 0 & \cdots & \cdots & 0 \\ 0 & \ddots & 0 & 0 & \vdots \\ \vdots & 0 & \lambda_d^U & 0 & \vdots \\ \cdots & 0 & 0 & \ddots & 0 \\ 0 & \cdots & \cdots & 0 & \lambda_D^U \end{bmatrix} \tag{5.7}$$

Where ϕ_D^U is a vector that illustrate the unstable DM, and λ_d^U is an element that signify its equivalent eigenvalue, where $d = 1,2,\ldots,D$ signifies the total number of DMs. $\phi_d^U(l)$ reflects every single lead of unstable DM, where $l = 1,2,\ldots,12$. Φ^S is the matrix having stable DMs, and Λ^S shows the diagonal matrix containing the equivalent eigen values, as follows:

$$\Phi^S = [\phi_1^S, \ldots, \phi_c^S, \ldots, \phi_C^S] \tag{5.8}$$

$$\Lambda^S = \begin{bmatrix} \lambda_1^S & 0 & \cdots & \cdots & 0 \\ 0 & \ddots & 0 & 0 & \vdots \\ \vdots & 0 & \lambda_c^S & 0 & \vdots \\ \cdots & 0 & 0 & \ddots & 0 \\ 0 & \cdots & \cdots & 0 & \lambda_C^S \end{bmatrix} \tag{5.9}$$

Where ϕ_c^S is a vector which demonstrate the stable DM and λ_c^S is the element that display its eigen value, where $c = 1,2,\ldots C$ and C reviews the integral number of stable DMs. $\phi_c^S(l)$ represents every single lead of stable DM. As the count of ECG leads is always less than the number of snapshots (k), the non-zero singular values marked by SVD, Y is smaller than both the number of leads and the overall snapshots $(k-1)$. Sometimes, the total number of DMs are inappropriate to fully record the dynamic activity of cardiac system. To process the overall functionality, the number of rows must be increased around twice the number of columns by loading the time-shifted versions of the original signal to obtain an augmented data matrix Y_{aug}. It should be noticed that DMD is applied on the augmented matrix Y_{aug}, rather than Y. Few results are obtained after implementation of DMD technique on MIT-BIH Arrhythmia DB of record 101 shown in Fig 5.1. The ECG signals of different datasets from physionet with corresponding spatial-temporal modes are displayed in Fig 5.2.
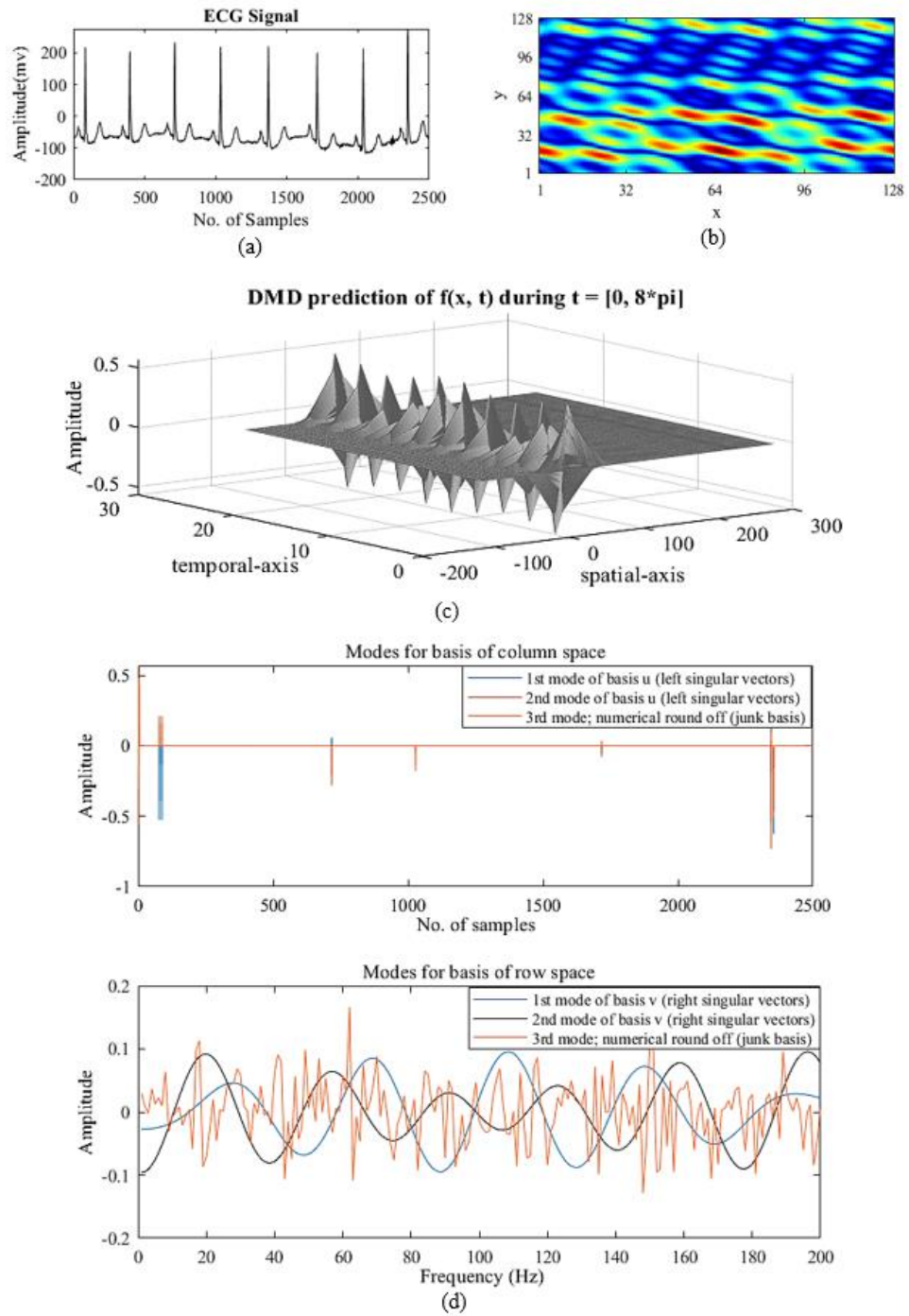
Fig 5.1 (a) ECG signal of MIT-BIHA record-101 (b) The sparse spatial dynamics for compressed DMD (c) Spatial-temporal patterns generated from DMD (d) The modes representing the left and right singular vectors of an arrhythmia record-101.
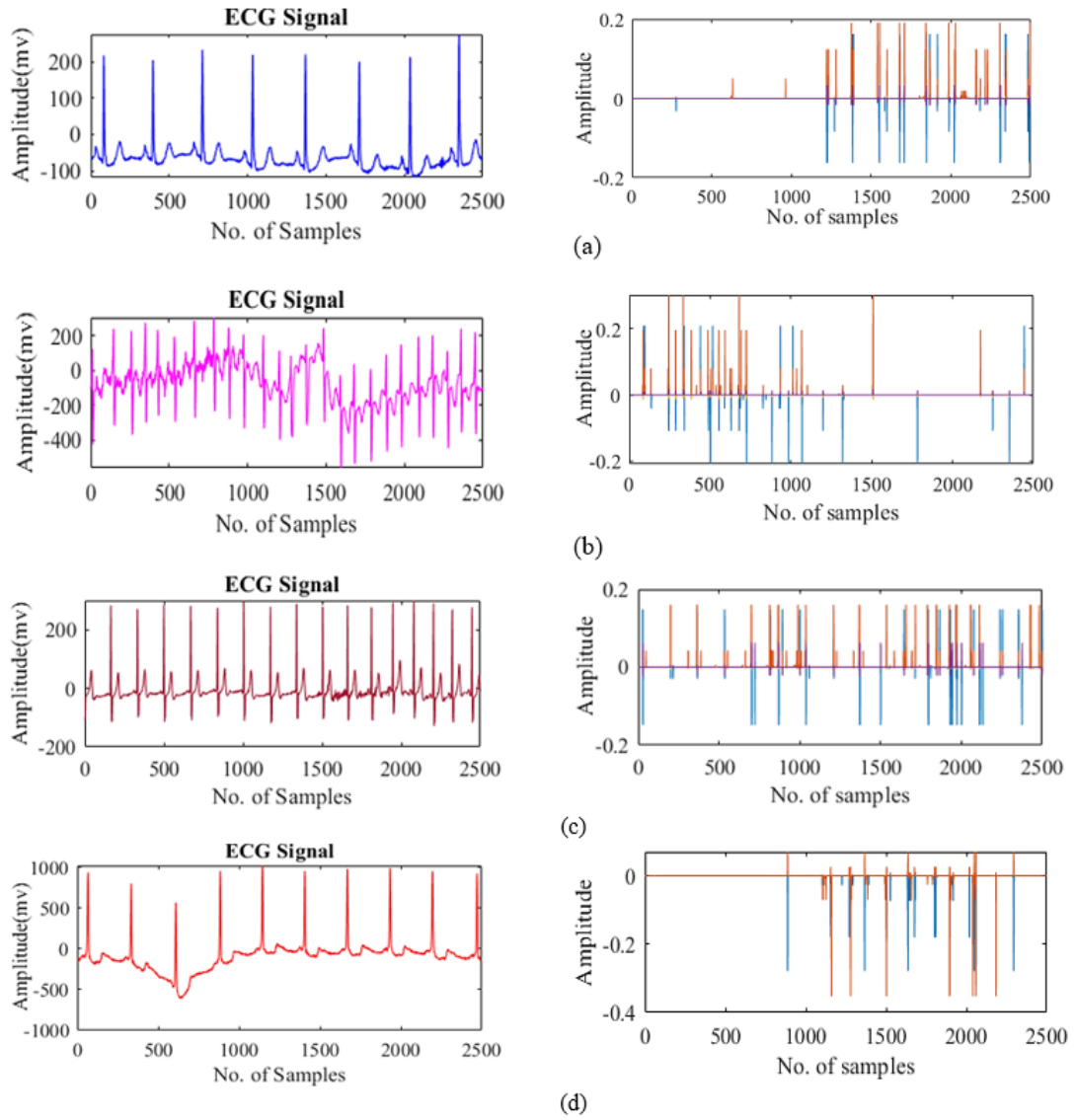
Fig 5.2 (a) The ECG signal of MIT-BIHA of record-101with spatial-temporal modes (b) MIT-BIH AF ECG signal of record 4015 with spatial-temporal modes. (c) Supraventricular Tachyarrhythmia ECG signal of record-800 with spatial-temporal modes (d) The CU Ventricular ECG signal of record-010 and the spatial-temporal modes.

Fig 5.2 represents the records of different ECG signals and correspondingly the spatial-temporal modes generated from DMD technique applied on the ECG signal. Each of the modes are associated with frequency and growth rates that computes the behaviour of the system. The spatial and temporal modes are analysed independently.

5.4 Feature Extraction Using Wavelet Scattering Transform

The feature extraction procedure acts in a unique way in recognition and classification of cardiac arrhythmia. The extraction of any small information which is used to categorise the disease can be considered as a feature.

In general, the feature extraction is divided into two types, i.e., time-domain and frequency-domain [88]. In time-domain, the peak points are efficiently used from the segmented ECG signal for feature extraction process [209]. There is a problem of generating a high dimensional feature vector and displacement of ECG signal from peak points. The RR interval, which fluctuates subtly and dynamically, is the space between successive R-peaks of ECG signal. It is best suited to record the heart rate variability which is a powerful method to consider as it is less affected by noise [210]. In frequency-domain, it is noticed by researchers that discrete wavelet transform (DWT) is more efficient to work on, due to the multi-resolution analysis [211]. Several statistical features can be extracted from DWT like mean, median, standard deviation, and many more. Along with it, more features like high order spectral, power spectral density, and hexadecimal local pattern can be extracted [212]. The features extracted not only depend on the QRS complexes but also on the P and T waves. In this work, WST is implemented for feature extraction of the dynamic modes generated from the DMD technique.

5.4.1 Wavelet Scattering Transform

The wavelet scattering transform [134] [135] constructs coherent, instructive, and translation-invariant signal depictions. It is rugged to dislocations, and conserves class discriminability that makes it especially efficient for feature extraction and categorisation. The method includes three step iterative signal transformation as wavelet convolution, modulation, and filtering. By using repetitive wavelet decomposition, local averaging, and complex modulus, the features of the signal are extracted [143]. In the end, the stability is maintained between invariance and the discrimination after clearing the signal through different scattering routes [136]. The endmost scattering matrix is a summation of all scattering coefficients of all orders to discuss the characteristics of the input signal. Due to the mean operation calculated by the low pass filter, the system is invariable to translations upto the invariance scale, which can be huge enough. The

features have a property of deformation stability due to the attributes take over from the wavelet transform. The scattering coefficients are formed that possess a low variance within a group and a high variance between the groups. From the above discussions, it has been reviewed that wavelet scattering notices the minute changes in the duration and amplitude of non-linear information which are difficult to calculate but conveys the state of the heart. Therefore, WST is implemented to generate the rugged formations of ECG heartbeat that decreases the difference in one category of arrhythmia during the maintenance of discriminability between different categories of arrhythmia. It is visualised that with the increase in the count of the layer, the energy level of scattering coefficients drops suddenly with initial two layers having 99% of the energy. We utilised a second-order scattering network for the extraction of features of ECG signal. It also minimizes the computational complexity by avoiding the calculations of higher order coefficients. The results obtained by the application of WST on the generated modes of DMD on MIT-BIH arrhythmia record 101, is illustrated in Fig 5.3.
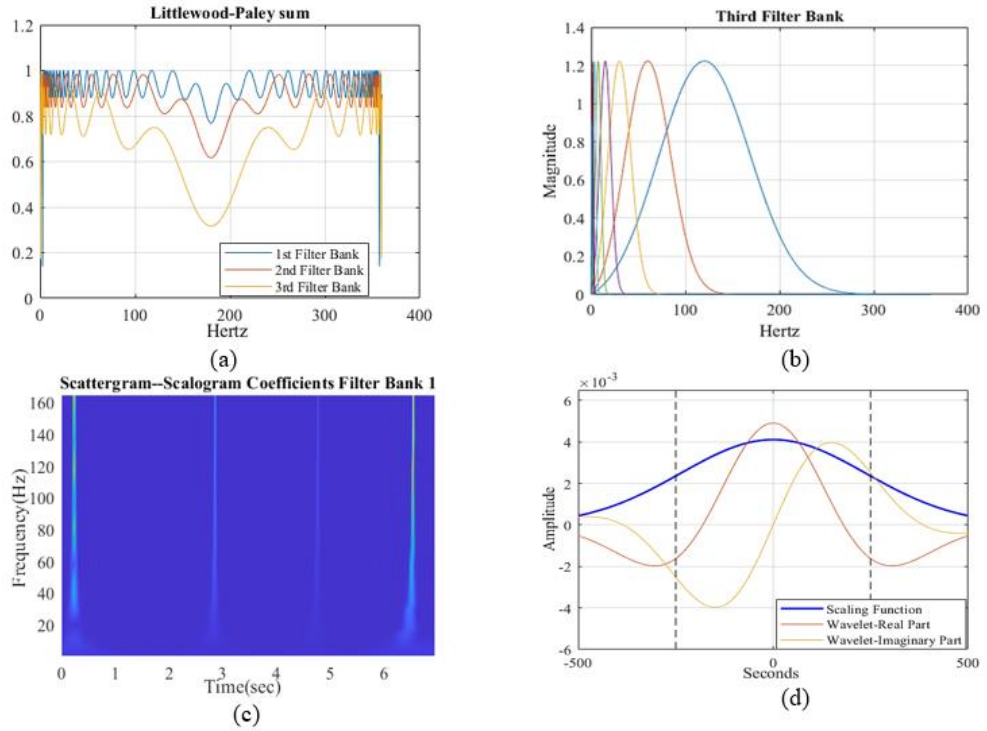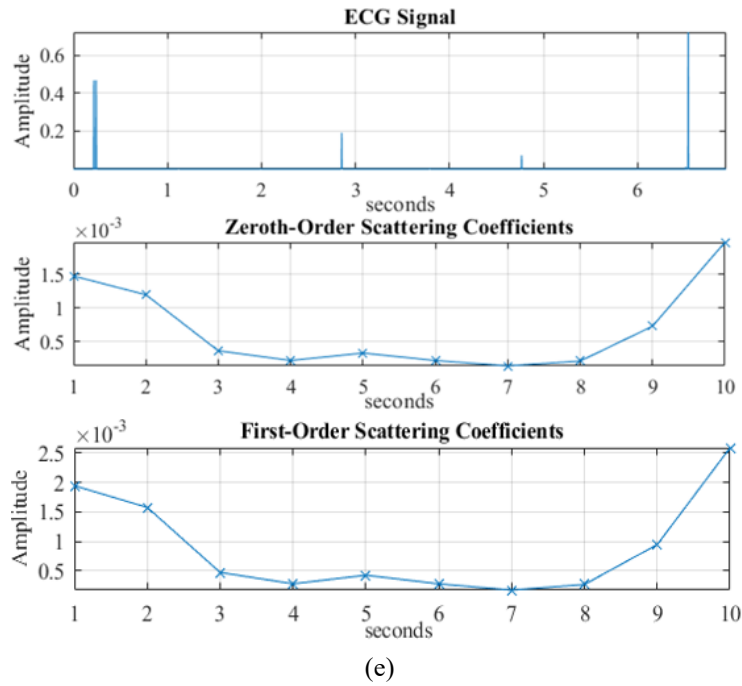
(e)

Fig 5.3. (a) The Littlewood-Paley sum of all three filter banks obtained from arrhythmia record-101 (b) The third filter bank obtained after execution of WST on the DMD output (generated through record-101). (c) The scattergram-scalogram coefficients of filter bank 1 is shown (d) invariance scale of filter bank 1 (e) The scattering coefficients with ECG signal generated after application of WST on DMD output (arrhythmia record-101).

5.5 Classification Techniques Used for Arrhythmia Detection and Classification

The implementation of classifier plays an important role in categorisation accuracy. The several classifiers imposed on the presented technique (DMD+WST) are explained in this section. The five-fold and ten-fold cross validation is implemented on the datasets that represents the variations in the evaluation parameters.

kNN (k-nearest neighbor): It predicts the similarity between the new data and the available data and keep the new data into the category which is similar to the available categories [213]. It basically stores the available data and classifies a new data point based on the similarity.

123

Algorithm 5.2: **Algorithm for ECG classification using _k_NN**

Step 1: Construct the data by scaling, missing value calculation, and dimensionality reduction.

Step 2: Load the training and test data.

Step 3: For every point in test data:

Evaluate the Euclidean distance to all training data points (Y, Yi) from $i = 1,2,3, ... , n$ where Y is the new data point, Yi is the training data.

Step 4: Keep the optimal value for k.

   Store the Euclidean distance in a list and organise it.

   From the list, choose the initial k points

Step 5: Allocate a class to the test point on the basis of majority of classes present in the selected points

   end

***SVM (Support Vector Machine)*:** It is the supervised learning algorithm used for both classification and regression problems [214]. The main aim of SVM is to calculate the best decision boundaries in an _N_- dimensional space, which can separate data points into classes, and the decision boundary as hyperplane.

Algorithm 5.3: Algorithm for ECG classification using SVM

Step 1: Load the input data.

Input: $D = [A, B]$;

$A \rightarrow$ array of input with m features,

   $B \rightarrow$ array of class labels

Output: Evaluate the performance of the system

Step 2: Train the array of input having class labels with different number of epochs.

train_svm $(A, B, epochs)$

Initialise the learning rate corresponding to the optimizer used.

Perform the iterations with distinct learning rates

   for i in A

   if $\big(B[i] * (A[i] * w)\big) < 1$ then

Update the weights corresponding to the learning rate and iterations

$$w = w + learning\ rate * ((X[i] * Y[i]) * (-2 * (1/epochs) * w)$$

else

$$w = w + learn\ rate * (2 * (1/epochs) * w)$$

end if

end

LDA (Linear Discriminant Analysis): It is a machine learning algorithm for categorisation [215]. It is operated by evaluating the mean and standard deviation for the input features by class labels. The linear algebraic operations are used to evaluate the essential quantities through matrix decomposition. The outcome is estimated from the probability that a new example belongs to each class label based on the data of every input feature. The class having the highest possibility is allotted to the example.

QDA (Quadratic Discriminant Analysis): It is a non-linear classification technique. Both LDA and QDA work on the principle of finding the boundary between the classifiers [216]. More parameters are required to estimate in QDA. A separate and individual covariance matrix will be there with QDA for every class. A quadratic decision boundary is used in QDA. The classifiers, LDA and QDA tries to evaluate the best decision boundary that increases the class separability.

Decision Tree: It is a tree-structured supervised learning technique that can be used for both categorisation and regression situations [217]. The internal nodes in the tree shows the features of the dataset, the decision rules and the outputs are reflected through the branches and each leaf node respectively. The decision is taken by the decision node and the leaf nodes are the outputs of those decision nodes. The decision is performed on the basis of the characteristics of the dataset.

5.6 DATASET USED FOR ARRHYTHMIA CLASSIFICATION

Physionet dataset (Dataset I): The presented work utilised four datasets accessed from Physionet [34] for decomposition, feature extraction, and classification. The dataset MIT-BIH AF [36], MIT-BIH SUVT [38], MIT-BIH Arrhythmia [35]and MIT-BIH CUVT are used as dataset I from physionet.

Mendeley-II dataset (Dataset II): The data is collected from 45 patients and only lead II recordings are used to mention the fragments. The dataset is fetched from the Mendeley-II and link is given in [45]. The ten-second duration of each fragment conveys some information about type of arrhythmia.
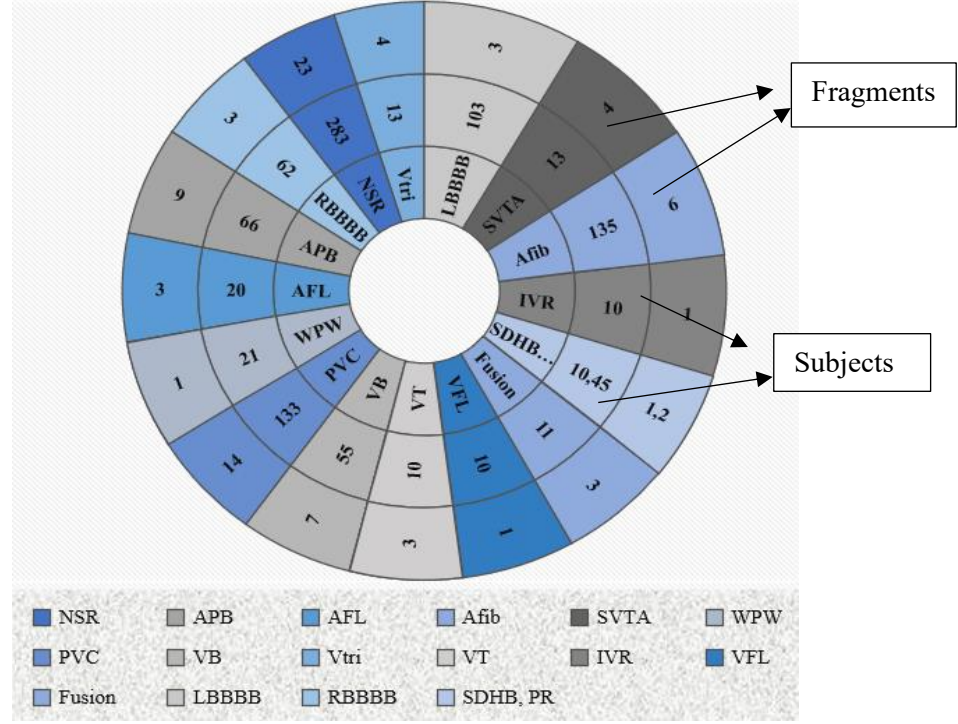
Fig 5.4. Summary of 1000 fragments of Mendeley-II dataset (17 classes) for arrhythmia classification

The fragments are sampled at sampling frequency of 360 Hz. The overall fragments with subjects are presented in Fig 5.4. The dataset II provides all the classes related to heart that helps in arrhythmia classification.

Real-time ECG dataset (Dataset III): The real-time dataset is captured with the use of iWorx LabScribe data recording device and analysis software, by placing the electrodes on the skin of human body. The three leads are used to record the data which are placed on the right arm, left arm and right limb, respectively. The representation of the leads signifies the formation of Einthoven's triangle. In this dataset, six subjects on the basis of different physical activity (exercise and limbs movement) are defined. Due to the movements in body, the motion artifacts and electromyographic noise are noticed. The data is recorded by the medical practitioners with the consent of the

subject. The captured data is of one minute which is segmented into ten-second duration. The transition in the heart rate is also measured during the recording of ECG. The real-time ECG data is recorded from three females and three males. The information gathered while recording the real-time ECG is discussed in Table 5.1 that represents the gender of the subject, physical state of the subject, and the artifacts noticed during recording of ECG.

Table 5.1 Summary of the real-time dataset recorded through iWorx LabScribe data recording device and analysis software under different physical state of the subjects.

Subject	Gender	Physical state of subject	Artifacts obtained
1	M	Resting position	Stable (no artifact)
2	M	Hand movements	Motion artifacts
3	F	Resting position	Stable (no artifact)
4	F	Cycling movements	Motion and Electromyographic artifacts
5	F	Exercising	Motion and Electromyographic artifacts
6	M	Body movements	Motion artifacts

(a)

(b)
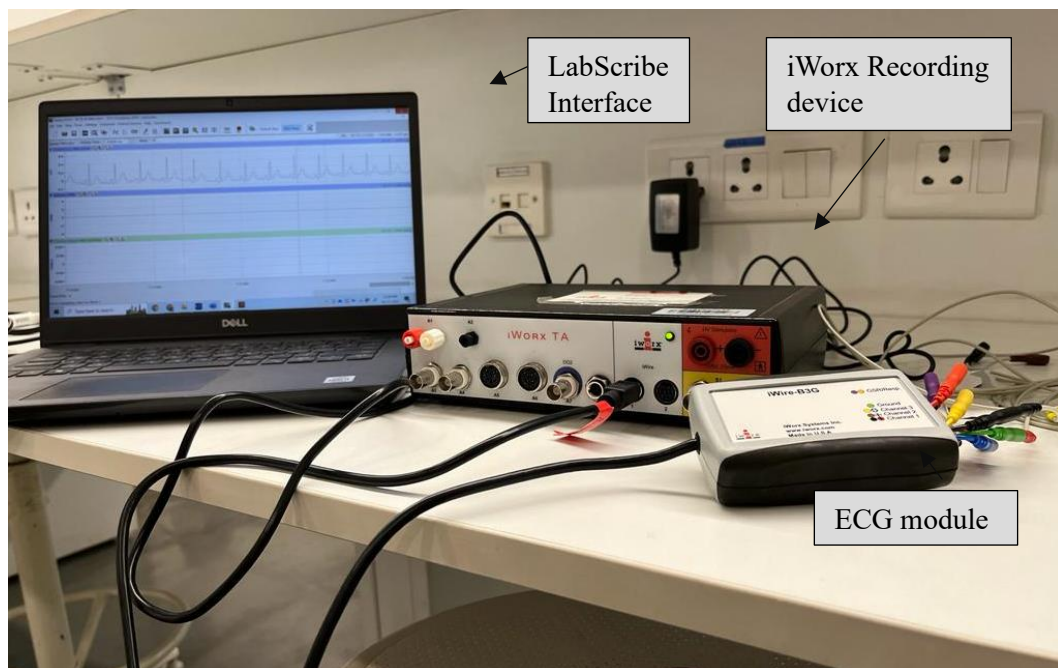
(c)

Fig 5.5. (a) The real-time ECG data is recorded using iWorx LabScribe data recording device and analysis software (b) The obtained real-time ECG waveform of the subject 1 (c) The experimental setup of iWorx LabScribe data recording device and analysis software for real-time ECG data.

The experimental setup of real-time ECG dataset recording with LabScribe interface, iWorx recorder, and the module used is shown in Fig 5.5

5.7 Implementation of DMD+WST over multiple datasets for arrhythmia classification

The overall process involves the data acquisition, preprocessing, feature extraction, and classification. This work is accomplished on three datasets namely, physionet dataset in four classes, Mendeley dataset in 17 classes, and real-time ECG dataset. Initially, preprocessing is fulfilled by performing segmentation and normalisation on each dataset and is segmented into eight second of duration. The segmented signals are fed to the decomposition technique, DMD which splits the non-linear ECG signal into dynamic modes (stable and unstable modes). The dynamic modes represent the IMFs that indicates the high and low frequency components of the signal. The sustainability of spatial-temporal modes is achieved by using the DMD technique. The decomposition step is imposed to produce a unique presentation of multicomponent signal as a sum of the mean-value and non-stationary mono component signals. The different modes generated are then applied to the WST for feature extraction. It provides the consistent, and translation invariant representation of signal. It exhibits zeroth, first, and second order scattering coefficients associated with different filter banks. The modes generated from DMD are individually applied to WST for feature extraction and also produce the scalograms that demonstrate the energy diagrams showing the intensity of the specified signal in terms of peaks. The creation of scalograms conveys the information associated with the non-linearity of the signal. The WST feature vector is a 3-dimensional tensor resulting the scattering route $\times$ wavelet scale $\times$ number of signals. The scattering coefficients of one ECG pulse are represented by a single layer of the tensor and the down sampling of the coefficients is performed according to the bandwidth of low pass filter. To make the outcome suited for the classifiers, refinement of the tensor into two-dimensional matrix is executed in which column and row represent the scattering route and the time frame, respectively. The acquired features are then applied to the machine learning algorithms where 80% data is used as training and 20% data is utilised for testing purposes. Several models as SVM, kNN, Bagged Trees, Boosted Trees, Optimized SVM, Optimized kNN, QDA, and LDA are employed on the extracted features to categorise them into multiple classes.

The same process is executed on dataset I, II and III, in which the normalisation is performed on the non-linear values of original ECG signal followed by the segmentation process. The DMD technique is applied on the segmented data, and reflects the spatial-temporal modes on which the WST is employed for feature extraction. After completing the following steps, features are then fed to the machine learning algorithms to focus on the specific categorisation of disease. Using dataset I, the classification is done in four classes i.e. Normal, AFib, SUVT, and CU_VT. Using dataset II, the categorization is made in 17 classes i.e. NSR, APB, AFL, Afib, SVTA, WPW, PVC, VB, Vtri, VT, IVR, VFL, Fusion, LBBBB, RBBBB, SDHB, and PR. Dataset III is based upon real-time ECG recording using iWorx LabScribe data recording device and analysis software that categorise the real-time ECG data of six subjects.

Here, the details of hyperparameters utilised for optimizable *k*NN machine learning model is described, where the count of 30 iterations is used, the Bayesian optimizer is utilised, and ten-fold cross validation is employed for classification mentioned in Fig 5.6. The hyperparameters are essential to tune for correct classification of the respective data.
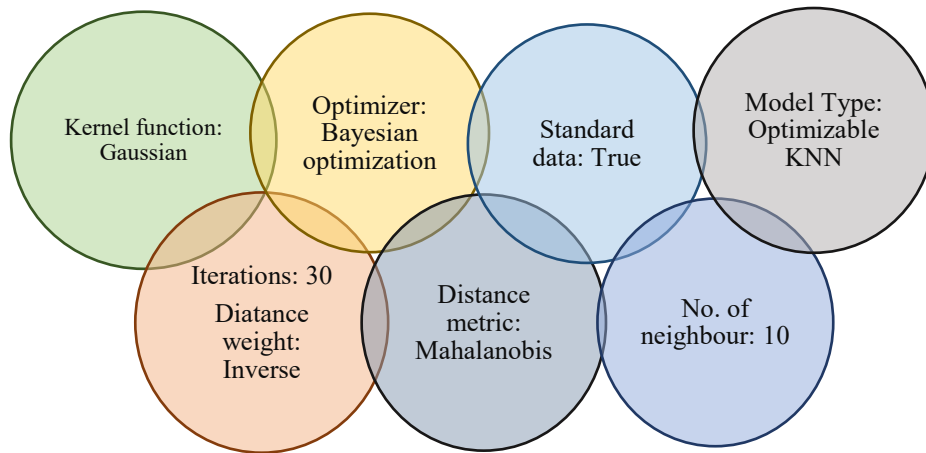
Fig 5.6 Illustrating the optimized hyperparameters (Bayesian optimization) utilised during the training step

The overall structure of presented methodology is illustrated in Fig 5.7 which includes the different steps like data acquisition from human heart followed by the preprocessing of the signal. The decomposition step is implemented followed by the feature extraction and at last, the detection and classification of ECG is performed.
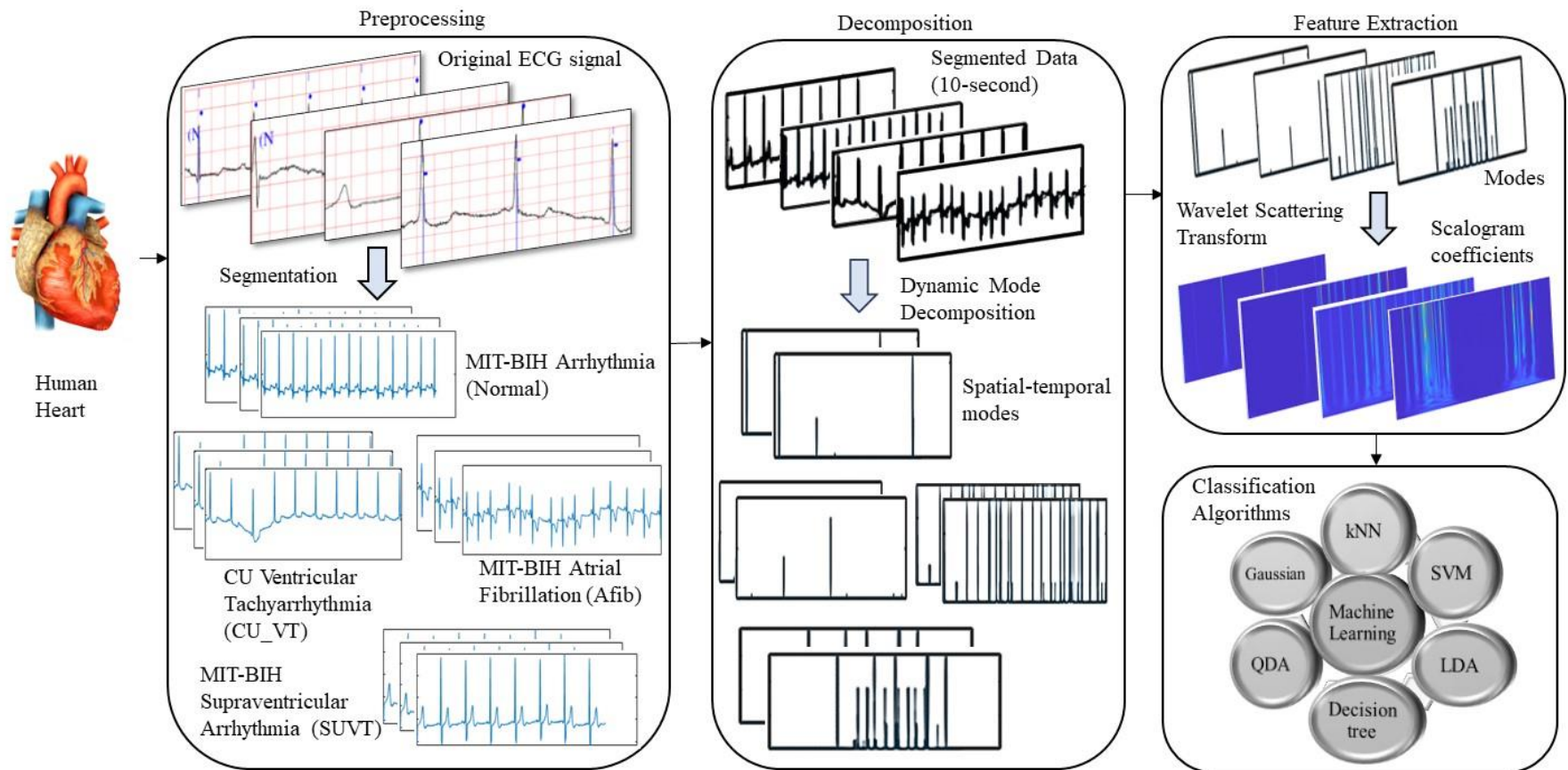
Fig 5.7 The framework of Dynamic Mode Decomposition with Wavelet Scattering Transform (DMD+WST) for multi-level classification

131

The presented algorithm (DMD+WST) over non-linear ECG signal is represented in Algorithm 5.4.

Algorithm 5.4 DMD+WST Algorithm over non-linear ECG Signal

INITIALISE Input: $y(n) \rightarrow$ Eight second ECG segment

$Y \rightarrow$ Raw data matrix of $r \times (s-1)$.

$r \rightarrow$ Number. of leads

$s \rightarrow$ Sampling time point

$Y^T \rightarrow$ Matrix whose columns are acquired by shifting those in Y by one time point.

$Z \rightarrow$ Linear operator deals with temporal succession from Y to Y^T.

Output: $C_m Y(t) \rightarrow$ feature matrix

Step1: Calculate the SVD of our first data matrix,

for $k \in [1,2,..,t]$ **do**

$$Y = U \sum V^*$$

Calculate $Y^T = ZU \sum V^*$

end

Step2: Evaluate the pseudo inverse of Y to obtain the matrix Z.

for $t \in [0, \ldots, 4 * pi]$ **do**

$Z = pinv(\Phi) * svd(f)$

end

Step 3: Predict Z onto the orthogonal decomposition modes of U to determine the value of $\tilde{Z}$ which signifies $\tilde{Z} = U^* Z U = U^* Y^T V \sum^{-1}$

Step 4: Evaluate the eigen decomposition of $\tilde{Z}$, implies $\tilde{Z} N = N \wedge$

$[N, \wedge] = eig(\tilde{Z})$

$N \rightarrow$ Matrix where columns of N are the eigenvectors of $\tilde{Z}$.

$\wedge \rightarrow$ Diagonal matrix representing the eigenvalues of matrix Z.

Step 5: Evaluate the dynamic modes of Y utilising the eigenvectors N and time-shifted snapshot matrix Y^T, $\Phi = Y^T V \sum^{-1} N$.

Eigen value, $\lambda = diag(\wedge)$

Step 6: Calculate the translation-invariant,

$$C_o Y(t) = Y * \phi_L(t); \ \phi_L(t) \rightarrow \text{Low pass filter}$$

Step 7: The first-order scattering coefficients are evaluated by taking the mean, which is given as

$$C_1 Y(t) = \left\{ \left| Y * \Psi_{l_1} \right| * \phi_L(t) \right\}_{l_1 \in \Lambda_1}$$

Step 8: The second-order scattering coefficient,

$$C_2 Y(t) = \left\{ \left| \left| Y * \Psi_{l_1} \right| * \Psi_{l_2} \right| * \phi_L(t) \right\}_{l_i \in \Lambda_i}, i = 1,2.$$

Step 9: Calculate the total scattering matrix, shows the feature matrix, followed the 2-layer process.

$$C_1 Y(t) + C_2 Y(t) = C_m Y(t)$$

$$C_m Y(t) = \sum_{l_i}^{\Lambda_i} \left\{ \left| \left| \left| Y * \Psi_{l_1} \right| * \ldots \right| * \Psi_{l_m} \right| * \phi_L(t) \right\}, \\ i = 1,2, \ldots, m.$$

Step 10: Apply the obtained matrix as the input to the KNN with 5-fold and 10-fold cross validation. Predict the specific class of disease.

5.8 Experimental Results

The performance of the model can be analysed with some parameters like accuracy, sensitivity, specificity, precision, F1-score, G-mean, MCC value, and Cohen's Kappa. We implemented the machine learning algorithms over MATLAB software. The simulations are performed with NVIDIA GEFORCE RTX 3070, 11th Gen Intel(R) Core (TM) i7-11370H @ 3.30GGHz, 64-bit operating system, x64-based processor.

5.8.1 Performance analysis on the basis of datasets

The feature extraction is initiated by employing the WST on the different modes generated by DMD technique. The outcome of feature extraction produces a matrix for each decomposed value generated by DMD. On the completion of feature extraction process, the combination of all the metrices is made and a balanced data is maintained according to the specific class. The extraction of features makes the classification process better for diagnosing the specific disease. The data in the form of matrix is applied to the machine learning algorithms for detection and categorisation into different arrhythmia classes namely, Normal, Afib, CU_VT, and SUVT. The different

classifiers, SVM, *k*NN, QDA, LDA, PCA, and Trees, are executed for acquiring the outcome of categorisation. With the help of categorised classes, the specific disease is treated without any delay for the cure of the patient. In overall, the optimized *k*NN proved the maximum validation and testing *Acc* over dataset I is 92.8% and 99.4%, respectively with the training time of 0.63987 seconds. The relevant results are obtained from optimizable SVM on the same dataset is 94.6% and 98.9% as validation and testing *Acc*, respectively. The overall value of *Sens, Spec, prec, F1-sc, MCC value*, and *Cohen's Kappa* obtained on dataset I are 98.1%, 99.6%, 98.8%, 98.9%, 0.92 and 0.99 respectively. In case of dataset II, the *k*NN algorithm reflects an overall *Acc* of 98.7% and categorised into 17 classes of arrhythmia i.e. NSR, APB, AFL, Afib, SVTA, WPW, PVC, VB, Vtri, VT, IVR, VFL, Fusion, LBBBB, RBBBB, SDHB, and PR.

The overall value of *Sens, Spec, prec, F1-sc, MCC value*, and *Cohen's Kappa* attained on dataset II are 97.1%, 99.1%, 98.2%, 97.7%, 0.91, and 0.94 respectively. The samples are recorded at a sampling rate of 360 Hz through lead II. In real-time dataset III, the overall testing *Acc* obtained from optimized *k*NN is 96.3%. The value achieved from other parameters, *Sens, Spec, prec, F1-sc, MCC value*, and *Cohen's Kappa* are 96.8%, 96.9%, 96.1%, 96.7%, 0.89, and 0.90 respectively.

Dataset I (Physionet dataset): The confusion metrics consisting the number of observations of each individual class after implementation of optimized *k*NN is represented in Fig 5.8. The confusion metrics representing the sensitivity of each class of dataset I after validating through optimized *k*NN is displayed in Fig 5.9. Each categorised class here represents the number of observations corresponding to the feature matrix generated by WST. The validation *Acc* of 92.8% is attained with ten-fold cross validation. The values of sensitivity or recall is equivalent to true positive rate (TPR), that always focus on the actual positive values. It predicts the correctly positives out of the actual true values. False negative rate (FNR) predicts the false negative out of the actual positives.

Fig 5.8. The confusion metrics representing the number of observations with validation accuracy of 92.8% after implementing the optimized *k*NN as classifier on dataset I.

Fig 5.9. The confusion metrics depicting the sensitivity of individual class after execution of the optimized *k*NN on dataset I.

The minimum classification error (MCE) is a well-known parameter to calculate the

error while performing classification. The validation of MCE is required to reduce the final classification error while dealing with any new dataset. The MCE representation is shown in Fig 5.10.
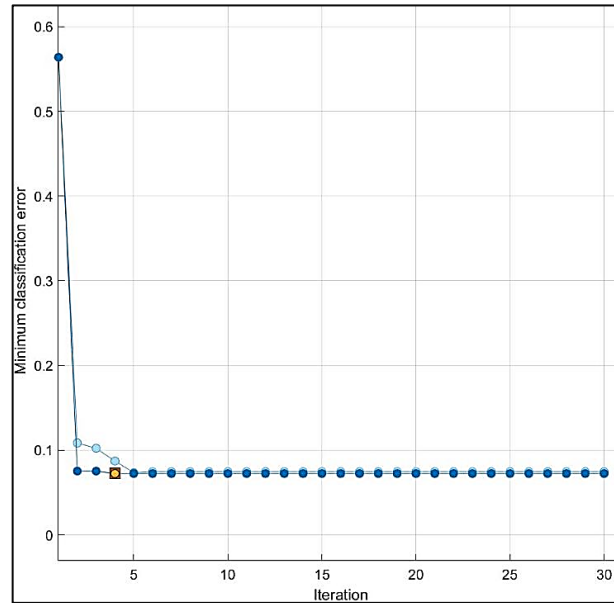
Fig 5.10. Illustration of the minimum classification error achieved with optimizable *k*NN algorithm under 30 iterations using Bayesian optimizer reflects the validation and testing accuracy of 92.8% and 99.4% respectively.
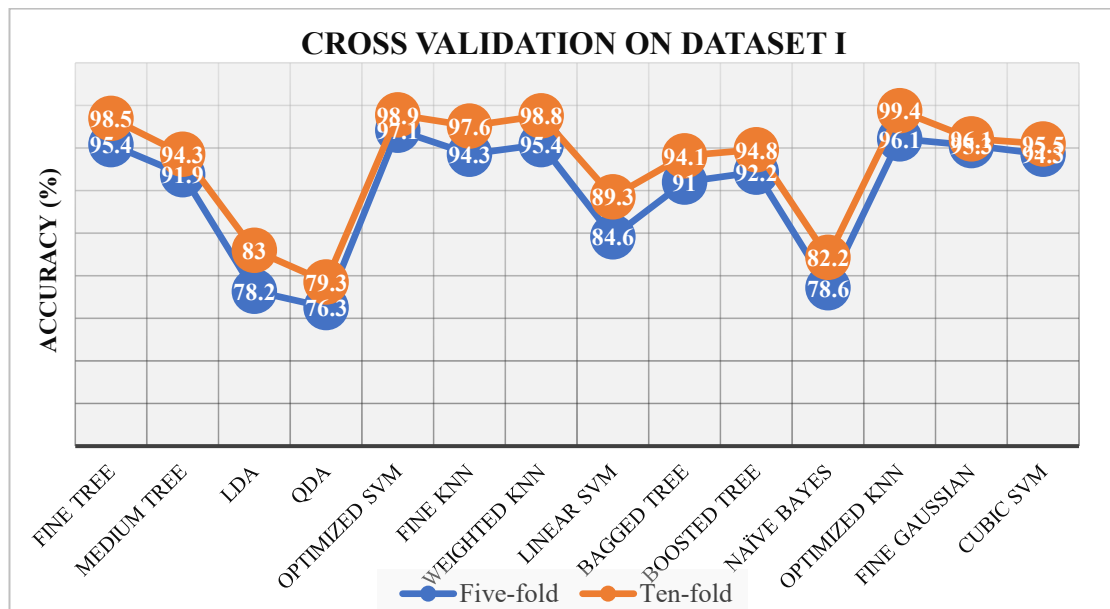
Fig 5.11. A line graph is drawn showing the overall accuracy on dataset I by employing 14 classifiers using five-fold and ten-fold cross validation.

The visualisation of 14 classifiers (Fine Tree, Medium Tree, LDA, QDA, Optimized SVM, Fine *k*NN, Weighted *k*NN, Linear SVM, Bagged Tree, Boosted Tree, Naïve Bayes, Cubic SVM, Fine Gaussian and Optimized *k*NN) is mentioned in Fig 5.11.

The graph indicates that ten-fold cross validation reflects more accurate and precise results than five-fold cross validation. Few evaluation parameters like sensitivity, specificity, precision, and F1-score are measured using 14 classifiers (Fine Tree, Medium Tree, LDA, QDA, Optimized SVM, Fine *k*NN, Weighted *k*NN, Linear SVM, Bagged Tree, Boosted Tree, Kernel Naïve Bayes, and Optimized *k*NN, Optimized SVM, and Fine Gaussian) on dataset I, is represented through radar plot in Fig 5.12.

The ten-fold cross validation is utilised for both training and testing purposes. The performance comprising the accuracy, sensitivity, specificity, precision, and F1-score acquired from SVM and KNN on dataset I is summarised in Table 5.2. Some more parameters (G-mean, MCC value, and Cohen's Kappa) are evaluated of all classifiers on dataset I are discussed in Table 5.3.

Dataset II (Mendeley II dataset): It consists of 17 classes of arrhythmia fetched from Mendeley-II, sampled at 360 Hz frequency. The records are maintained according to the fragments and the corresponding subjects. The results (accuracy, sensitivity, specificity, precision, F1-score, G-mean, MCC value, and Cohen's Kappa) obtained through optimized *k*NN classifier on dataset II is reported in Table 5.4 and 5.5.
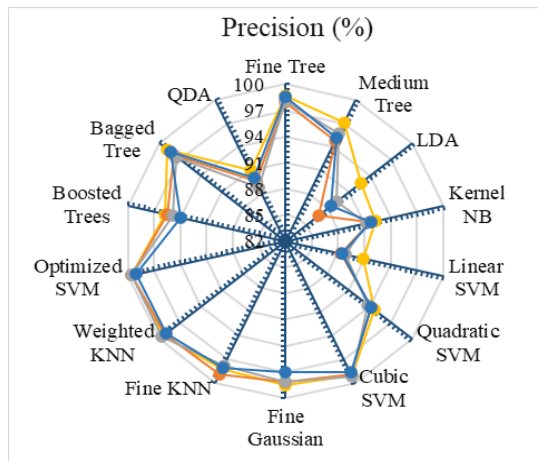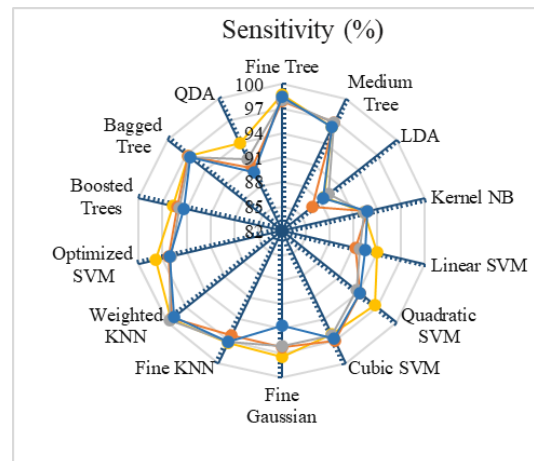
(a)   (b)
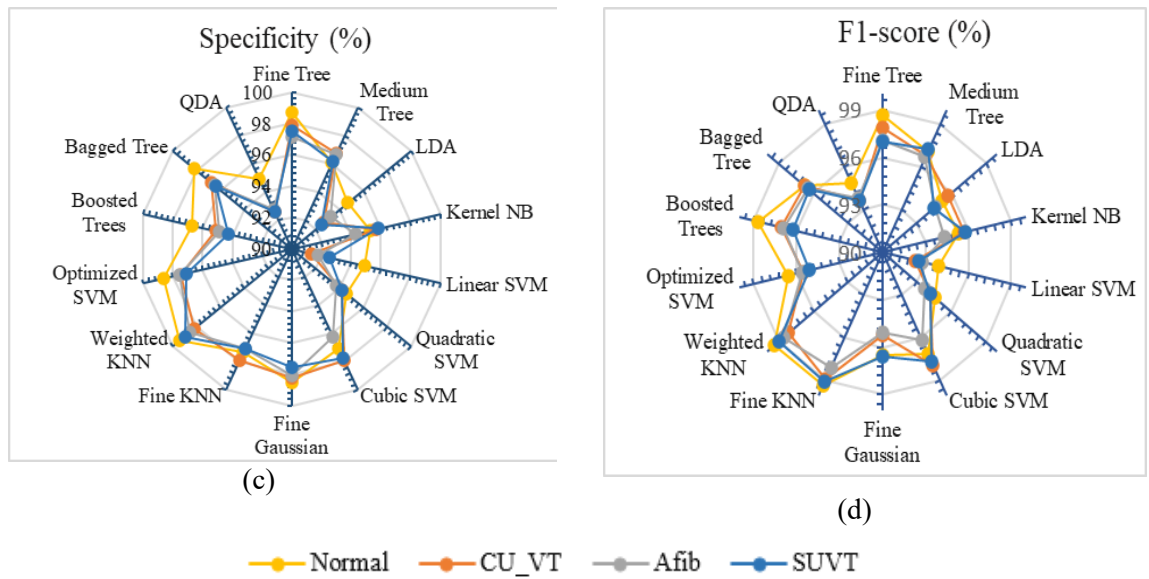
Fig 5.12. (a) The radar plot showing the percentage value of precision on Dataset I using 14 classifiers. (b) Depicting the percentage value of sensitivity on dataset I. (c) Representing the percentage of specificity of each class. (d) Depicting the percentage value of F1-score through radar plot.

The highest *Acc* is recorded with RBBB and VFL of 98.2%, while the maximum *Sens* of 98.1% is noted with IVR, VFL, and LBBBB. The highest attained value of *Spec* and *precision* is 98.9% and 98.3% with VFL respectively, while the maximum recorded value of *F1-sc* is 98.2% with PR and RBBBB.

Table 5.2 Classification summary (on test dataset) employing (DMD+WST) attained from SVM and optimized *k*NN as classifiers on dataset I (physionet).

Class	Acc (%)		Sens (%)		Spec (%)		Prec (%)		F1-sc (%)	
	SVM	*k*NN	SVM	*k*NN	SVM	*k*NN	SVM	*k*NN	SVM	*k*NN
Normal	97.6	99.1	96.8	98.7	97.7	100	97.1	98.9	97.0	98.6
CU_VT	96.8	98.9	96.2	98.3	95.7	99.2	96.4	99.3	96.5	97.4
SUVT	97.0	98.7	97.9	100	98.1	100	97.6	98.9	98.6	98.3
Afib	97.1	99.3	97.8	99.4	97.9	99.7	97.2	98.8	97.7	98.1

Table 5.3 The summary of the G-mean, MCC values, and Cohen's Kappa of the presented technique (DMD+WST) evaluated on dataset I (physionet) using several classifiers.

Parameter ↓	Classifier→ Classes↓	kNN	SVM	LDA	QDA	Fine Tree	Medium Tree	Bagged Tree	Boosted Tree	Naïve Bayes	Fine Gaussian
G-mean		0.990	0.941	0.876	0.882	0.843	0.887	0.862	0.832	0.768	0.832
MCC values	Normal	0.95	0.88	0.81	0.79	0.68	0.79	0.85	0.86	0.78	0.71
	CU_VT	0.87	0.83	0.73	0.75	0.63	0.74	0.80	0.82	0.71	0.65
	SUVT	0.94	0.85	0.78	0.77	0.69	0.73	0.83	0.81	0.70	0.69
	Afib	0.88	0.80	0.76	0.72	0.61	0.71	0.82	0.79	0.73	0.68
Cohen's Kappa	Normal	0.93	0.82	0.79	0.76	0.69	0.71	0.81	0.76	0.69	0.69
	CU_VT	0.85	0.78	0.77	0.72	0.66	0.69	0.73	0.77	0.68	0.65
	SUVT	0.92	0.80	0.71	0.73	0.67	0.70	0.79	0.80	0.63	0.63
	Afib	0.86	0.81	0.73	0.70	0.71	0.65	0.78	0.72	0.70	0.61

Table 5.4 Performance of evaluation parameters on dataset II (Mendeley II) with kNN as classifier using (DMD+WST) for arrhythmia classification.

Classes	Acc (%)	Sens (%)	Spec (%)	Prec (%)	F1-sc (%)	MCC value	Cohen's Kappa
NSR	97.6	96.8	97.9	96.9	96.6	0.89	0.82
APB	96.8	96.3	96.7	96.1	96.3	0.81	0.87
AFL	95.8	96.1	96.0	95.9	95.4	0.85	0.83
Afib	94.2	95.1	95.7	95.4	95.7	0.89	0.86
SVTA	95.8	96.2	96.8	96.2	96.8	0.92	0.89
WPW	96.7	97.1	97.8	96.5	96.8	0.84	0.79
PVC	96.2	96.8	97.3	96.7	96.9	0.96	0.88
VB	97.3	97.2	98.0	97.6	97.8	0.90	0.85
Vtri	96.3	97.6	96.2	96.5	96.1	0.82	0.79
Vtach	97.4	97.8	97.9	97.1	97.6	0.88	0.83
IVR	97.8	98.1	98.3	97.7	97.3	0.87	0.82
VFL	98.2	98.1	98.9	98.3	98.1	0.80	0.77
FVNB	97.9	97.3	98.1	97.3	97.6	0.97	0.91
LBBBB	97.2	98.1	98.6	97.1	97.4	0.94	0.90
RBBBB	98.2	97.7	98.4	97.3	98.2	0.83	0.81
SDHB	96.4	97.3	97.8	96.4	96.3	0.82	0.79
PR	97.4	97.9	98.3	97.1	98.2	0.86	0.83

Table 5.5 The summarised values of the G-mean calculated over the presented technique (DMD+WST) using dataset II (Mendeley II) with different classifiers

Classifier	kNN	SVM	LDA	QDA	Fine Tree	Medium Tree	Bagged Tree	Boosted Tree	Naïve Bayes	Fine Gaussian
Values	0.94	0.92	0.83	0.86	0.76	0.83	0.87	0.88	0.84	0.91

Dataset III: A few artifacts are noticed while recording the real-time ECG data using iWorx LabScribe data recording device and analysis software which is mentioned in Fig

5.13. The presented technique is being tested on real-time dataset and proves the reliability at all datasets. The evaluation parameters (Accuracy, Sensitivity, Specificity, Precision, F1-score, MCC value, and Cohen's Kappa) are calculated on dataset III, mentioned in Table 5.6 and the confusion metrics representing the testing sensitivity of dataset III of all six subjects implementing optimized kNN is displayed in Fig 5.14. The optimized kNN classifier is applied with ten-fold cross validation which results best in other classifiers. Several other classifiers like LDA, QDA, Medium Tree, Linear SVM and Optimized SVM are also implemented but optimized kNN reflects better. The overall results of all the datasets are mentioned in Fig 5.15 specifying the accuracy, sensitivity, specificity, precision, and F1-score.

(a)

(b)
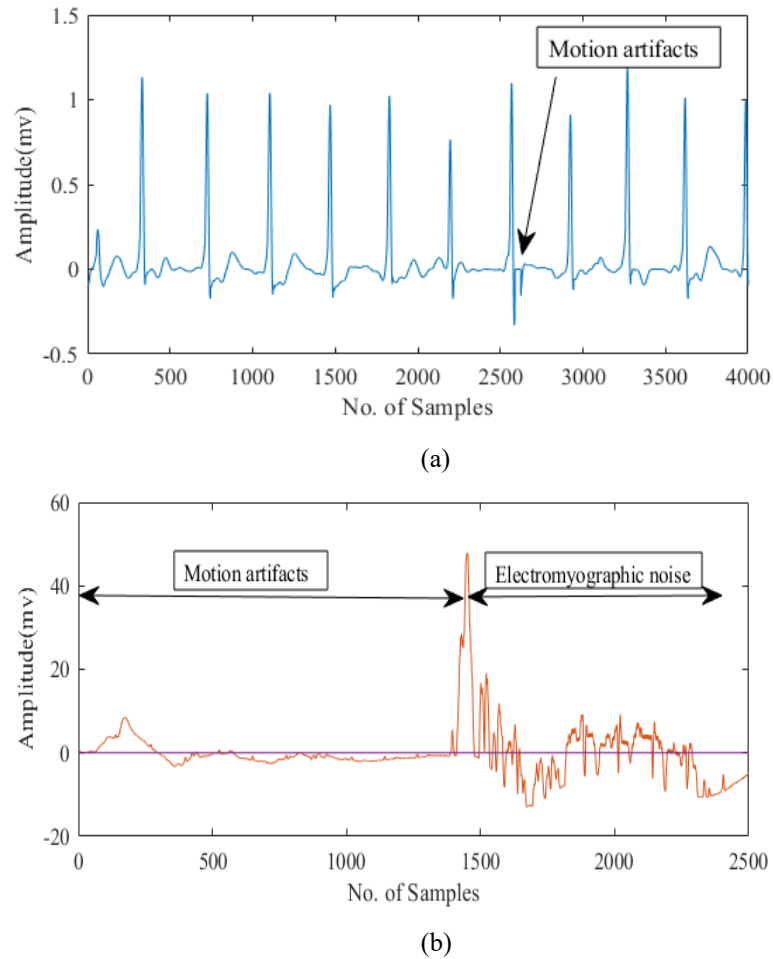
Fig 5.13. The artifacts noticed during recording of real-time ECG data using iWorx LabScribe data recording device and analysis software of subject 2 and subject 5 respectively.

141

Table 5.6 Summary of evaluation parameters calculated on test dataset with optimized *k*NN on dataset III (Real-time dataset).

Subject	Male/ Female	Acc (%)	Sens (%)	Spec (%)	Prec (%)	F1-sc (%)	MCC value	Cohen's *K*appa
1	M	93.7	89.8	94.3	99.3	98.3	0.82	0.83
2		97.2	97.4	97.8	96.4	97.3	0.84	0.80
3		98.1	97.2	97.9	93.3	96.7	0.81	0.84
4	F	94.3	92.0	94.1	97.5	97.9	0.84	0.86
5		96.8	96.6	97.2	92.7	96.8	0.92	0.87
6		98.4	98.6	98.9	93.2	97.4	0.91	0.91
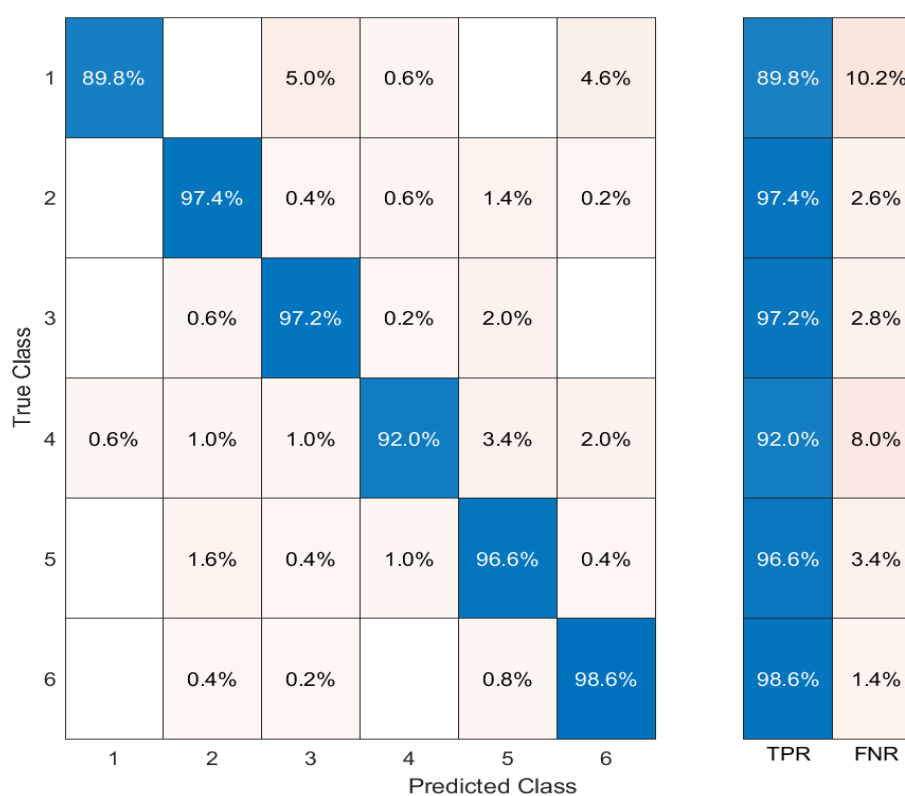
Fig 5.14. The confusion metrics depicting the testing sensitivity of individual subject after execution of the optimized *k*NN on dataset III (Real-time dataset).
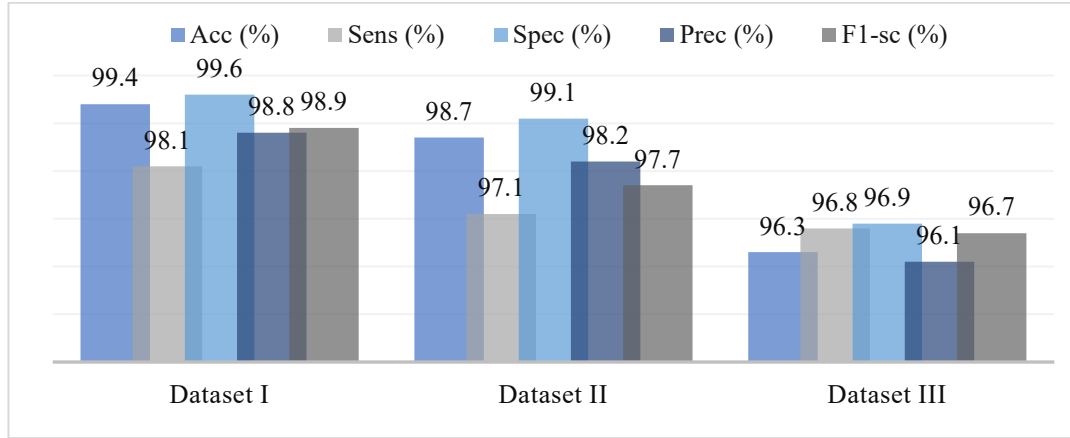
Fig 5.15 Illustration of graph showing the obtained values of evaluation parameters at dataset I, dataset II, and dataset III for arrhythmia classification using (DMD+WST).

5.8.2 Based on the comparison with existing methods

The experimental analysis is performed over three datasets with DMD+WST technique for arrhythmia classification. The results are recorded on the basis of evaluation parameters (*Acc, Sens, Spec, prec, F1-sc, G-mean, MCC value, and Cohen's Kappa*). The comparison mentions a few of the reported research results on the multilevel classification. The performance comparison is made between the presented method and the previous methods on the basis of multiple classes is mentioned in Table 5.7.

5.9 Discussions over DMD+WST using distinct datasets for arrhythmia classification

The work focuses at categorising the multilevel arrhythmia, particularly to recognise the subject is suffered from which disease. Three datasets are utilised to detect and classify the multiple disease. The classification is done for identifying the four different classes from Physionet dataset, 17 arrhythmia classes from Mendeley-II dataset, and the real-time ECG data which is recorded using iWorx LabScribe data recording device and analysis software. The purpose to work over the real-time ECG signals is to scrutinize the efficiency of the model, whether the model is able to identify the diseased patient or not. Here, the overall process consists of implementation of scattering transform on the decomposition modes. The DMD technique is imposed on the segmented data recorded from ECG. The spatial and temporal modes are generated that specifically defines the different frequency components.

Computational complexity of DMD:

In dynamic mode decomposition, for an $m \times n$ matrix:

Computational complexity of singular valued decomposition, SVD is $O(mn^2)$ (if $m > n$)

After SVD, DMD computes eigenvalues of an $r \times r$ matrix (where r is reduced rank).

$$\text{Eigen-decomposition computational complexity} = O(r^3)$$

Total Complexity of Standard DMD: $O(mn^2) + O(r^3)$

Since r^3 is tiny compared to mn^2. The computational complexity of standard Dynamic Mode Decomposition is dominated by the SVD step and is approximately $O(mn^2)$, while reduced-rank or randomized DMD reduces it to $O(mnr)$.

Table 5.7 Performance comparison of the presented method and the existing methods over multilevel arrhythmia classification.

Year	Model	Class/leads/records	Datasets	Performance
(2012) [187]	LDC+ EMCA	3 classes, 2 leads and 12 leads, 609 records	MIT-BIH Arrhythmia, SUP, ST, MITBIH-LT, INCART	*Acc*- 95.42
(2021) [218]	MS-ECG, MC-ECG	5 classes	CPSC [219]	*Prec*-84.62
(2020) [220]	STA-CRNN	8 classes of Arr and normal rhythm, 6877 records, 12 leads	CPSC	*F1-sc*- 83.50
(2019) [221]	Neural network	12 leads	China Intelligent Competition	*F1-sc*- 87.8 *Acc*- 83.60
(2023) [134]	WST + SVM	17 classes, 1000 fragments	Mendeley dataset	*Acc*- 98.90
(2017) [222]	Neural Net Fitting Model	3 leads, 4 classes	Real-time dataset: IOT+SNOMED coding system	*Acc*- 97.0 *MSE*- 0.0087
(2020) [223]	ECG sensor module AD8232	3 leads	Real-time dataset	*Acc*- 90.0

(2022) [178]	SLT+ DenseNet/ GoogleNet/ AlexNet	3 classes, ML II lead	MIT-BIH Arrhythmia, malignant, CU_VT Fantasia, AF term challenge,	*Acc*- 96.2
(2018a) [224]	SVM	17 classes, 744 fragments, MLII lead	MIT-BIH Arrhythmia	*Acc*- 98.99 *Spec*- 99.46
(2018b) [45]	SVM	17 classes, 1000 fragment, ML II lead	MIT-BIH Arrhythmia	*Acc*- 98.85 *Spec*- 99.39
(2021) [225]	CNN-LSTM+ RRHOS-LSTM	4 classes, (1, 3, and 5 beats)	MIT-BIH Arrhythmia	*Acc*- 95.81
(2018) [226]	Unidirectional LSTM, Bi-LSTM	5 classes, 360 sampled ECG signals	MIT-BIH Arrhythmia	*Acc*- 99.39
(2024) [227]	DMD+ WST+ *k*NN	4 Classes	MIT-BIH Arrhythmia, CU_VT, AFib, SUVT	*Acc*- 99.4%
	DMD+WST+ SVM			*Acc*- 98.9%
	DMD+ WST+ *k*NN	17 Classes, MLII	Mendeley dataset	*Acc*- 98.7%
	DMD+ WST+ *k*NN	3 leads, 6 Subjects	Real-time dataset	*Acc*- 96.3%

The WST is implemented on frequency components for feature extraction process. The machine learning algorithms are applied on the presented combination of DMD+WST for accurate classification. The selection of the particular classifier for multilevel classification is noted on the basis of the performance of evaluation parameters (accuracy, specificity, sensitivity, precision, F1-score, G-mean, MCC value, and Cohen's Kappa). To demonstrate the reliability of the presented method, a five-fold and ten-fold cross validation is executed after the model structure is framed. It is observed that optimized *k*NN proves the robustness with all datasets as compared to other reported classifiers.

5.10 Summary of DMD+WST over multiple classifiers for arrhythmia classification using real-time ECG signal

The work presented the arrhythmia classification on the basis of derived dynamic mode decomposition technique and wavelet scattering transform. The ECG signals are decomposed using DMD technique and rebuilds into stable and unstable modes of different frequency scales. The work also shows that the stability analysis of ECG

modes can expose the underlying spatiotemporal dynamics of the cardiac system and represent the status of the heart disease. Over the individual modes, WST is applied to extract the features. The data generated from WST is applied to the machine learning models. The optimized hyperparameters are utilised to train the distinct machine learning algorithms (SVM, kNN, LDA, QDA, Optimized kNN, Optimized SVM, Gaussian, Naïve Bayes, PCA, Medium Tree, Boosted Tree, and Bagged Tree) to perform the classification on utilised datasets. The presented method is validated over three datasets and acquired an overall *Acc* of 99.4%, 98.7%, and 96.3% on dataset I, dataset II, and dataset III respectively. The work reflects efficient results with decomposition technique and execution of WST on multilevel arrhythmia categorisation.

Chapter 6

Conclusion and Future Scope

6.1 Conclusion

This chapter summarises the conclusion of the presented work. Also, it compiles the future work related to the arrhythmia detection and classification using ECG signals.

✓ Firstly, we implemented a parallel cluster wavelet analysis (PCWA) technique using the Ricker wavelet for accurate R-peak detection in ECG signals. This is an unsupervised approach that effectively work over multiple datasets at a time. The technique isolates the characteristic peaks by leveraging the Ricker wavelet's sensitivity to sharp transitions. By processing multiple signal segments in parallel, the technique enhances computational efficiency and robustness, particularly in noisy or irregular ECG recordings. Our approach significantly improves the reliability of R-peak localization, by reducing the computational complexity and detection error rate which correspondingly enhance the efficiency. Hence, thereby supporting more precise arrhythmia detection and contributing to the development of advanced diagnostic tools in cardiac healthcare.

✓ Secondly, the implementation of the Wavelet Scattering Transform (WST) over pre-term infant ECG dataset for feature extraction has proven to be a powerful tool in the analysis of ECG signals. Although, the infant dataset includes variation in every step, the WST effectively captures both local and global signal characteristics by extracting translation-invariant and deformation-stable features, which are crucial to identify in heart-related diseases. Unlike traditional feature extraction methods, WST preserves the hierarchical structure of the signal while reducing sensitivity to noise and variability, making it highly suitable for clinical applications. It offers a robust and efficient feature extraction framework that significantly contributes to the development of accurate and automated heart disease diagnostic systems.

147

✓ Third, we applied Group Sparse Mode Decomposition (GSMD) technique to decompose ECG signals into a set of intrinsic mode functions (IMFs), enabling a deeper analysis of the underlying frequency and bandwidth characteristics. The sparsity constraint ensures the extraction of only the most significant modes, reducing redundancy and improving interpretability. This approach facilitates a more accurate and detailed characterization of arrhythmias, contributing to the development of robust and data-efficient diagnostic systems.

✓ Fourth, we employed the high resolution Superlet Transform to convert 1D ECG signal into 2D time-frequency representation. This technique is highly beneficial in capturing transient and non-stationary features associated with various arrhythmia conditions. The challenge of noise interruption in ECG signal, peak displacement, and avoidance of weak neighboring spectral peaks from dominating spectral peaks, is resolved by utilizing this 2D representation. It leads to the detection of QRS complexes consisting of short-term oscillations and also removes the extra denoising step by providing high intensity energy peaks. This advancement contributes to the development of more reliable, efficient, and automated diagnostic systems in the field of cardiovascular healthcare.

✓ Finally, we utilized Dynamic Mode Decomposition (DMD) to decompose ECG signals into a set of dynamic modes that capture the essential temporal and spectral characteristics of cardiac activity. It effectively isolates coherent patterns within the ECG, allowing for a compact and informative representation of underlying physiological processes. The integration of DMD with machine learning provided enhanced interpretability and classification performance by highlighting the dynamic structures associated with abnormal heart rhythms.

6.2 Future Scope

We aim to explore the above methodologies over different domain of healthcare for early detection, even for low quality signals to avoid any risk factor. Utilizing a new methodology for low-quality signals in every field is planned to further improve the performance by reducing complexity.

Integration into cloud-based health analytics platforms could enable scalable and centralized cardiac data processing, useful for population-level arrhythmia screening. It can be used for real-time implementation which implies optimizing the parallel architecture for time-domain signal.

R-peak detection in wearable or edge devices can enable continuous cardiac monitoring in remote or ambulatory settings. It is useful for other biomedical signals, as well as in fields like audio processing, structural health monitoring, and fault detection.

It can be used in structural health monitoring, speech signal analysis, and financial time-series forecasting, due to its versatile behaviour over signals.

Hybridization of deep learning models will be implemented for future perspectives.

The presented methods may be applied to other physiological signals, such as phonocardiography signals, to evaluate the stability and reliability of the method. This may help medical practitioners to adequately understand their underlying mechanisms and diagnose their related diseases.

It shows tremendous promise along with excellent accuracy for early detection of arrhythmia and may find widespread use in clinical investigations and different engineering-related applications.

LIST OF PUBLICATIONS

Journal Papers: <u>SCI/SCIE Indexed Journal Papers Published</u>

1. Singhal, Shikha, and Manjeet Kumar. "A systematic review on artificial intelligence-based techniques for diagnosis of cardiovascular arrhythmia diseases: Challenges and opportunities." *Archives of Computational Methods in Engineering* 30.2 (2023): 865-888, https://doi.org/10.1007/s11831-022-09823-7.

2. Singhal, Shikha, and Manjeet Kumar. "GSMD-SRST: Group sparse mode decomposition and superlet-transform-based technique for multilevel classification of cardiac arrhythmia." *IEEE Sensors Journal* 24.6 (2024): 8160-8169, <u>10.1109/JSEN.2024.3354113</u>.

3. Singhal, Shikha, and Manjeet Kumar. "SPTDMD-WST: Arrhythmia classification from spatiotemporal modes of dynamic mode decomposition using wavelet scattering transform." *Biomedical Signal Processing and Control* 92 (2024): 105983, <u>https://doi.org/10.1016/j.bspc.2024.105983</u>.

4. Singhal, Shikha, and Manjeet Kumar. "FrnOBSA: fractional order-based spectral analysis for arrhythmia detection." *Physical and Engineering Sciences in Medicine* (2025): 1-12, <u>https://doi.org/10.1007/s13246-025-01634-x</u>.

<u>Scopus Indexed International Conference Papers</u>

1. Singhal, Shikha, and Manjeet Kumar. "Cardiovascular diseases classification using high-resolution superlet transform on ECG and PCG signals." *2023 14th International Conference on Computing Communication and Networking Technologies (ICCCNT)*. IEEE, 2023.

2. Singhal, Shikha, and Manjeet Kumar. "R-Peak Detection Using Wavelet Scattering Transform for Pre-Term Infant ECG Dataset." *2024 2nd International Conference on Device Intelligence, Computing and Communication Technologies (DICCT)*. IEEE, 2024.

<u>SCI/SCIE Indexed Journal Papers Communicated</u>

1. Singhal, Shikha, and Manjeet Kumar. "PCWA-MSG: Parallel Cluster Wavelet Analysis with Multi-Spot Gaussian Over Low-Quality ECG Signals for Multi-Peak Detection" communicated in IEEE Sensors Journal.

2. Singhal, Shikha, and Manjeet Kumar. "Spectrogram-Based Energy Measures for Gauging Sleep Disorder Metamorphosis: Relationship of Sleep Disorder to Cardiac Arrhythmia" submitted revision in IEEE Internet of Things Journal.

3. Singhal, Shikha, and Manjeet Kumar. "F^2DM-TriAFormer: Fast Fourier Decomposition Method on Triplet Attention-Based Vision Transformer for RBD Sleep Disorder Detection Using ECG Signal" communicated in Signal, Image and Video processing journal.

REFERENCES

[1]   D. Prabhakaran, P. Jeemon, and A. Roy, "Cardiovascular Diseases in India," *Circulation*, vol. 133, no. 16, pp. 1605–1620, Apr. 2016, doi: 10.1161/CIRCULATIONAHA.114.008729.

[2]   T. Mar, S. Zaunseder, J. P. Martínez, M. Llamedo, and R. Poll, "Optimization of ECG Classification by Means of Feature Selection," *IEEE Trans Biomed Eng*, vol. 58, no. 8, pp. 2168–2177, Aug. 2011, doi: 10.1109/TBME.2011.2113395.

[3]   M. Barni, P. Failla, R. Lazzeretti, A.-R. Sadeghi, and T. Schneider, "Privacy-Preserving ECG Classification With Branching Programs and Neural Networks," *IEEE Transactions on Information Forensics and Security*, vol. 6, no. 2, pp. 452–468, Jun. 2011, doi: 10.1109/TIFS.2011.2108650.

[4]   A. S. Alvarado, C. Lakshminarayan, and J. C. Principe, "Time-Based Compression and Classification of Heartbeats," *IEEE Trans Biomed Eng*, vol. 59, no. 6, pp. 1641–1648, Jun. 2012, doi: 10.1109/TBME.2012.2191407.

[5]   M. A. Escalona-Moran, M. C. Soriano, I. Fischer, and C. R. Mirasso, "Electrocardiogram Classification Using Reservoir Computing With Logistic Regression," *IEEE J Biomed Health Inform*, vol. 19, no. 3, pp. 892–898, May 2015, doi: 10.1109/JBHI.2014.2332001.

[6]   S. Banerjee and M. Mitra, "Application of Cross Wavelet Transform for ECG Pattern Analysis and Classification," *IEEE Trans Instrum Meas*, vol. 63, no. 2, pp. 326–333, Feb. 2014, doi: 10.1109/TIM.2013.2279001.

[7]   S.-Y. Lee, J.-H. Hong, C.-H. Hsieh, M.-C. Liang, S.-Y. Chang Chien, and K.-H. Lin, "Low-Power Wireless ECG Acquisition and Classification System for Body Sensor Networks," *IEEE J Biomed Health Inform*, vol. 19, no. 1, pp. 236–246, Jan. 2015, doi: 10.1109/JBHI.2014.2310354.

[8]   K. Huang and L. Zhang, "Cardiology knowledge free ECG feature extraction using generalized tensor rank one discriminant analysis," *EURASIP J Adv Signal Process*, vol. 2014, no. 1, p. 2, Dec. 2014, doi: 10.1186/1687-6180-2014-2.

[9]   P. M. Tripathi, A. Kumar, R. Komaragiri, and M. Kumar, "A Review on Computational Methods for Denoising and Detecting ECG Signals to Detect Cardiovascular Diseases," *Archives of Computational Methods in Engineering*, vol. 29, no. 3, pp. 1875–1914, May 2022, doi: 10.1007/s11831-021-09642-2.

[10]   M. Wasimuddin, K. Elleithy, A.-S. Abuzneid, M. Faezipour, and O. Abuzaghleh, "Stages-Based ECG Signal Analysis From Traditional Signal Processing to Machine Learning Approaches: A Survey," *IEEE Access*, vol. 8, pp. 177782–177803, 2020, doi: 10.1109/ACCESS.2020.3026968.

[11]   Q. A. Rahman, L. G. Tereshchenko, M. Kongkatong, T. Abraham, M. R. Abraham, and H. Shatkay, "Utilizing ECG-Based Heartbeat Classification for Hypertrophic Cardiomyopathy Identification," *IEEE Trans Nanobioscience*, vol. 14, no. 5, pp. 505–512, Jul. 2015, doi: 10.1109/TNB.2015.2426213.

[12]   S. Murawwat, H. M. Asif, S. Ijaz, M. Imran Malik, and K. Raahemifar, "Denoising and classification of Arrhythmia using MEMD and ANN," *Alexandria Engineering Journal*, vol. 61, no. 4, pp. 2807–2823, Apr. 2022, doi: 10.1016/j.aej.2021.08.014.

[13]   J. Morales *et al.*, "Model-Based Evaluation of Methods for Respiratory Sinus Arrhythmia Estimation," *IEEE Trans Biomed Eng*, vol. 68, no. 6, pp. 1882–1893, Jun. 2021, doi: 10.1109/TBME.2020.3028204.

[14]   S. K. Jagtap and M. D. Uplane, "Digital Filter Approach for ECG in Signal Processing," 2013, pp. 1075–1082. doi: 10.1007/978-81-322-0740-5_131.

[15]   Y. Lee and D. Hwang, "Periodicity-based nonlocal-means denoising method for electrocardiography in low SNR non-white noisy conditions," *Biomed Signal Process Control*, vol. 39, pp. 284–293, Jan. 2018, doi: 10.1016/j.bspc.2017.08.006.

[16]   H. Yang and Z. Wei, "A Novel Approach for Heart Ventricular and Atrial Abnormalities Detection via an Ensemble Classification Algorithm Based on ECG Morphological Features," *IEEE Access*, vol. 9, pp. 54757–54774, 2021, doi: 10.1109/ACCESS.2021.3071273.

[17]   B. Ganguly, A. Ghosal, A. Das, D. Das, D. Chatterjee, and D. Rakshit, "Automated Detection and Classification of Arrhythmia From ECG Signals Using Feature-Induced Long Short-Term Memory Network," *IEEE Sens Lett*, vol. 4, no. 8, pp. 1–4, Aug. 2020, doi: 10.1109/LSENS.2020.3006756.

[18]   S. Shadmand and B. Mashoufi, "A new personalized ECG signal classification algorithm using Block-based Neural Network and Particle Swarm Optimization," *Biomed Signal Process Control*, vol. 25, pp. 12–23, Mar. 2016, doi: 10.1016/j.bspc.2015.10.008.

[19]   A. B. Rad *et al.*, "ECG-Based Classification of Resuscitation Cardiac Rhythms for Retrospective Data Analysis," *IEEE Trans Biomed Eng*, vol. 64, no. 10, pp. 2411–2418, Oct. 2017, doi: 10.1109/TBME.2017.2688380.

[20]   J. Oster, J. Behar, O. Sayadi, S. Nemati, A. E. W. Johnson, and G. D. Clifford, "Semisupervised ECG Ventricular Beat Classification With Novelty Detection Based on Switching Kalman Filters," *IEEE Trans Biomed Eng*, vol. 62, no. 9, pp. 2125–2134, Sep. 2015, doi: 10.1109/TBME.2015.2402236.

[21]   H. D. Hesar and M. Mohebbi, "An Adaptive Kalman Filter Bank for ECG Denoising," *IEEE J Biomed Health Inform*, vol. 25, no. 1, pp. 13–21, Jan. 2021, doi: 10.1109/JBHI.2020.2982935.

[22] U. Satija, B. Ramkumar, and M. S. Manikandan, "Automated ECG Noise Detection and Classification System for Unsupervised Healthcare Monitoring," *IEEE J Biomed Health Inform*, vol. 22, no. 3, pp. 722–732, May 2018, doi: 10.1109/JBHI.2017.2686436.

[23] K. K. Patro and P. R. Kumar, "Effective Feature Extraction of ECG for Biometric Application," *Procedia Comput Sci*, vol. 115, pp. 296–306, 2017, doi: 10.1016/j.procs.2017.09.138.

[24] Y. Li, Y. Pang, J. Wang, and X. Li, "Patient-specific ECG classification by deeper CNN from generic to dedicated," *Neurocomputing*, vol. 314, pp. 336–346, Nov. 2018, doi: 10.1016/j.neucom.2018.06.068.

[25] T. Teijeiro, P. Felix, J. Presedo, and D. Castro, "Heartbeat Classification Using Abstract Features From the Abductive Interpretation of the ECG," *IEEE J Biomed Health Inform*, vol. 22, no. 2, pp. 409–420, Mar. 2018, doi: 10.1109/JBHI.2016.2631247.

[26] M. Ayar and S. Sabamoniri, "An ECG-based feature selection and heartbeat classification model using a hybrid heuristic algorithm," *Inform Med Unlocked*, vol. 13, pp. 167–175, 2018, doi: 10.1016/j.imu.2018.06.002.

[27] S. G., K. P. T., and K. K. V., "Classification of ECG beats using deep belief network and active learning," *Med Biol Eng Comput*, vol. 56, no. 10, pp. 1887–1898, Oct. 2018, doi: 10.1007/s11517-018-1815-2.

[28] S. Celin and K. Vasanth, "ECG Signal Classification Using Various Machine Learning Techniques," *J Med Syst*, vol. 42, no. 12, p. 241, Dec. 2018, doi: 10.1007/s10916-018-1083-6.

[29] X. Zhai and C. Tin, "Automated ECG Classification Using Dual Heartbeat Coupling Based on Convolutional Neural Network," *IEEE Access*, vol. 6, pp. 27465–27472, 2018, doi: 10.1109/ACCESS.2018.2833841.

[30] W. Zhu, X. Chen, Y. Wang, and L. Wang, "Arrhythmia Recognition and Classification Using ECG Morphology and Segment Feature Analysis," *IEEE/ACM Trans Comput Biol Bioinform*, vol. 16, no. 1, pp. 131–138, Jan. 2019, doi: 10.1109/TCBB.2018.2846611.

[31] S. S. Xu, M.-W. Mak, and C.-C. Cheung, "Towards End-to-End ECG Classification With Raw Signal Extraction and Deep Neural Networks," *IEEE J Biomed Health Inform*, vol. 23, no. 4, pp. 1574–1584, Jul. 2019, doi: 10.1109/JBHI.2018.2871510.

[32] J. Niu, Y. Tang, Z. Sun, and W. Zhang, "Inter-Patient ECG Classification With Symbolic Representations and Multi-Perspective Convolutional Neural Networks," *IEEE J Biomed Health Inform*, vol. 24, no. 5, pp. 1321–1332, May 2020, doi: 10.1109/JBHI.2019.2942938.

[33] H. M. Lynn, S. B. Pan, and P. Kim, "A Deep Bidirectional GRU Network Model for Biometric Electrocardiogram Classification Based on Recurrent Neural Networks," *IEEE Access*, vol. 7, pp. 145395–145405, 2019, doi: 10.1109/ACCESS.2019.2939947.

[34] A. L. Goldberger *et al.*, "PhysioBank, PhysioToolkit, and PhysioNet," *Circulation*, vol. 101, no. 23, Jun. 2000, doi: 10.1161/01.CIR.101.23.e215.

[35] G. B. Moody and R. G. Mark, "The impact of the MIT-BIH Arrhythmia Database," *IEEE Engineering in Medicine and Biology Magazine*, vol. 20, no. 3, pp. 45–50, 2001, doi: 10.1109/51.932724.

[36] J. Lian, L. Wang, and D. Muessig, "A Simple Method to Detect Atrial Fibrillation Using RR Intervals," *Am J Cardiol*, vol. 107, no. 10, pp. 1494–1497, May 2011, doi: 10.1016/j.amjcard.2011.01.028.

[37] N. Iyengar, C. K. Peng, R. Morin, A. L. Goldberger, and L. A. Lipsitz, "Age-related alterations in the fractal scaling of cardiac interbeat interval dynamics," *American Journal of Physiology-Regulatory, Integrative and Comparative*

Physiology, vol. 271, no. 4, pp. R1078–R1084, Oct. 1996, doi: 10.1152/ajpregu.1996.271.4.R1078.

[38] S. D. Greenwald, R. S. Patil, and R. G. Mark, "Improved detection and classification of arrhythmias in noise-corrupted electrocardiograms using contextual information," in *[1990] Proceedings Computers in Cardiology*, IEEE Comput. Soc. Press, pp. 461–464. doi: 10.1109/CIC.1990.144257.

[39] A. Verma and X. Dong, "Detection of Ventricular Fibrillation Using Random Forest Classifier," *J Biomed Sci Eng*, vol. 09, no. 05, pp. 259–268, 2016, doi: 10.4236/jbise.2016.95019.

[40] S. Petrutiu, A. V. Sahakian, and S. Swiryn, "Abrupt changes in fibrillatory wave characteristics at the termination of paroxysmal atrial fibrillation in humans," *EP Europace*, vol. 9, no. 7, pp. 466–470, Jul. 2007, doi: 10.1093/europace/eum096.

[41] Q. A. Rahman, L. G. Tereshchenko, M. Kongkatong, T. Abraham, M. R. Abraham, and H. Shatkay, "Utilizing ECG-Based Heartbeat Classification for Hypertrophic Cardiomyopathy Identification," *IEEE Trans Nanobioscience*, vol. 14, no. 5, pp. 505–512, Jul. 2015, doi: 10.1109/TNB.2015.2426213.

[42] L. Wik, "Quality of Cardiopulmonary Resuscitation During Out-of-Hospital Cardiac Arrest," *JAMA*, vol. 293, no. 3, p. 299, Jan. 2005, doi: 10.1001/jama.293.3.299.

[43] J. Zhang, L. Wang, X. Liu, H. Zhu, and J. Dong, "Chinese Cardiovascular Disease Database (CCDD) and Its Management Tool," in *2010 IEEE International Conference on BioInformatics and BioEngineering*, IEEE, May 2010, pp. 66–72. doi: 10.1109/BIBE.2010.19.

[44] G. Clifford *et al.*, "AF Classification from a Short Single Lead ECG Recording: the Physionet Computing in Cardiology Challenge 2017," Sep. 2017. doi: 10.22489/CinC.2017.065-469.

[45] P. Pławiak, "Novel methodology of cardiac health recognition based on ECG signals and evolutionary-neural system," *Expert Syst Appl*, vol. 92, pp. 334–349, Feb. 2018, doi: 10.1016/j.eswa.2017.09.022.

[46] S. Singhal and M. Kumar, "A Systematic Review on Artificial Intelligence-Based Techniques for Diagnosis of Cardiovascular Arrhythmia Diseases: Challenges and Opportunities," *Archives of Computational Methods in Engineering*, vol. 30, no. 2, pp. 865–888, Mar. 2023, doi: 10.1007/s11831-022-09823-7.

[47] M. B. Hossain, S. K. Bashar, A. J. Walkey, D. D. McManus, and K. H. Chon, "An Accurate QRS Complex and P Wave Detection in ECG Signals Using Complete Ensemble Empirical Mode Decomposition with Adaptive Noise Approach," *IEEE Access*, vol. 7, pp. 128869–128880, 2019, doi: 10.1109/ACCESS.2019.2939943.

[48] C. B. Gungor, P. P. Mercier, and H. Toreyin, "A Stochastic Resonance Electrocardiogram Enhancement Algorithm for Robust QRS Detection," *IEEE J Biomed Health Inform*, vol. 26, no. 8, pp. 3743–3754, Aug. 2022, doi: 10.1109/JBHI.2022.3178109.

[49] Y. Zou *et al.*, "An Energy-Efficient Design for ECG Recording and R-Peak Detection Based on Wavelet Transform," *IEEE Transactions on Circuits and Systems II: Express Briefs*, vol. 62, no. 2, pp. 119–123, Feb. 2015, doi: 10.1109/TCSII.2014.2368619.

[50] G. J. J. Warmerdam, R. Vullings, L. Schmitt, J. O. E. H. Van Laar, and J. W. M. Bergmans, "Hierarchical Probabilistic Framework for Fetal R-Peak Detection, Using ECG Waveform and Heart Rate Information," *IEEE Transactions on Signal Processing*, vol. 66, no. 16, pp. 4388–4397, Aug. 2018, doi: 10.1109/TSP.2018.2853144.

[51] H. J. Davies, G. Hammour, M. Zylinski, A. Nassibi, L. Stanković, and D. P. Mandic, "The Deep-Match Framework: R-Peak Detection in Ear-ECG," *IEEE*

Trans Biomed Eng, vol. 71, no. 7, pp. 2014–2021, Jul. 2024, doi: 10.1109/TBME.2024.3359752.

[52] C. J. Deepu and Y. Lian, "A Joint QRS Detection and Data Compression Scheme for Wearable Sensors," *IEEE Trans Biomed Eng*, vol. 62, no. 1, pp. 165–175, Jan. 2015, doi: 10.1109/TBME.2014.2342879.

[53] N. Sabor, G. Gendy, H. Mohammed, G. Wang, and Y. Lian, "Robust Arrhythmia Classification Based on QRS Detection and a Compact 1D-CNN for Wearable ECG Devices," *IEEE J Biomed Health Inform*, vol. 26, no. 12, pp. 5918–5929, Dec. 2022, doi: 10.1109/JBHI.2022.3207456.

[54] L. Qiao, S. Hu, B. Xiao, X. Bi, W. Li, and X. Gao, "A Dual Self-Calibrating Framework for Noninvasive Fetal ECG R-Peak Detection," *IEEE Internet Things J*, vol. 10, no. 18, pp. 16579–16593, Sep. 2023, doi: 10.1109/JIOT.2023.3269096.

[55] Z. Hao, X. Zhang, and Z. Lai, "Adaptive R-Peak Detection Algorithm Based on Brown Exponential Smoothing Model," *IEEE Access*, vol. 10, pp. 114355–114363, 2022, doi: 10.1109/ACCESS.2022.3218308.

[56] E. De Giovanni, T. Teijeiro, G. P. Millet, and D. Atienza, "Adaptive R-Peak Detection on Wearable ECG Sensors for High-Intensity Exercise," *IEEE Trans Biomed Eng*, vol. 70, no. 3, pp. 941–953, Mar. 2023, doi: 10.1109/TBME.2022.3205304.

[57] H. Chen and K. Maharatna, "An Automatic R and T Peak Detection Method Based on the Combination of Hierarchical Clustering and Discrete Wavelet Transform," *IEEE J Biomed Health Inform*, vol. 24, no. 10, pp. 2825–2832, Oct. 2020, doi: 10.1109/JBHI.2020.2973982.

[58] X. Peng, H. Zhu, X. Zhou, C. Pan, and Z. Ke, "ECG Signals Segmentation Using Deep Spatiotemporal Feature Fusion U-Net for QRS Complexes and R-Peak Detection," *IEEE Trans Instrum Meas*, vol. 72, pp. 1–12, 2023, doi: 10.1109/TIM.2023.3241997.

[59] A. Kumar, M. Kumar, and R. Komaragiri, "Design of a Biorthogonal Wavelet Transform Based R-Peak Detection and Data Compression Scheme for Implantable Cardiac Pacemaker Systems," *J Med Syst*, vol. 42, no. 6, p. 102, Jun. 2018, doi: 10.1007/s10916-018-0953-2.

[60] W. Cai and D. Hu, "QRS Complex Detection Using Novel Deep Learning Neural Networks," *IEEE Access*, vol. 8, pp. 97082–97089, 2020, doi: 10.1109/ACCESS.2020.2997473.

[61] M. Gabbouj *et al.*, "Robust Peak Detection for Holter ECGs by Self-Organized Operational Neural Networks," *IEEE Trans Neural Netw Learn Syst*, vol. 34, no. 11, pp. 9363–9374, Nov. 2023, doi: 10.1109/TNNLS.2022.3158867.

[62] M. Jia, F. Li, J. Wu, Z. Chen, and Y. Pu, "Robust QRS Detection Using High-Resolution Wavelet Packet Decomposition and Time-Attention Convolutional Neural Network," *IEEE Access*, vol. 8, pp. 16979–16988, 2020, doi: 10.1109/ACCESS.2020.2967775.

[63] V V. N., H. Cao, and L. Peyrodie, "Variational Mode Decomposition-Based Simultaneous R Peak Detection and Noise Suppression for Automatic ECG Analysis," *IEEE Sens J*, vol. 23, no. 8, pp. 8703–8713, Apr. 2023, doi: 10.1109/JSEN.2023.3257332.

[64] V. Gupta, M. Mittal, V. Mittal, and Y. Chaturvedi, "Detection of R-peaks using fractional Fourier transform and principal component analysis," *J Ambient Intell Humaniz Comput*, vol. 13, no. 2, pp. 961–972, Feb. 2022, doi: 10.1007/s12652-021-03484-3.

[65] F. Tueche, Y. Mohamadou, A. Djeukam, L. C. N. Kouekeu, R. Seujip, and M. Tonka, "Embedded Algorithm for QRS Detection Based on Signal Shape," *IEEE Trans Instrum Meas*, vol. 70, pp. 1–12, 2021, doi: 10.1109/TIM.2021.3051412.

[66] A. Habib, C. Karmakar, and J. Yearwood, "Domain Agnostic Post-Processing for QRS Detection Using Recurrent Neural Network," *IEEE J Biomed Health*

Inform, vol. 27, no. 8, pp. 3748–3759, Aug. 2023, doi: 10.1109/JBHI.2023.3235341.

[67] C. Nayak, S. K. Saha, R. Kar, and D. Mandal, "An Efficient and Robust Digital Fractional Order Differentiator Based ECG Pre-Processor Design for QRS Detection," *IEEE Trans Biomed Circuits Syst*, vol. 13, no. 4, pp. 682–696, Aug. 2019, doi: 10.1109/TBCAS.2019.2916676.

[68] M. U. Zahid *et al.*, "Robust R-Peak Detection in Low-Quality Holter ECGs Using 1D Convolutional Neural Network," *IEEE Trans Biomed Eng*, vol. 69, no. 1, pp. 119–128, Jan. 2022, doi: 10.1109/TBME.2021.3088218.

[69] D. Yun *et al.*, "Robust R-peak detection in an electrocardiogram with stationary wavelet transformation and separable convolution," *Sci Rep*, vol. 12, no. 1, p. 19638, Nov. 2022, doi: 10.1038/s41598-022-19495-9.

[70] S. K. Bashar, Y. Noh, A. J. Walkey, D. D. McManus, and K. H. Chon, "VERB: VFCDM-Based Electrocardiogram Reconstruction and Beat Detection Algorithm," *IEEE Access*, vol. 7, pp. 13856–13866, 2019, doi: 10.1109/ACCESS.2019.2894092.

[71] W. Li and J. Li, "Local Deep Field for Electrocardiogram Beat Classification," *IEEE Sens J*, vol. 18, no. 4, pp. 1656–1664, Feb. 2018, doi: 10.1109/JSEN.2017.2772031.

[72] V. Atanasoski *et al.*, "A Morphology-Preserving Algorithm for Denoising of EMG-Contaminated ECG Signals," *IEEE Open J Eng Med Biol*, vol. 5, pp. 296–305, 2024, doi: 10.1109/OJEMB.2024.3380352.

[73] E. Brophy, B. Hennelly, M. De Vos, G. Boylan, and T. Ward, "Improved Electrode Motion Artefact Denoising in ECG Using Convolutional Neural Networks and a Custom Loss Function," *IEEE Access*, vol. 10, pp. 54891–54898, 2022, doi: 10.1109/ACCESS.2022.3176971.

[74] A. Ghafari, N. Pourjafari, and A. Ghaffari, "Vector-Based Postprocessing Method for Improving ECG Denoising Techniques by Re-Establishing Lead Relationships," *IEEE Trans Instrum Meas*, vol. 73, pp. 1–9, 2024, doi: 10.1109/TIM.2023.3335528.

[75] C. Li, Y. Wu, H. Lin, J. Li, F. Zhang, and Y. Yang, "ECG Denoising Method Based on an Improved VMD Algorithm," *IEEE Sens J*, vol. 22, no. 23, pp. 22725–22733, Dec. 2022, doi: 10.1109/JSEN.2022.3214239.

[76] H. Shi, R. Liu, C. Chen, M. Shu, and Y. Wang, "ECG Baseline Estimation and Denoising With Group Sparse Regularization," *IEEE Access*, vol. 9, pp. 23595–23607, 2021, doi: 10.1109/ACCESS.2021.3056459.

[77] K. Wang *et al.*, "Noise Removal in Single-Lead Capacitive ECG With Adaptive Filtering and Singular Value Decomposition," *IEEE Access*, vol. 12, pp. 152777–152785, 2024, doi: 10.1109/ACCESS.2024.3478779.

[78] E. K. Wang, X. Zhang, and L. Pan, "Automatic Classification of CAD ECG Signals With SDAE and Bidirectional Long Short-Term Network," *IEEE Access*, vol. 7, pp. 182873–182880, 2019, doi: 10.1109/ACCESS.2019.2936525.

[79] X. Bian, W. Xu, Y. Wang, L. Lu, and S. Wang, "Direct Feature Extraction and Diagnosis of ECG Signal in the Compressed Domain," *IEEE Sens J*, vol. 21, no. 15, pp. 17096–17106, Aug. 2021, doi: 10.1109/JSEN.2021.3081577.

[80] J. Yang and R. Yan, "A Multidimensional Feature Extraction and Selection Method for ECG Arrhythmias Classification," *IEEE Sens J*, vol. 21, no. 13, pp. 14180–14190, Jul. 2021, doi: 10.1109/JSEN.2020.3047962.

[81] M. Ayar and S. Sabamoniri, "An ECG-based feature selection and heartbeat classification model using a hybrid heuristic algorithm," *Inform Med Unlocked*, vol. 13, pp. 167–175, 2018, doi: 10.1016/j.imu.2018.06.002.

[82] S. Saadatnejad, M. Oveisi, and M. Hashemi, "LSTM-Based ECG Classification for Continuous Monitoring on Personal Wearable Devices," *IEEE J Biomed Health Inform*, vol. 24, no. 2, pp. 515–523, Feb. 2020, doi: 10.1109/JBHI.2019.2911367.

[83] H. Zakaria, E. S. H. Nurdiniyah, A. M. Kurniawati, D. Naufal, and N. Sutisna, "Morphological Arrhythmia Classification Based on Inter-Patient and Two Leads ECG Using Machine Learning," *IEEE Access*, vol. 12, pp. 147372–147386, 2024, doi: 10.1109/ACCESS.2024.3469640.

[84] S. G., K. P. T., and K. K. V., "Classification of ECG beats using deep belief network and active learning," *Med Biol Eng Comput*, vol. 56, no. 10, pp. 1887–1898, Oct. 2018, doi: 10.1007/s11517-018-1815-2.

[85] M. Sharma, R.-S. Tan, and U. R. Acharya, "Automated heartbeat classification and detection of arrhythmia using optimal orthogonal wavelet filters," *Inform Med Unlocked*, vol. 16, p. 100221, 2019, doi: 10.1016/j.imu.2019.100221.

[86] F. I. Alarsan and M. Younes, "Analysis and classification of heart diseases using heartbeat features and machine learning algorithms," *J Big Data*, vol. 6, no. 1, p. 81, Dec. 2019, doi: 10.1186/s40537-019-0244-x.

[87] Z. Sun, C. Wang, Y. Zhao, and C. Yan, "Multi-Label ECG Signal Classification Based on Ensemble Classifier," *IEEE Access*, vol. 8, pp. 117986–117996, 2020, doi: 10.1109/ACCESS.2020.3004908.

[88] H. Yang and Z. Wei, "Arrhythmia Recognition and Classification Using Combined Parametric and Visual Pattern Features of ECG Morphology," *IEEE Access*, vol. 8, pp. 47103–47117, 2020, doi: 10.1109/ACCESS.2020.2979256.

[89] Q. Wang, Y. W. Mao, L. Ren, Z. Li, and H. Liu, "Automatic Classification of ECG Data Quality for Each Channel," *IEEE Access*, vol. 8, pp. 196094–196101, 2020, doi: 10.1109/ACCESS.2020.3034449.

[90] A. Diker, E. Avci, E. Tanyildizi, and M. Gedikpinar, "A novel ECG signal classification method using DEA-ELM," *Med Hypotheses*, vol. 136, p. 109515, Mar. 2020, doi: 10.1016/j.mehy.2019.109515.

[91] J. Lu *et al.*, "Efficient Hardware Architecture of Convolutional Neural Network for ECG Classification in Wearable Healthcare Device," *IEEE Transactions on Circuits and Systems I: Regular Papers*, vol. 68, no. 7, pp. 2976–2985, Jul. 2021, doi: 10.1109/TCSI.2021.3072622.

[92] B.-H. Kung, P.-Y. Hu, C.-C. Huang, C.-C. Lee, C.-Y. Yao, and C.-H. Kuan, "An Efficient ECG Classification System Using Resource-Saving Architecture and Random Forest," *IEEE J Biomed Health Inform*, vol. 25, no. 6, pp. 1904–1914, Jun. 2021, doi: 10.1109/JBHI.2020.3035191.

[93] P. Darsana and V. N. Kumar, "Extracting Fetal ECG Signals Through a Hybrid Technique Utilizing Two Wavelet-Based Denoising Algorithms," *IEEE Access*, vol. 11, pp. 91696–91708, 2023, doi: 10.1109/ACCESS.2023.3308409.

[94] M. Sharma, R.-S. Tan, and U. R. Acharya, "Automated heartbeat classification and detection of arrhythmia using optimal orthogonal wavelet filters," *Inform Med Unlocked*, vol. 16, p. 100221, 2019, doi: 10.1016/j.imu.2019.100221.

[95] Y. Hou, R. Liu, M. Shu, X. Xie, and C. Chen, "Deep Neural Network Denoising Model Based on Sparse Representation Algorithm for ECG Signal," *IEEE Trans Instrum Meas*, vol. 72, pp. 1–11, 2023, doi: 10.1109/TIM.2023.3251408.

[96] W. Ji and D. Zhu, "ECG Classification Exercise Health Analysis Algorithm Based on GRU and Convolutional Neural Network," *IEEE Access*, vol. 12, pp. 59842–59850, 2024, doi: 10.1109/ACCESS.2024.3392965.

[97] S. Hao *et al.*, "G2-ResNeXt: A Novel Model for ECG Signal Classification," *IEEE Access*, vol. 11, pp. 34808–34820, 2023, doi: 10.1109/ACCESS.2023.3265305.

[98]   T. H. Rafi and Y. Woong Ko, "HeartNet: Self Multihead Attention Mechanism via Convolutional Network With Adversarial Data Synthesis for ECG-Based Arrhythmia Classification," *IEEE Access*, vol. 10, pp. 100501–100512, 2022, doi: 10.1109/ACCESS.2022.3206431.

[99]   M. U. Zahid, S. Kiranyaz, and M. Gabbouj, "Global ECG Classification by Self-Operational Neural Networks With Feature Injection," *IEEE Trans Biomed Eng*, vol. 70, no. 1, pp. 205–215, Jan. 2023, doi: 10.1109/TBME.2022.3187874.

[100] H. Bechinia, D. Benmerzoug, and N. Khlifa, "Approach Based Lightweight Custom Convolutional Neural Network and Fine-Tuned MobileNet-V2 for ECG Arrhythmia Signals Classification," *IEEE Access*, vol. 12, pp. 40827–40841, 2024, doi: 10.1109/ACCESS.2024.3378730.

[101] Y. Guan, Y. An, J. Xu, N. Liu, and J. Wang, "HA-ResNet: Residual Neural Network With Hidden Attention for ECG Arrhythmia Detection Using Two-Dimensional Signal," *IEEE/ACM Trans Comput Biol Bioinform*, vol. 20, no. 6, pp. 3389–3398, Nov. 2023, doi: 10.1109/TCBB.2022.3198998.

[102] J. Chen, B. Fang, H. Li, L.-B. Zhang, Y. Teng, and G. Fortino, "EMCNet: Ensemble Multiscale Convolutional Neural Network for Single-Lead ECG Classification in Wearable Devices," *IEEE Sens J*, vol. 24, no. 6, pp. 8754–8762, Mar. 2024, doi: 10.1109/JSEN.2024.3358997.

[103] S. Yang, C. Lian, Z. Zeng, B. Xu, J. Zang, and Z. Zhang, "A Multi-View Multi-Scale Neural Network for Multi-Label ECG Classification," *IEEE Trans Emerg Top Comput Intell*, vol. 7, no. 3, pp. 648–660, Jun. 2023, doi: 10.1109/TETCI.2023.3235374.

[104] G. M., V. Ravi, S. V, G. E.A, and S. K.P, "Explainable Deep Learning-Based Approach for Multilabel Classification of Electrocardiogram," *IEEE Trans Eng Manag*, vol. 70, no. 8, pp. 2787–2799, Aug. 2023, doi: 10.1109/TEM.2021.3104751.

[105] G. Sannino and G. De Pietro, "A deep learning approach for ECG-based heartbeat classification for arrhythmia detection," *Future Generation Computer Systems*, vol. 86, pp. 446–455, Sep. 2018, doi: 10.1016/j.future.2018.03.057.

[106] J. Niu, Y. Tang, Z. Sun, and W. Zhang, "Inter-Patient ECG Classification With Symbolic Representations and Multi-Perspective Convolutional Neural Networks," *IEEE J Biomed Health Inform*, vol. 24, no. 5, pp. 1321–1332, May 2020, doi: 10.1109/JBHI.2019.2942938.

[107] H. M. Lynn, S. B. Pan, and P. Kim, "A Deep Bidirectional GRU Network Model for Biometric Electrocardiogram Classification Based on Recurrent Neural Networks," *IEEE Access*, vol. 7, pp. 145395–145405, 2019, doi: 10.1109/ACCESS.2019.2939947.

[108] Y. Li, Y. Pang, J. Wang, and X. Li, "Patient-specific ECG classification by deeper CNN from generic to dedicated," *Neurocomputing*, vol. 314, pp. 336–346, Nov. 2018, doi: 10.1016/j.neucom.2018.06.068.

[109] M. M. Al Rahhal, Y. Bazi, H. Almubarak, N. Alajlan, and M. Al Zuair, "Dense Convolutional Networks With Focal Loss and Image Generation for Electrocardiogram Classification," *IEEE Access*, vol. 7, pp. 182225–182237, 2019, doi: 10.1109/ACCESS.2019.2960116.

[110] J. Huang, B. Chen, B. Yao, and W. He, "ECG Arrhythmia Classification Using STFT-Based Spectrogram and Convolutional Neural Network," *IEEE Access*, vol. 7, pp. 92871–92880, 2019, doi: 10.1109/ACCESS.2019.2928017.

[111] A. Amirshahi and M. Hashemi, "ECG Classification Algorithm Based on STDP and R-STDP Neural Networks for Real-Time Monitoring on Ultra Low-Power Personal Wearable Devices," *IEEE Trans Biomed Circuits Syst*, vol. 13, no. 6, pp. 1483–1493, Dec. 2019, doi: 10.1109/TBCAS.2019.2948920.

[112] J. Wu, F. Li, Z. Chen, Y. Pu, and M. Zhan, "A Neural Network-Based ECG Classification Processor With Exploitation of Heartbeat Similarity," *IEEE*

Access, vol. 7, pp. 172774–172782, 2019, doi: 10.1109/ACCESS.2019.2956179.

[113] W. Li, "Deep Intermediate Representation and In-Set Voting Scheme for Multiple-Beat Electrocardiogram Classification," *IEEE Sens J*, vol. 19, no. 16, pp. 6895–6904, Aug. 2019, doi: 10.1109/JSEN.2019.2910853.

[114] N. Feng, S. Xu, Y. Liang, and K. Liu, "A Probabilistic Process Neural Network and Its Application in ECG Classification," *IEEE Access*, vol. 7, pp. 50431–50439, 2019, doi: 10.1109/ACCESS.2019.2910880.

[115] J. Hua, Y. Xu, J. Tang, J. Liu, and J. Zhang, "ECG heartbeat classification in compressive domain for wearable devices," *Journal of Systems Architecture*, vol. 104, p. 101687, Mar. 2020, doi: 10.1016/j.sysarc.2019.101687.

[116] A. M. Shaker, M. Tantawi, H. A. Shedeed, and M. F. Tolba, "Generalization of Convolutional Neural Networks for ECG Classification Using Generative Adversarial Networks," *IEEE Access*, vol. 8, pp. 35592–35605, 2020, doi: 10.1109/ACCESS.2020.2974712.

[117] X. Xu and H. Liu, "ECG Heartbeat Classification Using Convolutional Neural Networks," *IEEE Access*, vol. 8, pp. 8614–8619, 2020, doi: 10.1109/ACCESS.2020.2964749.

[118] T. F. Romdhane, H. Alhichri, R. Ouni, and M. Atri, "Electrocardiogram heartbeat classification based on a deep convolutional neural network and focal loss," *Comput Biol Med*, vol. 123, p. 103866, Aug. 2020, doi: 10.1016/j.compbiomed.2020.103866.

[119] M.-L. Huang and Y.-S. Wu, "Classification of atrial fibrillation and normal sinus rhythm based on convolutional neural network," *Biomed Eng Lett*, vol. 10, no. 2, pp. 183–193, May 2020, doi: 10.1007/s13534-020-00146-9.

[120] X. Song, G. Yang, K. Wang, Y. Huang, F. Yuan, and Y. Yin, "Short Term ECG Classification with Residual-Concatenate Network and Metric Learning,"

Multimed Tools Appl, vol. 79, no. 31–32, pp. 22325–22336, Aug. 2020, doi: 10.1007/s11042-020-09035-w.

[121] Z. Dokur and T. Ölmez, "Heartbeat classification by using a convolutional neural network trained with Walsh functions," *Neural Comput Appl*, vol. 32, no. 16, pp. 12515–12534, Aug. 2020, doi: 10.1007/s00521-020-04709-w.

[122] J.-S. Huang, B.-Q. Chen, N.-Y. Zeng, X.-C. Cao, and Y. Li, "Accurate classification of ECG arrhythmia using MOWPT enhanced fast compression deep learning networks," *J Ambient Intell Humaniz Comput*, vol. 14, no. 5, pp. 5703–5720, May 2023, doi: 10.1007/s12652-020-02110-y.

[123] Z. Yan, J. Zhou, and W.-F. Wong, "Energy efficient ECG classification with spiking neural network," *Biomed Signal Process Control*, vol. 63, p. 102170, Jan. 2021, doi: 10.1016/j.bspc.2020.102170.

[124] E. Essa and X. Xie, "An Ensemble of Deep Learning-Based Multi-Model for ECG Heartbeats Arrhythmia Classification," *IEEE Access*, vol. 9, pp. 103452–103464, 2021, doi: 10.1109/ACCESS.2021.3098986.

[125] T. Mahmud, S. A. Fattah, and M. Saquib, "DeepArrNet: An Efficient Deep CNN Architecture for Automatic Arrhythmia Detection and Classification From Denoised ECG Beats," *IEEE Access*, vol. 8, pp. 104788–104800, 2020, doi: 10.1109/ACCESS.2020.2998788.

[126] S. Nurmaini *et al.*, "Beat-to-Beat Electrocardiogram Waveform Classification Based on a Stacked Convolutional and Bidirectional Long Short-Term Memory," *IEEE Access*, vol. 9, pp. 92600–92613, 2021, doi: 10.1109/ACCESS.2021.3092631.

[127] E. H. Houssein, D. S. Abdelminaam, I. E. Ibrahim, M. Hassaballah, and Y. M. Wazery, "A Hybrid Heartbeats Classification Approach Based on Marine Predators Algorithm and Convolution Neural Networks," *IEEE Access*, vol. 9, pp. 86194–86206, 2021, doi: 10.1109/ACCESS.2021.3088783.

[128] J. Li, G. Wang, M. Chen, Z. Ding, and H. Yang, "Mixup Asymmetric Tri-Training for Heartbeat Classification Under Domain Shift," *IEEE Signal Process Lett*, vol. 28, pp. 718–722, 2021, doi: 10.1109/LSP.2021.3066068.

[129] Z. Ahmad, A. Tabassum, L. Guan, and N. M. Khan, "ECG Heartbeat Classification Using Multimodal Fusion," *IEEE Access*, vol. 9, pp. 100615–100626, 2021, doi: 10.1109/ACCESS.2021.3097614.

[130] M. Kolhar and A. M. Al Rajeh, "Deep learning hybrid model ECG classification using AlexNet and parallel dual branch fusion network model," *Sci Rep*, vol. 14, no. 1, p. 26919, Nov. 2024, doi: 10.1038/s41598-024-78028-8.

[131] S. K. Pandey, R. R. Janghel, and V. Vani, "Patient Specific Machine Learning Models for ECG Signal Classification," *Procedia Comput Sci*, vol. 167, pp. 2181–2190, 2020, doi: 10.1016/j.procs.2020.03.269.

[132] Y. Zhou, J. Ma, F. Li, B. Chen, T. Xian, and X. Wei, "An Improved Algorithm for Peak Detection Based on Weighted Continuous Wavelet Transform," *IEEE Access*, vol. 10, pp. 118779–118788, 2022, doi: 10.1109/ACCESS.2022.3220640.

[133] Z. Hao, X. Zhang, and Z. Lai, "Adaptive R-Peak Detection Algorithm Based on Brown Exponential Smoothing Model," *IEEE Access*, vol. 10, pp. 114355–114363, 2022, doi: 10.1109/ACCESS.2022.3218308.

[134] S. Nahak, A. Pathak, and G. Saha, "Fragment-level classification of ECG arrhythmia using wavelet scattering transform," *Expert Syst Appl*, vol. 224, p. 120019, Aug. 2023, doi: 10.1016/j.eswa.2023.120019.

[135] Z. Liu, G. Yao, Q. Zhang, J. Zhang, and X. Zeng, "Wavelet Scattering Transform for ECG Beat Classification," *Comput Math Methods Med*, vol. 2020, pp. 1–11, Oct. 2020, doi: 10.1155/2020/3215681.

[136] H. A. Marzog and Haider. J. Abd, "Machine Learning ECG Classification Using Wavelet Scattering of Feature Extraction," *Applied Computational Intelligence and Soft Computing*, vol. 2022, pp. 1–8, Sep. 2022, doi: 10.1155/2022/9884076.

[137] A. H. Gee, R. Barbieri, D. Paydarfar, and P. Indic, "Predicting Bradycardia in Preterm Infants Using Point Process Analysis of Heart Rate," *IEEE Trans Biomed Eng*, vol. 64, no. 9, pp. 2300–2308, Sep. 2017, doi: 10.1109/TBME.2016.2632746.

[138] A. Matonia *et al.*, "Fetal electrocardiograms, direct and abdominal with reference heartbeat annotations," *Sci Data*, vol. 7, no. 1, p. 200, Jun. 2020, doi: 10.1038/s41597-020-0538-z.

[139] X. Peng, H. Zhu, X. Zhou, C. Pan, and Z. Ke, "ECG Signals Segmentation Using Deep Spatiotemporal Feature Fusion U-Net for QRS Complexes and R-Peak Detection," *IEEE Trans Instrum Meas*, vol. 72, pp. 1–12, 2023, doi: 10.1109/TIM.2023.3241997.

[140] D. Yun *et al.*, "Robust R-peak detection in an electrocardiogram with stationary wavelet transformation and separable convolution," *Sci Rep*, vol. 12, no. 1, p. 19638, Nov. 2022, doi: 10.1038/s41598-022-19495-9.

[141] E. Celik *et al.*, "DSD-R: Deep Learning Based Segmentation for the Detection of R peaks in ECG Signals," in *2022 Medical Technologies Congress (TIPTEKNO)*, IEEE, Oct. 2022, pp. 1–4. doi: 10.1109/TIPTEKNO56568.2022.9960181.

[142] S. Das, S. Mukherjee, S. Chatterjee, and H. K. Chatterjee, "Noise elimination and ECG R peak detection using wavelet transform," in *2016 IEEE 7th Annual Ubiquitous Computing, Electronics & Mobile Communication Conference (UEMCON)*, IEEE, Oct. 2016, pp. 1–5. doi: 10.1109/UEMCON.2016.7777876.

[143] S. Singhal and M. Kumar, "R-Peak Detection Using Wavelet Scattering Transform for Pre-Term Infant ECG Dataset," in *2024 2nd International Conference on Device Intelligence, Computing and Communication*

Technologies (DICCT), IEEE, Mar. 2024, pp. 676–680. doi: 10.1109/DICCT61038.2024.10532950.

[144] J. Pan and W. J. Tompkins, "A Real-Time QRS Detection Algorithm," *IEEE Trans Biomed Eng*, vol. BME-32, no. 3, pp. 230–236, Mar. 1985, doi: 10.1109/TBME.1985.325532.

[145] H. Chen and K. Maharatna, "An Automatic R and T Peak Detection Method Based on the Combination of Hierarchical Clustering and Discrete Wavelet Transform," *IEEE J Biomed Health Inform*, vol. 24, no. 10, pp. 2825–2832, Oct. 2020, doi: 10.1109/JBHI.2020.2973982.

[146] K. Zhao, Y. Li, G. Wang, Y. Pu, and Y. Lian, "A robust QRS detection and accurate R-peak identification algorithm for wearable ECG sensors," *Science China Information Sciences*, vol. 64, no. 8, p. 182401, Aug. 2021, doi: 10.1007/s11432-020-3150-2.

[147] A. Habib, C. Karmakar, and J. Yearwood, "Domain Agnostic Post-Processing for QRS Detection Using Recurrent Neural Network," *IEEE J Biomed Health Inform*, vol. 27, no. 8, pp. 3748–3759, Aug. 2023, doi: 10.1109/JBHI.2023.3235341.

[148] Z. Hao, X. Zhang, and Z. Lai, "Adaptive R-Peak Detection Algorithm Based on Brown Exponential Smoothing Model," *IEEE Access*, vol. 10, pp. 114355–114363, 2022, doi: 10.1109/ACCESS.2022.3218308.

[149] M. Jia, F. Li, J. Wu, Z. Chen, and Y. Pu, "Robust QRS Detection Using High-Resolution Wavelet Packet Decomposition and Time-Attention Convolutional Neural Network," *IEEE Access*, vol. 8, pp. 16979–16988, 2020, doi: 10.1109/ACCESS.2020.2967775.

[150] V. Ganjalizadeh, G. G. Meena, T. A. Wall, M. A. Stott, A. R. Hawkins, and H. Schmidt, "Fast custom wavelet analysis technique for single molecule detection and identification," *Nat Commun*, vol. 13, no. 1, p. 1035, Feb. 2022, doi: 10.1038/s41467-022-28703-z.

[151] T. Guo, T. Zhang, E. Lim, M. Lopez-Benitez, F. Ma, and L. Yu, "A Review of Wavelet Analysis and Its Applications: Challenges and Opportunities," *IEEE Access*, vol. 10, pp. 58869–58903, 2022, doi: 10.1109/ACCESS.2022.3179517.

[152] P. Du, W. A. Kibbe, and S. M. Lin, "Improved peak detection in mass spectrum by incorporating continuous wavelet transform-based pattern matching," *Bioinformatics*, vol. 22, no. 17, pp. 2059–2065, Sep. 2006, doi: 10.1093/bioinformatics/btl355.

[153] Z.-M. Zhang *et al.*, "Multiscale peak detection in wavelet space," *Analyst*, vol. 140, no. 23, pp. 7955–7964, 2015, doi: 10.1039/C5AN01816A.

[154] F. Tueche, Y. Mohamadou, A. Djeukam, L. C. N. Kouekeu, R. Seujip, and M. Tonka, "Embedded Algorithm for QRS Detection Based on Signal Shape," *IEEE Trans Instrum Meas*, vol. 70, pp. 1–12, 2021, doi: 10.1109/TIM.2021.3051412.

[155] M. U. Zahid *et al.*, "Robust R-Peak Detection in Low-Quality Holter ECGs Using 1D Convolutional Neural Network," *IEEE Trans Biomed Eng*, vol. 69, no. 1, pp. 119–128, Jan. 2022, doi: 10.1109/TBME.2021.3088218.

[156] V. Gupta, M. Mittal, V. Mittal, and Y. Chaturvedi, "Detection of R-peaks using fractional Fourier transform and principal component analysis," *J Ambient Intell Humaniz Comput*, vol. 13, no. 2, pp. 961–972, Feb. 2022, doi: 10.1007/s12652-021-03484-3.

[157] D. Yun *et al.*, "Robust R-peak detection in an electrocardiogram with stationary wavelet transformation and separable convolution," *Sci Rep*, vol. 12, no. 1, p. 19638, Nov. 2022, doi: 10.1038/s41598-022-19495-9.

[158] V V. N., H. Cao, and L. Peyrodie, "Variational Mode Decomposition-Based Simultaneous R Peak Detection and Noise Suppression for Automatic ECG Analysis," *IEEE Sens J*, vol. 23, no. 8, pp. 8703–8713, Apr. 2023, doi: 10.1109/JSEN.2023.3257332.

[159] H. Xiong, M. Liang, and J. Liu, "A Real-Time QRS Detection Algorithm Based on Energy Segmentation for Exercise Electrocardiogram," *Circuits Syst Signal Process*, vol. 40, no. 10, pp. 4969–4985, Oct. 2021, doi: 10.1007/s00034-021-01702-z.

[160] T. Pander, "A new approach to adaptive threshold based method for QRS detection with fuzzy clustering," *Biocybern Biomed Eng*, vol. 42, no. 1, pp. 404–425, Jan. 2022, doi: 10.1016/j.bbe.2022.02.007.

[161] N. E. Huang *et al.*, "The empirical mode decomposition and the Hilbert spectrum for nonlinear and non-stationary time series analysis," *Proceedings of the Royal Society of London. Series A: Mathematical, Physical and Engineering Sciences*, vol. 454, no. 1971, pp. 903–995, Mar. 1998, doi: 10.1098/rspa.1998.0193.

[162] P. C. CHU, C. FAN, and N. HUANG, "COMPACT EMPIRICAL MODE DECOMPOSITION: AN ALGORITHM TO REDUCE MODE MIXING, END EFFECT, AND DETREND UNCERTAINTY," *Adv Adapt Data Anal*, vol. 04, no. 03, p. 1250017, Jul. 2012, doi: 10.1142/S1793536912500173.

[163] M. Nazari and S. M. Sakhaei, "Successive variational mode decomposition," *Signal Processing*, vol. 174, p. 107610, Sep. 2020, doi: 10.1016/j.sigpro.2020.107610.

[164] P. Singh, S. D. Joshi, R. K. Patney, and K. Saha, "The Fourier decomposition method for nonlinear and non-stationary time series analysis," *Proceedings of the Royal Society A: Mathematical, Physical and Engineering Sciences*, vol. 473, no. 2199, p. 20160871, Mar. 2017, doi: 10.1098/rspa.2016.0871.

[165] N. Mourad, "Group-sparse mode decomposition: A signal decomposition algorithm based on group-sparsity in the frequency domain," *Digit Signal Process*, vol. 122, p. 103375, Apr. 2022, doi: 10.1016/j.dsp.2021.103375.

[166] El Hadji S Diop, R. Alexandre, and A. O. Boudraa, "Analysis of Intrinsic Mode Functions: A PDE Approach," *IEEE Signal Process Lett*, vol. 17, no. 4, pp. 398–401, Apr. 2010, doi: 10.1109/LSP.2009.2038770.

[167] N. Ahmed, T. Natarajan, and K. R. Rao, "Discrete Cosine Transform," *IEEE Transactions on Computers*, vol. C–23, no. 1, pp. 90–93, Jan. 1974, doi: 10.1109/T-C.1974.223784.

[168] M. J. BUCKLEY, "Fast computation of a discretized thin-plate smoothing spline for image data," *Biometrika*, vol. 81, no. 2, pp. 247–258, 1994, doi: 10.1093/biomet/81.2.247.

[169] V. V. Moca, H. Bârzan, A. Nagy-Dăbâcan, and R. C. Mureșan, "Time-frequency super-resolution with superlets," *Nat Commun*, vol. 12, no. 1, p. 337, Jan. 2021, doi: 10.1038/s41467-020-20539-9.

[170] M. Bansal, M. Kumar, M. Sachdeva, and A. Mittal, "Transfer learning for image classification using VGG19: Caltech-101 image data set," *J Ambient Intell Humaniz Comput*, vol. 14, no. 4, pp. 3609–3620, Apr. 2023, doi: 10.1007/s12652-021-03488-z.

[171] J. Deng, W. Dong, R. Socher, L.-J. Li, Kai Li, and Li Fei-Fei, "ImageNet: A large-scale hierarchical image database," in *2009 IEEE Conference on Computer Vision and Pattern Recognition*, IEEE, Jun. 2009, pp. 248–255. doi: 10.1109/CVPR.2009.5206848.

[172] K. He, X. Zhang, S. Ren, and J. Sun, "Deep Residual Learning for Image Recognition," in *2016 IEEE Conference on Computer Vision and Pattern Recognition (CVPR)*, IEEE, Jun. 2016, pp. 770–778. doi: 10.1109/CVPR.2016.90.

[173] C. Szegedy *et al.*, "Going deeper with convolutions," in *2015 IEEE Conference on Computer Vision and Pattern Recognition (CVPR)*, IEEE, Jun. 2015, pp. 1–9. doi: 10.1109/CVPR.2015.7298594.

[174] A. Krizhevsky, I. Sutskever, and G. E. Hinton, "ImageNet classification with deep convolutional neural networks," *Commun ACM*, vol. 60, no. 6, pp. 84–90, May 2017, doi: 10.1145/3065386.

[175] F. Setiawan and C.-W. Lin, "A Deep Learning Framework for Automatic Sleep Apnea Classification Based on Empirical Mode Decomposition Derived from Single-Lead Electrocardiogram," *Life*, vol. 12, no. 10, p. 1509, Sep. 2022, doi: 10.3390/life12101509.

[176] S. Singhal and M. Kumar, "GSMD-SRST: Group Sparse Mode Decomposition and Superlet-Transform-Based Technique for Multilevel Classification of Cardiac Arrhythmia," *IEEE Sens J*, vol. 24, no. 6, pp. 8160–8169, Mar. 2024, doi: 10.1109/JSEN.2024.3354113.

[177] A. Kumar, V. K. Mehla, H. Tomar, M. Kumar, and R. Komaragiri, "Classification of Normal and Abnormal ECG signals using Support Vector Machine and Fourier Decomposition Method," in *2020 IEEE International Symposium on Smart Electronic Systems (iSES) (Formerly iNiS)*, IEEE, Dec. 2020, pp. 161–166. doi: 10.1109/iSES50453.2020.00044.

[178] P. M. Tripathi, A. Kumar, M. Kumar, and R. Komaragiri, "Multilevel Classification and Detection of Cardiac Arrhythmias With High-Resolution Superlet Transform and Deep Convolution Neural Network," *IEEE Trans Instrum Meas*, vol. 71, pp. 1–13, 2022, doi: 10.1109/TIM.2022.3186355.

[179] B. M. Mathunjwa, Y.-T. Lin, C.-H. Lin, M. F. Abbod, and J.-S. Shieh, "ECG arrhythmia classification by using a recurrence plot and convolutional neural network," *Biomed Signal Process Control*, vol. 64, p. 102262, Feb. 2021, doi: 10.1016/j.bspc.2020.102262.

[180] D. Lai, Y. Bu, Y. Su, X. Zhang, and C.-S. Ma, "Non-Standardized Patch-Based ECG Lead Together With Deep Learning Based Algorithm for Automatic Screening of Atrial Fibrillation," *IEEE J Biomed Health Inform*, vol. 24, no. 6, pp. 1569–1578, Jun. 2020, doi: 10.1109/JBHI.2020.2980454.

[181] H. Dang, M. Sun, G. Zhang, X. Qi, X. Zhou, and Q. Chang, "A Novel Deep Arrhythmia-Diagnosis Network for Atrial Fibrillation Classification Using Electrocardiogram Signals," *IEEE Access*, vol. 7, pp. 75577–75590, 2019, doi: 10.1109/ACCESS.2019.2918792.

[182] X. Fan, Q. Yao, Y. Cai, F. Miao, F. Sun, and Y. Li, "Multiscaled Fusion of Deep Convolutional Neural Networks for Screening Atrial Fibrillation From Single Lead Short ECG Recordings," *IEEE J Biomed Health Inform*, vol. 22, no. 6, pp. 1744–1753, Nov. 2018, doi: 10.1109/JBHI.2018.2858789.

[183] M. R. Rajeshwari and K. S. Kavitha, "Arrhythmia ventricular fibrillation classification on ECG signal using ensemble feature selection and deep neural network," *Cluster Comput*, vol. 25, no. 5, pp. 3085–3102, Oct. 2022, doi: 10.1007/s10586-022-03547-w.

[184] S. D. Reddy, R. Murugan, A. Nandi, and T. Goel, "Classification of arrhythmia disease through electrocardiogram signals using sampling vector random forest classifier," *Multimed Tools Appl*, vol. 82, no. 17, pp. 26797–26827, Jul. 2023, doi: 10.1007/s11042-022-14304-x.

[185] A. S. Eltrass, M. B. Tayel, and A. I. Ammar, "Automated ECG multi-class classification system based on combining deep learning features with HRV and ECG measures," *Neural Comput Appl*, vol. 34, no. 11, pp. 8755–8775, Jun. 2022, doi: 10.1007/s00521-022-06889-z.

[186] M. Baygin, T. Tuncer, S. Dogan, R.-S. Tan, and U. R. Acharya, "Automated arrhythmia detection with homeomorphically irreducible tree technique using more than 10,000 individual subject ECG records," *Inf Sci (N Y)*, vol. 575, pp. 323–337, Oct. 2021, doi: 10.1016/j.ins.2021.06.022.

[187] M. Llamedo and J. P. Martinez, "An Automatic Patient-Adapted ECG Heartbeat Classifier Allowing Expert Assistance," *IEEE Trans Biomed Eng*, vol. 59, no. 8, pp. 2312–2320, Aug. 2012, doi: 10.1109/TBME.2012.2202662.

176

[188] E. Essa and X. Xie, "An Ensemble of Deep Learning-Based Multi-Model for ECG Heartbeats Arrhythmia Classification," *IEEE Access*, vol. 9, pp. 103452–103464, 2021, doi: 10.1109/ACCESS.2021.3098986.

[189] S. Singhal and M. Kumar, "Cardiovascular Diseases Classification Using High-Resolution Superlet Transform on ECG and PCG Signals," in *2023 14th International Conference on Computing Communication and Networking Technologies (ICCCNT)*, IEEE, Jul. 2023, pp. 1–5. doi: 10.1109/ICCCNT56998.2023.10308338.

[190] M. Bansal, M. Kumar, M. Sachdeva, and A. Mittal, "Transfer learning for image classification using VGG19: Caltech-101 image data set," *J Ambient Intell Humaniz Comput*, vol. 14, no. 4, pp. 3609–3620, Apr. 2023, doi: 10.1007/s12652-021-03488-z.

[191] S. Kim, J. Lim, and J. Jang, "SeqAFNet: A Beat-Wise Sequential Neural Network for Atrial Fibrillation Classification in Adhesive Patch-Type Electrocardiographs," *IEEE J Biomed Health Inform*, vol. 28, no. 9, pp. 5260–5269, Sep. 2024, doi: 10.1109/JBHI.2024.3411056.

[192] Y. K. Kim, M. Lee, H. S. Song, and S.-W. Lee, "Automatic Cardiac Arrhythmia Classification Using Residual Network Combined With Long Short-Term Memory," *IEEE Trans Instrum Meas*, vol. 71, pp. 1–17, 2022, doi: 10.1109/TIM.2022.3181276.

[193] H. Dang, M. Sun, G. Zhang, X. Qi, X. Zhou, and Q. Chang, "A Novel Deep Arrhythmia-Diagnosis Network for Atrial Fibrillation Classification Using Electrocardiogram Signals," *IEEE Access*, vol. 7, pp. 75577–75590, 2019, doi: 10.1109/ACCESS.2019.2918792.

[194] A. S. Udawat and P. Singh, "An automated detection of atrial fibrillation from single-lead ECG using HRV features and machine learning," *J Electrocardiol*, vol. 75, pp. 70–81, Nov. 2022, doi: 10.1016/j.jelectrocard.2022.07.069.

[195] R. Pereira and R. V. Andreão, "Correction to: Inter-patient detection of atrial fibrillation in short ECG segments based on LSTM network with multiple input layers," *Research on Biomedical Engineering*, vol. 38, no. 2, pp. 779–779, Jun. 2022, doi: 10.1007/s42600-022-00208-0.

[196] Shikha Singhal, and Manjeet Kumar, "FrnOBSA: Fractional Order-Based Spectral Analysis for Arrhythmia Detection", accepted in Physical and Engineering Sciences in Medicine (Springer), 2025. (DOI:10.1007/s13246-025-01634-x) (Impact factor: 2.0) (Science Citation Index Expanded) Electronic ISSN: 2662-4737 Print ISSN: 2662-4729.

[197] E. H. Houssein, I. E. Ibrahim, N. Neggaz, M. Hassaballah, and Y. M. Wazery, "An efficient ECG arrhythmia classification method based on Manta ray foraging optimization," *Expert Syst Appl*, vol. 181, p. 115131, Nov. 2021, doi: 10.1016/j.eswa.2021.115131.

[198] A. S. Eltrass, M. B. Tayel, and A. I. Ammar, "A new automated CNN deep learning approach for identification of ECG congestive heart failure and arrhythmia using constant-Q non-stationary Gabor transform," *Biomed Signal Process Control*, vol. 65, p. 102326, Mar. 2021, doi: 10.1016/j.bspc.2020.102326.

[199] D. K. Atal and M. Singh, "Arrhythmia Classification with ECG signals based on the Optimization-Enabled Deep Convolutional Neural Network," *Comput Methods Programs Biomed*, vol. 196, p. 105607, Nov. 2020, doi: 10.1016/j.cmpb.2020.105607.

[200] W. Zhu, L. Zheng, A. Cheng, L. Qiu, Y. Chen, and L. Wang, "Two-stage detection method of supraventricular and ventricular ectopic beats based on sequential artificial features and heartbeats," *Biomed Signal Process Control*, vol. 85, p. 104804, Aug. 2023, doi: 10.1016/j.bspc.2023.104804.

[201] M. Mohanty, S. Sahoo, P. Biswal, and S. Sabut, "Efficient classification of ventricular arrhythmias using feature selection and C4.5 classifier," *Biomed*

Signal Process Control, vol. 44, pp. 200–208, Jul. 2018, doi: 10.1016/j.bspc.2018.04.005.

[202] O. Perlman, A. Katz, G. Amit, and Y. Zigel, "Supraventricular Tachycardia Classification in the 12-Lead ECG Using Atrial Waves Detection and a Clinically Based Tree Scheme," *IEEE J Biomed Health Inform*, vol. 20, no. 6, pp. 1513–1520, Nov. 2016, doi: 10.1109/JBHI.2015.2478076.

[203] J. Malik, O. C. Devecioglu, S. Kiranyaz, T. Ince, and M. Gabbouj, "Real-Time Patient-Specific ECG Classification by 1D Self-Operational Neural Networks," *IEEE Trans Biomed Eng*, vol. 69, no. 5, pp. 1788–1801, May 2022, doi: 10.1109/TBME.2021.3135622.

[204] Z. WU and N. E. HUANG, "ENSEMBLE EMPIRICAL MODE DECOMPOSITION: A NOISE-ASSISTED DATA ANALYSIS METHOD," *Adv Adapt Data Anal*, vol. 01, no. 01, pp. 1–41, Jan. 2009, doi: 10.1142/S1793536909000047.

[205] N. Rehman and D. P. Mandic, "Multivariate empirical mode decomposition," *Proceedings of the Royal Society A: Mathematical, Physical and Engineering Sciences*, vol. 466, no. 2117, pp. 1291–1302, May 2010, doi: 10.1098/rspa.2009.0502.

[206] A. Smruthy and M. Suchetha, "Real-Time Classification of Healthy and Apnea Subjects Using ECG Signals With Variational Mode Decomposition," *IEEE Sens J*, vol. 17, no. 10, pp. 3092–3099, May 2017, doi: 10.1109/JSEN.2017.2690805.

[207] H. Niyigena Ingabire *et al.*, "Analysis of ECG Signals by Dynamic Mode Decomposition," *IEEE J Biomed Health Inform*, vol. 26, no. 5, pp. 2124–2135, May 2022, doi: 10.1109/JBHI.2021.3130275.

[208] B. W. Brunton, L. A. Johnson, J. G. Ojemann, and J. N. Kutz, "Extracting spatial–temporal coherent patterns in large-scale neural recordings using

dynamic mode decomposition," *J Neurosci Methods*, vol. 258, pp. 1–15, Jan. 2016, doi: 10.1016/j.jneumeth.2015.10.010.

[209] Y. Özbay and G. Tezel, "A new method for classification of ECG arrhythmias using neural network with adaptive activation function," *Digit Signal Process*, vol. 20, no. 4, pp. 1040–1049, Jul. 2010, doi: 10.1016/j.dsp.2009.10.016.

[210] M. G. Tsipouras and D. I. Fotiadis, "Automatic arrhythmia detection based on time and time–frequency analysis of heart rate variability," *Comput Methods Programs Biomed*, vol. 74, no. 2, pp. 95–108, May 2004, doi: 10.1016/S0169-2607(03)00079-8.

[211] C. LIN, Y. DU, and T. CHEN, "Adaptive wavelet network for multiple cardiac arrhythmias recognition," *Expert Syst Appl*, vol. 34, no. 4, pp. 2601–2611, May 2008, doi: 10.1016/j.eswa.2007.05.008.

[212] T. Tuncer, S. Dogan, P. Pławiak, and U. Rajendra Acharya, "Automated arrhythmia detection using novel hexadecimal local pattern and multilevel wavelet transform with ECG signals," *Knowl Based Syst*, vol. 186, p. 104923, Dec. 2019, doi: 10.1016/j.knosys.2019.104923.

[213] Z. Zhang, "Introduction to machine learning: k-nearest neighbors," *Ann Transl Med*, vol. 4, no. 11, pp. 218–218, Jun. 2016, doi: 10.21037/atm.2016.03.37.

[214] M. A. Hearst, S. T. Dumais, E. Osuna, J. Platt, and B. Scholkopf, "Support vector machines," *IEEE Intelligent Systems and their Applications*, vol. 13, no. 4, pp. 18–28, Jul. 1998, doi: 10.1109/5254.708428.

[215] P. Xanthopoulos, P. M. Pardalos, and T. B. Trafalis, "Linear Discriminant Analysis," 2013, pp. 27–33. doi: 10.1007/978-1-4419-9878-1_4.

[216] A. Araveeporn, "Comparing the Linear and Quadratic Discriminant Analysis of Diabetes Disease Classification Based on Data Multicollinearity," *Int J Math Math Sci*, vol. 2022, pp. 1–11, Sep. 2022, doi: 10.1155/2022/7829795.

[217] A. Navada, A. N. Ansari, S. Patil, and B. A. Sonkamble, "Overview of use of decision tree algorithms in machine learning," in *2011 IEEE Control and System Graduate Research Colloquium*, IEEE, Jun. 2011, pp. 37–42. doi: 10.1109/ICSGRC.2011.5991826.

[218] Y. Li, Z. Zhang, F. Zhou, Y. Xing, J. Li, and C. Liu, "Multi-Label Classification of Arrhythmia for Long-Term Electrocardiogram Signals With Feature Learning," *IEEE Trans Instrum Meas*, vol. 70, pp. 1–11, 2021, doi: 10.1109/TIM.2021.3077667.

[219] F. Liu *et al.*, "An Open Access Database for Evaluating the Algorithms of Electrocardiogram Rhythm and Morphology Abnormality Detection," *J Med Imaging Health Inform*, vol. 8, no. 7, pp. 1368–1373, Sep. 2018, doi: 10.1166/jmihi.2018.2442.

[220] J. Zhang, A. Liu, M. Gao, X. Chen, X. Zhang, and X. Chen, "ECG-based multi-class arrhythmia detection using spatio-temporal attention-based convolutional recurrent neural network," *Artif Intell Med*, vol. 106, p. 101856, Jun. 2020, doi: 10.1016/j.artmed.2020.101856.

[221] Z. Xia *et al.*, "Automatic Multi-label Classification in 12-Lead ECGs Using Neural Networks and Characteristic Points," 2019, pp. 80–87. doi: 10.1007/978-3-030-33327-0_10.

[222] A. Walinjkar and J. Woods, "Personalized wearable systems for real-time ECG classification and healthcare interoperability: Real-time ECG classification and FHIR interoperability," in *2017 Internet Technologies and Applications (ITA)*, IEEE, Sep. 2017, pp. 9–14. doi: 10.1109/ITECHA.2017.8101902.

[223] T. Bhat, Akanksha, Shrikara, S. Bhat, and M. T, "A Real-Time IoT Based Arrhythmia Classifier Using Convolutional Neural Networks," in *2020 IEEE International Conference on Distributed Computing, VLSI, Electrical Circuits and Robotics (DISCOVER)*, IEEE, Oct. 2020, pp. 79–83. doi: 10.1109/DISCOVER50404.2020.9278059.

[224] P. Pławiak, "Novel genetic ensembles of classifiers applied to myocardium dysfunction recognition based on ECG signals," *Swarm Evol Comput*, vol. 39, pp. 192–208, Apr. 2018, doi: 10.1016/j.swevo.2017.10.002.

[225] E. Essa and X. Xie, "Multi-model Deep Learning Ensemble for ECG Heartbeat Arrhythmia Classification," in *2020 28th European Signal Processing Conference (EUSIPCO)*, IEEE, Jan. 2021, pp. 1085–1089. doi: 10.23919/Eusipco47968.2020.9287520.

[226] Ö. Yildirim, "A novel wavelet sequence based on deep bidirectional LSTM network model for ECG signal classification," *Comput Biol Med*, vol. 96, pp. 189–202, May 2018, doi: 10.1016/j.compbiomed.2018.03.016.

[227] S. Singhal and M. Kumar, "SPTDMD-WST: Arrhythmia classification from spatiotemporal modes of dynamic mode decomposition using wavelet scattering transform," *Biomed Signal Process Control*, vol. 92, p. 105983, Jun. 2024, doi: 10.1016/j.bspc.2024.105983.

SHIKHA SINGHAL

Email: ggshikha12@gmail.com
Phone: 7289994418
Location: Delhi
LinkedIn Profile

PROFESSIONAL SUMMARY

Dedicated and energetic teaching professional with a strong academic background and extensive experience in modern and innovative teaching techniques. Thrives in a competitive team environment where efforts are recognized and achievements are celebrated. Committed to delivering top-quality education and fostering a dynamic learning atmosphere that supports student success and growth.

EXPERIENCE

Total Experience: 5 years

Organization: *Delhi Technological University*
Designation: *Research Scholar | Jan 2021 – 2025*

Organization: *Panipat Institute of Engineering & Technology, Samalkha, Haryana*
Affiliation: *Kurukshetra University, Kurukshetra*
Designation: *Assistant Professor | Jan 2016 – Jan 2021 (5 years)*
Nature of Experience: *Assistant Professor*

Currently working as an Assistant professor in the department of Electronics & Communication Engineering at Panipat Institute of Engineering & Technology, affiliated with K.U.K. from July, 31, 2025.

Expertise in Areas

Basics of Electronics & Engineering, Digital Electronics, Analog Communication, Machine Learning, Deep Learning, Artificial Intelligence, Python, MATLAB, LT Spice, Proteus, TinkerCAD, VLSI, Digital Communication, Biomedical Signal Processing.

Journal Papers: SCI/SCIE/Scopus Indexed Journal Papers Published

1) **Singhal, S**., & Kumar, M. (2025). FrnOBSA: fractional order-based spectral analysis for arrhythmia detection. ***Physical and Engineering Sciences in Medicine***, 1-12. **(I.F: 2.0)**
2) **Singhal, S**., & Kumar, M. (2024). SPTDMD-WST: Arrhythmia classification from spatiotemporal modes of dynamic mode decomposition using wavelet scattering transform. ***Biomedical Signal Processing and Control***, *92*, 105983. **(I.F: 4.9)**
3) **Singhal, S**., & Kumar, M. (2024). GSMD-SRST: Group sparse mode decomposition and superlet-transform-based technique for multilevel classification of cardiac arrhythmia. ***IEEE Sensors Journal***, *24*(6), 8160-8169. **(I.F: 4.5)**
4) **Singhal, S**., & Kumar, M. (2023). A systematic review on artificial intelligence-based techniques for diagnosis of cardiovascular arrhythmia diseases: Challenges and opportunities. ***Archives of Computational Methods in Engineering***, *30*(2), 865-888. **(I.F: 12.1)**

5) SINGHAL, S., JAIN, V., TAYAL, S., SCHOLAR, M. T., & PANIPAT, P. SIMULATIVE & COMPARATIVE STUDY OF CMOS TECHNIQUES USING FULL ADDER.

Scopus Indexed International Conference Papers

1) Singhal, S., & Kumar, M. (2023, July). Cardiovascular diseases classification using high-resolution superlet transform on ECG and PCG signals. In *2023 14th International Conference on Computing Communication and Networking Technologies (ICCCNT)* (pp. 1-5). IEEE.
2) Singhal, S., & Kumar, M. (2024, March). R-Peak Detection Using Wavelet Scattering Transform for Pre-Term Infant ECG Dataset. In *2024 2nd International Conference on Device Intelligence, Computing and Communication Technologies (DICCT)* (pp. 676-680). IEEE.

SUBJECTS TAUGHT

Basics of Electronics & Engineering, Digital Electronics, Analog Communication, Digital data communication, Optical communication, Computer Communication and networking, Satellite Communication.

ACADEMIC PROFILE

Ph.D. *(Biomedical signal processing using Machine learning & Deep learning)*
Delhi Technological University | *January 2021 – June 2025*
Thesis Title: *"Efficient Technique for Arrhythmia Detection and Classification Using ECG Signals"*

M.Tech *(ECE)*
Kurukshetra University (Panipat Institute of Engineering & Technology) | *2013 – 2015*
Thesis Title: *"Simulative and Comparative Study of CMOS Techniques using full adder"*
Percentile: *73.9*

B.Tech *(Electronics & Communication Engineering)*
Kurukshetra University (Panipat Institute of Engineering & Technology) | *2007 – 2011*
Percentile: *72.9*

12th *(CBSE)*
S.S.D.S.B.M Punjabi Bagh, Delhi | *2007*
Percentile: *63.8*

10th *(CBSE)*
Mahendra Model School, Rohtak, Haryana | *2005*
Percentile: *68*

FDP/STC/WORKSHOP ATTENDED

- Attended 5 days Online Faculty Development Programme on "**AI for Multimedia Processing and Security**" organized by the Department of Computer Science and Engineering, NIT Patna, held from 18th -22nd February 2023.
- Attended 40 hours online Program on "**Medical Image Processing**" jointly organized by the Electronics and ICT Academies at IIT Roorkee, MNIT Jaipur, NIT Patna, PDPM IIITDM Jabalpur, and NIT Warangal during August 22 – September 2, 2022, under the

"Scheme of financial assistance for setting up of Electronics and ICT Academies" of the Ministry of Electronics and Information Technology (MeitY), Government of India

- Attended two days IEEE workshop on "INTERNET OF THINGS (IOT): THE FUTURE OF CONNECTIVITY" on (28-29 Oct 2021).
- One Week **AICTE-ISTE Induction Program on Recent Advancements in ML and AI** (16th-22nd Dec-2021)- BVCOE, New Delhi.
- Participated one-week Online Faculty Development Programme on "Advancements and Research Opportunities in Electronics and Communication Engineering" from 4th-8th August 2020 organized by Bharti Vidyapeeth College of Engineering, Pune.
- Participated one-week Online Faculty Development Programme on "Recent trends in Computational Technologies" from 13th-18th July 2020 organized by the Department of ECE and CSE, Ashoka Institute of Engineering and Technology, Malkapur.
- Participated in one-week Short Term Course on Outcome Based Education for Program Accreditation (Online Mode) organized by the Department of Computer Science and Engineering, National Institute of Technical Teachers Training & Research (NITTTR), Chandigarh, India from 06-10 July 2020 under AICTE Margdarshan Scheme.
- Participated in the 1st Virtual National Faculty Development Programme on 'Teaching Pedagogy and Research Skills Post COVID-19' held from 22nd – 28th June 2020.
- Participated in the Online Faculty Programme on "Big Data Engineering" organized by the Department of Computer Science and Engineering from 1st June to 5th June 2020 at Kings Engineering College, Chennai.
- Participated in One-week webinar series on "Wireless Communication towards 5G" organized by the Department of Electronics and Telecommunication Engineering from 25th May to 29th May 2020 by Singhad Institute of Technology and Science, Narhe, Pune.
- Participated in AICTE Recognized Faculty Development Programme on "Embedded Systems and IOT" conducted by Electrical Engineering Department from 27th Jan to 31st Jan,2020 at PIET, Samalkha by NITTTR, CHANDIGARH.
- Participated in AICTE Recognized Faculty Development Programme on "Strengthening Industry-Academia Integration in Technical Institutions" conducted by Entrepreneurship Development and Industrial Coordination Department from 9th Dec to 13th Dec, 19 at PIET, Samalkha by NITTTR, CHANDIGARH.
- Participated in an International Workshop on "Mobile Multimedia Internet" conducted by Dr. Seshadri Mohan, Professor, UA Little Rock, USA held at P.I.E.T., Samalkha, Panipat from 6th -10th August 2018.
- Participated in a Faculty Development Program on "Class Room Communication " held at P.I.E.T., Samalkha, Panipat from 28th May -1st June 2018.
- Participated in one day workshop on "IOT & Raspberry-pi" conducted by APTRON at P.I.E.T., Samalkha, Panipat on 16th February, 2017.
- Participated in an AICTE recognized Short Term Course on "Wireless and Mobile Communication" conducted by NITTTR through ICT at P.I.E.T. Samalkha Panipat from 3rd -7th October 2016
- Participated in a Faculty Development Program on "Recent Trends In Communication Technologies" held at P.I.E.T. Samalkha, Panipat from 4th -10th JULY, 2016.

AWARDS & ACHIEVEMENTS

- Guest Speaker in Workshop on "**AI in Healthcare**" conducted at Amity University on 17th June,2025.

- Honored with **"Research Excellence Award"** at Delhi Technological University in September, **2025** & **2024**, Delhi.
- Won 1st prize in **Group Paper Presentation Competition** in PIET.
- Coordinated as a team member in **National Conference** in PIET.

Other Departmental Work

- Class Incharge.
- Lab Incharge.
- Coordinator in Alumni Association.
- Coordinator in Cultural committee.
- Departmental Coordinator of student achievements in academics.
- Coordinator of letter to parents.

OTHER INFORMATION

- Languages: English, Hindi.
- Interest: Chess and Badminton.

SHIKHA SINGHAL

BIBLIOGRAPGY

Shikha Singhal received the B.Tech. and M.Tech. degree in Electronics and Communication Engineering from Kurukshetra University, Kurukshetra, India, in 2011 and 2015 respectively. She is currently pursuing the Ph.D. degree with the Department of Electronics and Communication Engineering of Delhi Technological University, Shahbad Daulatpur, Delhi, India. She has worked with the Panipat Institute of Engineering and Technology as an Assistant Professor from January, 2016 to January, 2021. Her research interests include biomedical signal processing, artificial intelligence in healthcare, and image processing. She is honored with Research Excellence Award in 2024 and 2025 at Delhi Technological University, Delhi.